Universidade de Brasília
IG | Instituto de Geociências

OS COMPLEXOS MÁFICO-ULTRAMÁFICOS MINERALIZADOS (Fe-Ti±V±Cu±Cr) DE FLORESTA E BODOCÓ NA PORÇÃO OCIDENTAL DA PROVÍNCIA BORBOREMA E SUAS IMPLICAÇÕES GEODINÂMICAS PARA A EVOLUÇÃO DA PARTE OESTE DA ZONA TRANSVERSAL

DISSERTAÇÃO DE MESTRADO Nº 337

Dissertação de Mestrado

Geysson de Almeida Lages

Orientador: Elton Luiz Dantas

Brasília

2014

Universidade de Brasília
IG | Instituto de Geociências

OS COMPLEXOS MÁFICO-ULTRAMÁFICOS MINERALIZADOS (Fe-Ti±V±Cu±Cr) DE FLORESTA E BODOCÓ NA PORÇÃO OCIDENTAL DA PROVÍNCIA BORBOREMA E SUAS IMPLICAÇÕES GEODINÂMICAS PARA A EVOLUÇÃO DA PARTE OESTE DA ZONA TRANSVERSAL

Geysson de Almeida Lages

Dissertação de Mestrado Nº 337

Banca Examinadora:

Prof. Dr. Elton Luiz Dantas – UnB (Orientador)

Prof. Dr. Cesar Fonseca Ferreira Filho (Membro interno)

Prof. Dr. Edilton José dos Santos (Membro externo)

Brasília

2014

RELATÓRIO DE DEFESA DE DISSERTAÇÃO

MESTRADO

Universidade de Brasília - UnB
Decanato de Pesquisa e Pós-Graduação - DPP
Secretaria de Administração Acadêmica - SAA

1 - Identificação do Aluno

Nome	Matrícula
Geysson de Almeida Lages	12/0047861

Curso: Geologia

Área de Concentração	Código	Departamento
Prospecção e Geologia Econômica	1627	IGD

2 - Sessão de Defesa de Dissertação

Título

"OS COMPLEXOS MÁFICO-ULTRAMÁFICOS MINERALIZADOS (Fe-Ti±V±Cu±Cr) DE FLORESTA E BODOCÓ NA PORÇÃO OCIDENTAL DA PROVÍNCIA BORBOREMA E SUAS IMPLICAÇÕES GEODINÂMICAS PARA A EVOLUÇÃO DA PARTE OESTE DA ZONA TRANSVERSAL"

3 - Comissão Examinadora

Nome	Função	Assinatura
ELTON LUIZ DANTAS (Doutor)	Membro Interno vinculado ao programa (Presidente) Instituto de Geociências	
CESAR FONSECA FERREIRA FILHO (Doutor)	Membro Interno vinculado ao programa Instituto de Geociências	
EDILTON JOSÉ DOS SANTOS (Doutor)	Membro Externo não vinculado ao programa COMPANHIA DE PESQUISA DE RECURSOS MINERAIS	
REINHARDT ADOLFO FUCK (Doutor)	Membro Interno vinculado ao programa (Suplente) Fundação Universidade de Brasília	

4 - Resultado

A Comissão Examinadora, em 25/11/2014 após exame da **Defesa de Dissertação** e argüição do candidato, decidiu:

- [ ] Pela aprovação da **Dissertação**
- [x] Pela aprovação da **Dissertação**, com revisão de forma, indicando o prazo de até 30 dias para apresentação definitiva do trabalho revisado.
- [ ] Pela reprovação da **Dissertação**
- [ ] Pela reformulação da **Dissertação**, indicando o prazo de _____ para nova versão.

Preencher somente em caso de revisão de forma:

- [ ] O aluno apresentou a revisão de forma e a **Dissertação** foi aprovada.
- [ ] O aluno apresentou a revisão de forma e a **Dissertação** foi reprovada.
- [ ] O aluno não apresentou a revisão de forma.

Autenticação
Presidente da Comissão Examinadora

25 / 11 / 2014 (Data) _____ (Assinatura/Carimbo)

Autenticação
Coordenador do Curso

25/11/2014 (Data) _____ (Assinatura/Carimbo)
Valnir da Silva Souza
Coordenador do Curso de Pós-Graduação em Geologia - UnB

Ciente
Aluno

25/11/14 (Data) Gy Almeida Lages (Assinatura/Aluno)

Este relatório não é conclusivo e não tem efeitos legais sem a aprovação do Decanato de Pesquisa e Pós-graduação da Universidade de Brasília.

Aprovação do Decanato de Pesquisa e Pós-Graduação

Decisão:

- [ ] Homologar

___/___/___ (Data) _____ (Assinatura do Decano)

Sumário

LISTA DE FIGURAS DA DISSERTAÇÃO

INTRODUÇÃO

CONTEXTO GEOLÓGICO REGIONAL

As ocorrências do sistema Fe-Ti-O na Zona Transversal

AGRADECIMENTOS

A gratidão e o senso de justiça devem permear qualquer meio social no qual os seres vivos se inter-relacionam. Estas nobres virtudes, não são exclusividade do "homem que pensa". Elas estão presentes no *pet* que espera ansiosamente seu dono, na baleia que agradece ao mergulhador por livrar-lhe dos restos de uma rede ou até mesmo pelo predador que ataca para alimentar-se.

Não irei ousar agradecer a todos nominalmente pois sendo assim, incorro no risco de esquecer nesse exato momento de alguém que contribuiu consideravelmente para eu concluir este trabalho.

Dentre todos, quero agradecer a Débora, minha mãe que até hoje não entende o nosso trabalho, meu pai e irmãos.

A CPRM de Recife, especialmente ao gerente Adeilson e todos meus amigos de trabalho, Roberta, Cleide, Silvana"s" que são duas, Gusmão, Ana Claúdia, Vladimir, Alan Miranda (ex-CPRM).

A CPRM de Brasília, também com uma menção especial para Joseneusa e Valdir.

A todo o pessoal do laboratório de geocronologia, MEV, microssonda que com certeza este trabalho não teria sido feito.

Aos amigos que fiz na UnB, Lauro, Praxedinho, Solon, Adriana Zappa...

A todos com quem cursei disciplinas e os professores da instituição UnB, o meu muito obrigado.

RESUMO

Os complexos máfico-ultramáficos na região de Floresta (Suíte Serrote das Pedras Pretas) e Bodocó (Fazenda Esperança), Pernambuco, na Província Borborema são constituidos por rochas ultramáficas que incluem metadunitos, olivina cumulados, piroxenitos, cromititos (ocorrem em Bodocó), ilmenomagnetititos, mostrando texturas cumuláticas e membros máficos compostos por granada anfibolitos e meta-horblenditos grossos. Estas rochas encontram-se recristalizadas apresentando textura reliquiares de fases que atingiram condições de alta-pressão.

A presença de uma borda horblendítica em vários corpos, aliado a inexistência de ortopiroxênio, conteúdo de Al em piroxênios cálcicos, enriquecimento em Fe^{3+} dos cromo-espinélios, enriquecimento dos ETRL em relação aos ETRP, são compatíveis com um magma hidratado de composição olivina-toleítico a ferro-picrítico enriquecido em Ti. Neste caso, estes complexos e depósitos minerais não são comparados com os modelos clássicos de depósitos de Ferro-titânio mundiais associados a complexos acamadados, anortosíticos e/ou alcalinos, e se assemelham aos exemplos de fragmentos reliquiares de produtos relacionados à subducção, como complexos de cumulados de arco, similares a complexos do tipo Alaska. Este tipo de complexo é amplamente considerado como formados em zonas de suprasubducção sendo representantes de magmas associados a arco ou como complexos formados nas raízes de arco, podendo representar sequências ofiolíticas.

Uma amostra de meta-horblendito da mina Serrote das Pedras Pretas foi datada por U-Pb em zircão (LA-ICPMS). As idades obtidas em núcleos de zircões ígneos podem ser interpretadas como representativas da idade de cristalização em torno de 950 Ma, enquanto que zircões mostrando bordas espessas com baixa razão Th/U (0,008-0,038), são representativos da idade do metamorfismo eclogítico/retro-eclogítico sofrido por estas rochas no brasiliano (idade concórdia de 625 ± 6 Ma). Adicionalmente, a idade do protólito ígneo é bem marcada em uma isócrona de Sm-Nd em 947 ± 58 Ma (n=18). Esta idade é considerada como formada durante a cristalização magmática do protólito.

Valores de εNd_t positivos entre +0,2 e +4,69 é compatível com um manto empobrecido ou uma fonte com valores próximos ao reservatório condritico na era Mesoproterozóica paras os corpos máfico-ultramáficos estudados. A variação das idades modelo T_{DM} entre 1,2-1,6 Ga são condizentes com fonte juvenil mesoproterozóica ou mistura entre fonte antiga (paleoproterozóica) e jovem (neoproterozóica). A dispersão

das razões iniciais de $^{87}Sr/^{86}Sr$ (0,701581–0,709031) junto ao fracionamento de ETRL em relação ao ETRP sugerem que a fonte foi metassomatizada/enriquecida por introdução de fusões/fluidos relacionados a subducção.

Os complexos metamáfico-ultramáficos e as rochas gnáissicas, metavulcânicas e metassedimentares associadas podem constituir um sistema de arco marginal/bacia de retro-arco desenvolvido entre 1000 e 950 Ma onde, posteriormente, podem ter se envolvido em processos de subducção de uma bacia oceânica mais jovem durante a convergência Pan-Africana/Brasiliana envolvendo estes complexos em condições de alta pressão, fazendo parte da amalgamação do supercontinente Gondwana ocidental.

Os depósitos econômicos de Fe-Ti associados aos corpos ultramáficos e máficos e inclusos em granito cedo-ediacarano devem estar associados em parte por: acumulação primária cumulática a intercumulática nos membros ultramáficos e secundariamente por: formação de rutilo (até 12 %) gerado pelo particionamento mineral do titânio entre as fases silicáticas e óxidos durante o estágio metamórfico de alto grau; e finalmente, pelas interações hidrotermais durante o encapsulamento destes corpos como xenólitos pelo granito durante a sua colocação.

ABSTRACT

The mafic-ultramafic complexes in Floresta (Serrote das Pedras Pretas suite) and Bodocó (Fazenda Esperança), Pernambuco, Borborema Province are constituded by ultramafic rocks that include metadunites, olivine cumulate rocks, metapyroxenites, chromitites, ilmenomagnetitites showing evidence of extensive cumulus textures, and mafic members including garnet amphibolites and coarse metahornblendites. These rocks were recrystallized showing relict texture stages that reached high-pressure conditions.

Features like hornblenditic aureole in several bodies, lack of orthopyroxene, Al content in calcium pyroxenes, enrichment in Fe^{3+} of chrome-spinel and enrichment of LREE relative to HREE in whole-rock chemistry are compatible with hydrous magma with olivine tholeiitic or high-Ti ferropicrit composition. In this way, these ore bodies aren't comparable with classical models of world titanium deposits associated to layered, anorthositic and alkaline complexes, and resemble relics of subduction products such as arc-cumulate complexes, similar to Alaskan-type complexes. This kind of complex is widely considered to have formed above subduction zones (supra-subduction zones) as representants of arc magmas or arc–root complexes.

A coarse metahornblendite from Serrote das Pedras Pretas mine were dated by U-Pb zircon (LA-ICPMS). Ages cores obtained from igneous zircons can be interpreted as representing the age of crystallisation at around 950 Ma, whereas zircon showing coarse rims with low Th/U ratios (0.008-0.038), are representative of the age of the eclogitic/retro-eclogitic metamorphism underwent by these rocks during brazilian event (concordia age of 625 ± 6 Ma). Additionally, the age of the igneous protolith is well marked in an Sm-Nd isochron in 947 ± 58 Ma (n = 18). This age is considered to be formed during magmatic crystallisation of the protolith.

Positive εNd values between +0.2 and +4.69 is compatible with a depleted mantle or a source close to the chondritic reservoir during the Mesoproterozoic era for the mafic ultramafic bodies studied. The T_{DM} model ages between 1.28 to 1.6 Ga are consistent with juvenile Mesoproterozoic source or mixing between old (Paleoproterozoic) and young (Neoproterozoic) sources. The dispersion of initial ratios

of ^{87}Sr / ^{86}Sr (0.701581-0.709031) and the high fractionation of LREE relative to HREE suggest that the source was metasomatized by subduction related melts /fluids.

The mafic–ultramafic complexes and contemporary granitic and volcanic rocks, together with a possible back-arc basin constitute a Cariris Velhos marginal arc–back-arc basin system evolved between 1000 and 950 Ma and subsequently, these rocks could be underwent by deformation under high pressure conditions during late Pan-African Brazilian convergence.

The economic deposits of Ti associated with ultramafic bodies and enclosed within early ediacaran granite should be linked in part and combined by: early accumulation as cumulus and intercumulus under magmatic conditons; posterior enrichment in rutile (up to 12%) generated by mineral partition between the titanium silicate and oxide phases during the eclogitic stage; and finally, by hydrothermal interactions in ruptile-ductile conditions during granite emplacement and encapsulation of ultramafic bodies as xenoliths.

1. INTRODUÇÃO

1.1. Apresentação e objetivos

A afinidade e origem de sequencias de rochas máfica-ultramáficas permitem a reconstrução de modelos de ambientes geotectônicos mais depurados, bem como, a definição de parâmetros prospectivos para determinados bens minerais.

A ocorrência de rochas desta natureza encontradas de modo disrupto ao longo do registro litológico do Domínio Alto Pajeú, Zona Tranversal (ZT) da Província Borborema, constitui uma importante associação petrotectônica que carece, sobretudo, de dados geocronológicos, geoquímicos e isotópicos a fim de que, possa se caracterizar corretamente sua ambiência tectônica.

A principal característica do Domínio Alto Pajeú, diz repeito, ao Evento Cariris Velhos (Brito Neves et al., 1995) responsável pela geração de rochas de idade toniana.

A origem do evento é alvo de debates sendo que, pode representar um ciclo wilsoniano completo com criação e consumo de placa oceânica, provavelmente pertencente a um ambiente de arco-subducção intrudidos por granitos sincolisionais (Santos 1995; Brito Neves et al. 1995, 2001a; Kozuch 2003; Santos et al. 2010a). Alternativamente, aborda-se este evento magmático como possuindo geração de crosta oceânica ausente ou restrita e deposição em ambiente extensional intracontinental (Neves & Mariano 2001; Neves et al. 2009).

De acordo com Santos (1995) e Beurlen et al. (1992), estes complexo máfico-ultramáfico metamorfisados em pressão alta, portam mineralizações incomuns de Fe-Ti±Cr e química compatível com uma origem oceânica toleítica picrítica e peridotitos oceânicos modificados.

Nosso estudo será focalizado na sequência de rochas metamáfica-ultramáficas portadoras de associações Fe-Ti-V-Cu da região de Floresta/PE - Suíte Serrote das Pedras Pretas (FMUC) e Cr-Fe-Ti de Fazenda Esperança - Bodocó/PE (BMUC) que ocorrem nos limites do Domínio Alto Pajeú (oeste da Zona Transversal, nordeste brasileiro).

Dentre os objetivos desta dissertação, destacam-se (i) caracterização isotópica e geocronológica de FMUC para delimitar as idades de geração e da provável eclogitização; (ii) reavaliação química (rocha-total e mineral) dos dados disponíveis

sobre BMUC aliados a dados químicos (rocha-total e mineral) disponíveis e inéditos para FMUC. Desse modo pretende-se, acessar o provável protolito desses complexos máfico-ultramáficos para auxiliar no entendimento do arcabouço tectônico da área de estudo.

1.2. Localização

A área de estudo situa-se no estado da Pernambuco (região do sertão do oeste pernambucano) (Fig.1). As cidades mais importantes da região circunvizinha à área estudada são Floresta, Carnaubeiras da Penha e Bodocó. A localidade de Floresta encontra-se distante cerca de 420 km da capital de Pernambuco, Recife. O acesso à região de Floresta se dá pela BR-232, partindo-se de Recife. Após passar a cidade de Arco Verde, segue-se pela BR-110 até o município de Ibimirim onde acessa a cidade de Floresta através da rodovia PE-360. A partir daí o acesso a área se dá em estrada não pavimentada que liga a cidade de Floresta à cidade de Carnaubeira da Penha e outras vias vicinais.

Para acessar Bodocó, segue-se a BR-232 até a mesma tornar-se a BR-316 onde se converge para a BR-122 até Bodocó distando cerca de 640 km de Recife.

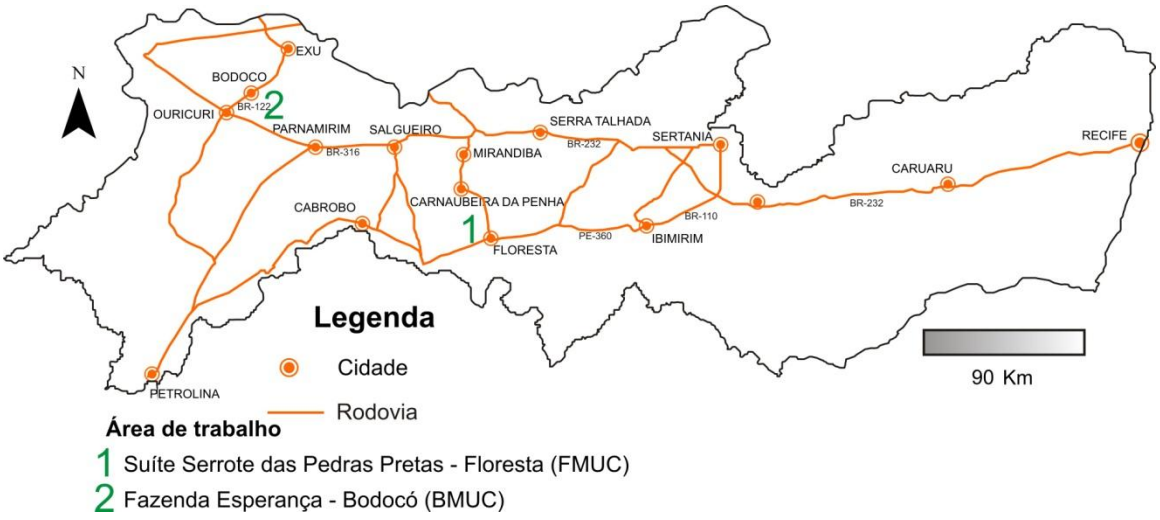

Figura 1 – Localização geográfica da região de Floresta e Bodocó (Pernambuco) (área de estudo).

1.3. Justificativas do tema proposto

A Suíte Serrote das Pedras Pretas (Veronese et al., 1985; Santos, 1995) que compreende o complexo metamáfico-ultramáfico de Floresta (FMUC) é formada por um conjunto de rochas metamáfica-ultramáficas, que estão encaixadas nas rochas supracrustais do Complexo São Caetano ou ocorrem como mega-xenólitos no Granito Riacho do Icó. Na sua área-tipo a norte de Floresta/PE, no serrote homônimo possui diversos depósitos de Fe-Ti-V±Cu associados e é formada por "metaperidotitos", metapiroxenitos, tremolititos, crossititos com ou sem granada, metagabros e metabasaltos.

Beurlen (1988) descreveu no depósito de Riacho da Posse (Floresta/PE): tremolita-clorita xistos gradando para tremolititos mineralizados, metaolivina cumulatos mineralizados, minério de Fe-Ti maciço, crossititos (termo descontinuado pela IMA - Leake et al., 1997 passando a constituir uma solução sólida entre riebeckita-glaucofana) com ou sem granada e metagabros subordinados.

Santos (1995) analisou as rochas não-anômalas (menos enriquecidas em Fe-Ti) da associação (na região do Complexo granítico Lagoa das Pedras), observando tratar-se de rochas similares a basaltos e picritos de uma série toleítica com características dos elementos maiores similares ao MORB.

Parte das mineralizações com olivina/granada-cumulados mineralizados com ilmenita-magnetita intercumulus e ilmenomagnetititos maciços formam xenólitos e/ou menos provavelmente fazem parte de *roof pendants* em granito porfirítico do Riacho do Icó (Santos, 1999).

Esta assembleia litológica conforme descrito acima, colocadas possivelmente junto a rochas de natureza marinha (psamitos) como é o caso, merecem atenção pois possuem condições de comporem fragmentos de crosta oceânica obductada (Gass, 1980) capazes de portar mineralizações de Cr do tipo podiforme e a possibilidade de novas ocorrências de Fe-Ti-V. Possíveis fases eclogíticas reportadas por Beurlen & Villarroel (1990) e Beurlen et al. (1992) reforçam esta suposição ao passo que requerem uma explanação sobre a origem das mineralizações de Fe-Ti já que, eclogitos não geram depósitos ilmeníticos, apenas neoformam rutilo a partir de fontes enriquecidas como ferrobasaltos/ferrogabros (Force, 1991).

A execução desse projeto de mestrado contribuirá para a elaboração de modelo geotectônico mais refinado para a evolução destas rochas ao passo que tentará delimitar a origem dos depósitos e possíveis idades de geração. Esse modelo mais refinado poderá auxiliar na localização e correta contextualização de novos alvos metalogenéticos.

1.4. Materiais e métodos

A proposta desta dissertação baseia-se em estudar as rochas hospedeiras metamáficas e ultramáficas e o minério maciço de Fe-Ti-V±Cu que ocorrem no Complexo metamáfico-ultramáfico de Floresta (Suíte Serrote das Pedras Pretas) com base em litogeoquímica, química mineral, geologia isotópica e geocronologia. Para isso foi realizada um levantamento de detalhe nas seções disponíveis em minas e trincheiras de pesquisa da região. Os dados disponíveis em (Beurlen, 1988) para a área de Bodocó (Faz. Esperança) e Floresta (Riacho da Posse) foram compilados.

1.4.1. Litogeoquímica

A utilização de análises químicas de múltiplos elementos para estudos petrológicos constitui atividade corriqueira da pesquisa geocientífica. Parte das amostras preparadas foram enviadas para serem analizadas no laboratório ACME *Analytycal Laboratories* Ltda (Vancouver – Canadá), por digestão de ácido nítrico diluído, fusão de 0,2g de amostra com $LiBO_2$, seguido de analise via ICP-ES para os principais óxidos e ICP-MS para elementos menores. Outra parte foi enviada para a SGS/GEOSOL e digeridas por multiácidos para análises em fluorescência de raios-X (FRX) para elementos maiores e fusão por metaborato de lítio para análises via ICP-MS para os elementos menores, traços e de terras raras.

1.4.2. Geocronologia e geoquímica isotópica

O método se baseia no decaimento dos isótopos radiogênicos de U e Th para os isótopos estáveis de Pb tendo suas composições isotópicas medidas por espectrometria de massa com a premissa básica de que os minerais utilizados mantiveram-se fechados

para estes elementos após sua formação (temperatura de fechamento). As análises isotópicas de U-Pb, foram realizadas no laboratório de geocronologia da Universidade de Brasilia. Para estas análises, as amostras foram quebradas a partir de aproximadamente 10 kg de rocha com auxilio de marreta, martelo e a utilização de britador de mandíbula. Os concentrados de minerais pesados foram separados através de separação gravimétrica utilizando batéias, feito isso os concentrados de zircões foram separados através de separador magnético (Frantz isodynamic separator). Os grãos de zircão foram separados através de catação manual, utilizando-se lupa binocular.

Os grãos de zircão foram ionizados gerando uma solução mista de ^{205}Pb-^{235}U sendo posteriormente U e Pb separados, utilizando procedimentos próprios do Laboratório do Geocronologia do IG/UnB. As incertezas nos cálculos e teores derivados da medição em ICP/MS são da ordem de ±0,5%. Isótopos radiogênicos de Pb foram corrigidos para valores originais de isótopos radiogênicos segundo o modelo para a idade aproximada da amostra de Stacey e Kramers (1975). As constantes de decaimento usadas foram as de Steiger e Jager (1977) e são de $0{,}155125 \times 10^{-9}$ por ano para ^{238}U e $0{,}98485 \times 10^{-9}$ por ano para ^{235}U. Os dados ^{207}Pb-^{235}U e ^{206}Pb-^{238}U de 40 análises foram corrigidos e lançados em um diagrama convencional de "curva concórdia" usando o programa ISOPLOT (Ludwig 2001).

Seguindo os procedimentos analíticos descritos por Bühn *et al.* (2009) e Matteini *et al.* (2009), utilizou-seis padrões internacionais de zircão, o padrão GJ-1 (Jackson *et al.*, 2004) foi usado como amostra padrão para balanço de massa e correção de desvios. O fator de correção resultante de cada amostra é procedente da posição relativa entre 4 análises, sendo duas referentes ao padrão e duas em branco (Albarède *et al.*, 2004). Já o padrão Temora2 (Black *et al.*, 2004) foi rodado no início e no fim de cada sessão analítica, apresentando acurácia em torno de 2% e precisão por volta de 1% (1σ). Os erros analíticos foram propagados pela soma quadrática de incerteza externa observada para os padrões de reprodutibilidade e precisão de cada análise desconhecida. Adicionalmente os cristais com razão $^{206}Pb/^{204}Pb$ menores que 1.000 foram excluídos das análises.

O método de Sm-Nd tem seu desenvolvimento baseado na baixa taxa de decaimento, pouca mobilidade e baixa solubilidade dos elementos envolvidos, o mesmo tem ampla aplicação tanto para fins geocronológicos quanto para fins petrológicos/petrogenéticos partindo do pressuposto que o Sm fraciona-se em relação ao

Nd somente em processos como diferenciação magmática entre manto e crosta. Uma de suas aplicações refere-se ao uso em sedimentos para indicar a origem/localização das áreas-fontes, no entanto, em áreas envolvidas em eventos metamórficos de médio a alto grau esta razão pode-se alterar a nível de minerais com a redistribuição de Sm e Nd entre os minerais neoformados ao longo da recristalização metamórfica. Como exemplo pode-se citar a afinidade da granada em reter Sm em sua estrutura cristalina. Desse modo, sugere-se o cálculo de idades-modelo baseados numa evolução de duplo estágio para os períodos mais susceptíveis aos eventos metamórficos/metassomáticos na Província Borborema para os dados disponíveis nesta área. Também segundo os dados disponíveis na literatura para está região, a alta razão isotópica de Sm/Nd reforçam que tal fracionamento ocorreu e portanto, a necessidade da revisão/aplicação de um método voltado para esta realidade.

As análises isotópicas Sm-Nd, seguiram o método descrito por Gioia e Pimentel (2000). A alíquota das amostras pulverizadas foi misturada com solução em *spike* ^{149}Sm-^{150}Nd e dissolvidas em capsulas do tipo Savillex. A extração de Sm e Nd das amostras de rocha total, seguiram técnicas convencionais de troca catiônica, usando colunas de teflon, contendo resina do tipo LN-SPEC (HEHP – ácido dietilexil fosfórico em PTFE).

Amostras de Sm e Nd foram então inseridas em filamentos de Re, e as analises isotópicas foram realizadas no espectrômetro de massa multi-colector Finnigan MAT 262 em modo estático. As incertezas Sm^{147}/Nd^{144} e $^{143}Nd/^{144}Nd$ são melhores que ± 0,4% e 0,005% respectivamente, baseado em analises repetidas de em padrões de rocha internacionais (BHVO-1 e BCR-1).

As razões isotópicas de $^{143}Nd/^{144}Nd$ foram normalizadas a 0.7210 de $^{146}Nd/^{144}Nd$ e a constante de decaimento utilizada foi de $6{,}54 \times 10^{-12}$. As idades modelo T_{DM} foram calculadas utilizando o modelo de DePaolo (1981). As analises Sm-Nd também foram realizadas no laboratório de geocronologia da Universidade de Brasilia.

As análises de isótopos de Sr foram separados pela técnica cromatográfica de troca iônica, segundo método descrito por Gioia e Pimentel (2000). As composições isotópicas de Sr foram obtidas através do espectrômetro de massa FINIGAN multicoletor, de modo estático. Os brancos totais para Sr foram de ordem de 0,2 ng. As incertezas 2σ para as razões $^{87}Sr/^{86}Sr$ foram menores que 0,01% e 0,005%, respectivamente. As idades registradas referem-se a intervalos de 95% de confiança.

Imagens por retro-espalhamento e suporte para analises elementares semi-quantitativas em laminas e mounts foram efetuadas utilizando um microscópio eletrônico de varredura com EDS acoplado modelo FEI Quanta 450 utilizando os parâmetros WD ~ 10mm e voltagem de aceleração de 20 kV.

1.4.3. Química mineral

Após o polimento das seções micropetrográficas, as análises de microssonda eletrônica foram efetuadas num equipamento Jeol JXA-8230 com 5 espectrômetros WDS e um EDS. Os cristais analisadores disponíveis (TAPJ, LIF, LIFH, PETJ, PETH, LDE1 e LDE2) permitem que sejam dosados todos os elementos químicos com número atômico superior a 4. As condições de rotina de análise foram: a) corrente do feixe de 1.002E-008 A; b) diametro do feixe de 3 μ; and c) voltagem de aceleração de 15 kV.

1.5.Plano de dissertação

A dissertação foi organizada na forma de um artigo assim distribuído:

1) "**Early Tonian Floresta and Bodocó mafic-ultramafic arc cumulate-type complexes and their retrogressed high Fe-Ti eclogites: Neoproterozoic metamorphism in Central Domain, western Borborema Province, Brazil**" a ser submetido a um periódico internacional. Este artigo representa a conclusão da dissertação com a exposição da evolução tectônica das rochas hospedeiras das mineralizações de Fe-Ti-V±Cu na região de Floresta e Bodocó (Pernambuco), com base em dados de litogeoquímica, química mineral, geocronologia e química isotópica.

2. CONTEXTO GEOLÓGICO REGIONAL

2.1. Introdução sobre a Província Borborema

A Província Borborema (PB) (Almeida et al., 1977; 1981) (Fig.2) constitui uma faixa móvel brasiliana, formada a partir da convergência dos cratons Oeste Africano-São Luís, São Francisco-Congo e Amazônico, durante a aglutinação do Gondwana Ocidental (Trompette, 1994).

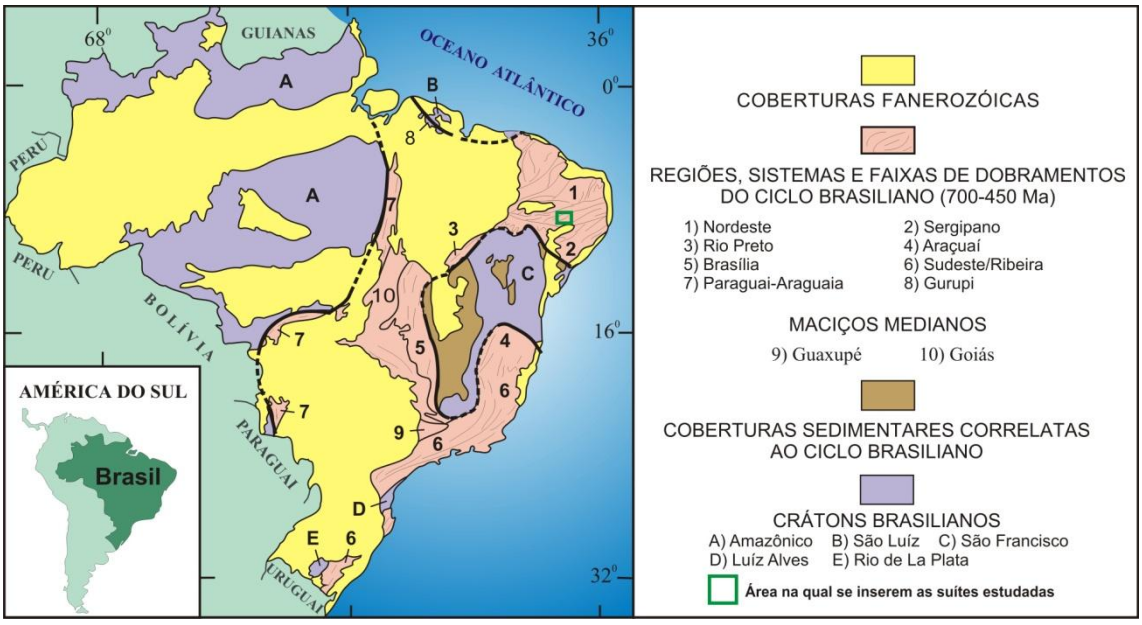

Figura 2 – Compartimentação tectônica do território brasileiro sobre a Plataforma Sul-Americana, segundo Schobbenhaus *et al.* (1984). A Província Borborema de Almeida *et al.* (1981), compreende a Região de Dobramentos Nordeste (número 1 na figura) e a Faixa Sergipana (número 2 na figura). A área de estudo se encontra assinala como o polígono verde.

O arcabouço tectônico da PB possui uma estruturação complexa que inclui *inliers* paleoproterozóicos com menores núcleos arqueanos, magmatismo intraplaca de idade estateriana/caliminiana sobrepostas por várias sequencias supracrustais metamorfizadas em variados graus. A província foi recortada por diversos cinturões de cisalhamento continentais de alta temperatura (Corsini et al. 1991; Jardim de Sá 1994; Vauchez et al. 1995) que controlaram, durante o Ciclo Brasiliano, a intrusão de extenso plutonismo associado (Brito Neves, 1975; Almeida et al., 1977; Ferreira et al. 1998; Santos & Medeiros 1999; Neves et al. 2000; Nascimento et al. 2000 e 2008; Guimarães et al. 2004; Van Schmus et al. 2011)

Ao longo de décadas, diversos modelos de compartimentação tectônica conforme o enfoque e o avanço dos métodos de pesquisa foram propostos (dentre eles: Brito Neves 1975 e 1983; Santos & Brito Neves 1984; Jardim de Sá et al. 1992; Jardim de Sá 1994; Van Schmus et al. 1995, 2011; Santos et al. 1999; Santos & Medeiros 1999; Brito Neves et al. 2000, 2001a e b, 2005; Santos et al. 2002; Oliveira 2008).

Os modelos de mosaico de terrenos exóticos/alóctones (Coney et al. 1980, Coney 1989 e Howell 1995) foram mais bem contextualizados na década de 90 por Jardim de Sá et al. (1992), Santos (1996) e Santos et al. (1999).

De uma maneira geral, a Província Borborema pode ser dividida internamente (por ex. Van Schmus *et al.*, 1995; 2008; Brito Neves *et al.*, 2000; Santos *et al.*, 2000;

2010a) em três subprovincias: Norte ou Setentrional, Central ou Zona Transversal e Meridional ou Externa.

A área em estudo insere-se no contexto da Zona Transversal (Fig.3) pelo referido modelo de terrenos tectono-estratigráficos (alóctones) da Província Borborema (Santos 1997; Santos et al. 1999), nos quais se considera os domínios supracitados como segmentos crustais com estratigrafia e evolução tectônica características e distintas dos terrenos adjacentes, estando delimitados por zonas de cisalhamento marcantes/profundas (suturas).

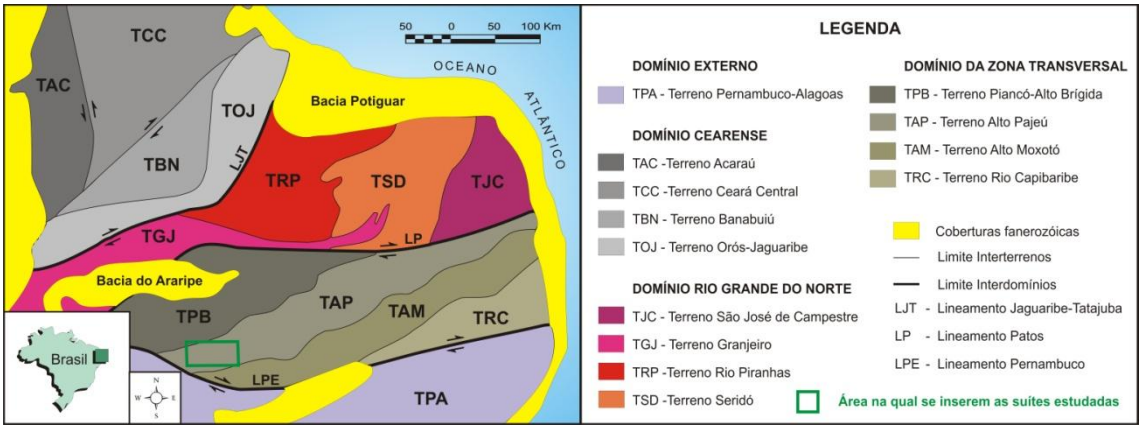

Figura 3 - Compartimentação do segmento central ou Domínio da Zona Transversal (fica as suítes máfica-ultramáficas estudadas), norte (domínios Rio Grande do Norte e Cearense) e externo da Província Borborema em domínios (ou superterrenos) e terrenos tectono-estratigráficos, segundo Santos et al. (1999).

Algumas zonas de cisalhamento com potencial para serem consideradas estruturas profundas/suturas foram propostas pela interpretação de dados gravimétricos, sendo elas dispostas conforme sua magnitude e ordem de probabilidade: Patos, Sobral-Pedro II, Picuí-João Câmara, Remígio-Pocinhos, Senador Pompeu, Tauá e Portalegre (Jardim de Sá et al. 1997; Campelo 1999).

A divisão da província segundo Oliveira (2008) destaca os domínios geofísico-tectônicos Setentrional (subdomínios Rio Piranhas, Granjeiro-Seridó e São José do Campestre) e Central ou Domínio da Zona Transversal – ZT (Van Schmus et al. 1995; Brito Neves et al. 2000) (Piancó Alto Brígida, Alto Pajeú, Alto Moxotó, Rio Capibaribe) e os domínios pertencentes ao maciço Pernambuco-Alagoas, Faixa Riacho do Pontal e Sergipana. Esta compartimentação da Província Borborema em domínios e subdomínios geofísico-tectônicos é baseada em interpretações de dados gravimétricos regionais e magnéticos de alta densidade de amostragem.

Com o incremento do acervo de dados isotópicos, geoquímicos e estruturais da porção leste da Província Borborema é retomada a discussão acerca da aplicação e relevância do conceito de terrenos tectono-estratigráficos para esta porção da província (Neves 2003; Neves et al. 2006, 2009).

Embora sistematicamente os dados de idade-modelo Sm-Nd apontem para contribuição arqueana nas fontes profundas da ZT de alguns setores, terrenos arqueanos são descritas somente fora da ZT no Domínio Rio Grande do Norte (Dantas, 1996), Rio Coruripe e oeste do Domínio Pernambuco-Alagoas (Cruz et al., 2010).

As análises de zircões detríticos a partir de rochas de sequencias metassedimentares revelam principalmente idades de deposição tardi-neoproterozóica para as rochas supracrustais do Domínio Rio Grande do Norte (Van Schmus et al. 2003).

Já em relação à Zona Transversal, as análises de zircões detríticos contam uma história mais complexa em detrimento de diversas idades de deposição que vão do paleoproterozóico ao cedo a tardi-neoproterozóico (Santos et al. 2004; Neves et al. 2006 e 2009; Guimarães et al. 2012).

Parte dos picos de idades paleoproterozoicas encontrados em diversas análises de proveniência de sedimentos possuem fontes ortoderivadas correspondentes bem representadas tais como: 2,2 a 2,05 Ga (Santos, 1995; Melo, 1998; Kozuch, 2003; Neves et al., 2006, 2014; Santos et al. 2004, 2008, 2010b; Lages et al. 2010; Rodrigues et al. 2010; Van Schmus et al. 2011; Lages no prelo; Lira Santos et al., 2014; dentre outros) indo até 2,4 Ga (Lira Santos et al., 2014).

Notadamente, o período de transição do paleoproterozóico/mesoproterozóico do Estateriano ao Caliminiano – 1,75 a 1,5 Ga foi confirmado na parte oriental da Zona Transversal onde além comprovar parte dos picos de proveniência de zircões detríticos destas idades nas rochas supracrustais também passa a constituir um importante evento magmático de espessamento/criação de crosta siálica na parte oriental da zona Transversal com diversas ocorrências de rochas neste domínio (Sá et al. 1997; Accioly 2000; Brasilino et al. 2009; Lages no prelo; Lages et al., 2013; Brasilino & Miranda no prelo; Lira Santos 2012; Lira Santos et al., 2014) sendo a grande parte caracterizado por magmatismo intraplaca.

A assembleia de rochas que data o início do Neoproterozoico vastamente documentadas na província (Brito Neves et al., 1995; Van Schmus et al., 1995; Kozuch et al., 1997; Brito Neves et al., 2000, 2001a, 2001b; Kozuch, 2003; dentre outros)

denota um evento inicialmente formalizado como orogenia Cariris Velhos (Brito Neves et al., 1995). Nesta concepção, vários autores, dentre os supracitados, relacionam as sucessões de rochas metavulcânicas e metassedimentares ocorrentes, sobretudo no Domínio Alto Pajeú como pertencentes a um ambiente de arco-subducção intrudidas por granitos sincolisionais. Entretanto, existem discussões acerca de um possível rifte intracontinental (Neves e Mariano 2001; Neves et al. 2009) e assinaturas geoquímicas de magmas intraplacas (Bittar et al. 2001; Neves 2003; Guimarães e Brito Neves 2004; dentre outros) obtidas para rochas metavulcânicas e metaplutônicas deste domínio propondo outro significado para o evento Cariris Velhos.

A zona de cisalhamento Afogados da Ingazeira é sugerida como limite leste para o evento Cariris Velhos (Kozuch 2003; Guimarães et al. 2012) por conter as maiores exposições de rochas desta idade dentro da ZT. Outras ocorrências de rochas plutônicas e vulcânicas são descritas a leste desta zona (rochas plutônicas - Brito Neves et al. 2001a; Lages et al., 2014; e rochas vulcânicas - Accioly et al. 2007) e no domínio meridional (Oliveira et al. 2010).

Nestas abordagens, uma importante associação petrotectônica de ambiente orogenéticos ou extensionais carece de dados, sobretudo de dados geocronológicos e isotópicos que são as sequencias máfico-ultramáficas encontradas de modo disrupto ao longo do registro litológico da ZT.

Uma característica peculiar a estas rochas na ZT, é a associação de mineralizações de Fe-Ti-(V) associado às ocorrências de rochas metaultramáficas e metamáficas estudadas até o momento, constituindo quase sempre corpos maciços de minério por vezes com alta razão ilmenita/magnetita (Beurlen et al., 1992).

Picos de proveniência esteniana a toniana – 1000 a 860 Ma (Brito Neves et al. 2001a; Kozuch 2003; Neves et al. 2011) são encontrados no qual o termo Evento Cariris Velhos (Brito Neves et al. 1995) constitui um importante período de criação de crosta no subdomínio Alto Pajeú.

As rochas supracrustais da Zona Tranversal incluem os Complexos considerados tonianos São Caetano (metavulcânicas e metassedimentares; Santos et al., 1984; Santos, 1995; Kozuch, 2003) e Riacho Gravatá (metavulcânicas; Brito Neves et al., 1995; Van Schmus et al., 1995; Kozuch, 2003), Complexo Salgueiro e o Grupo Cachoeirinha (Barbosa 1970; Silva Filho 1984) de idade ediacarana.

Em um *sheet* riodacítico deformado intercalado junto aos biotita xistos próximo à cidade de Salgueiro obteve-se uma idade toniana (962 Ma) para este Complexo

(Brito & Cruz 2009). Contudo esse complexo é considerado como cronocorrelato ao Grupo Cachoeirinha por alguns autores

O Grupo Cachoeirinha tem unidades litológicas similares ao Complexo Salgueiro mas apresenta gradiente metamórfico mais baixo que o referido complexo. Idades U-Pb em riolitos apresentaram resultados do Criogeniano ao Ediacarano para esta sequência (650 – 625 Ma a partir de rochas metavulcanicas; Kozuch et al., 1997; Kozuch, 2003; Medeiros, 2004).

Vários modelos estratigráficos foram propostos para o Grupo Cachoeirinha (por ex. Campos Neto, 1994; Brito Neves et al., 1995; Bittar, 1998; Medeiros & Sá, 2009). Medeiros & Sá (2009) propõe um modelo de bacia do tipo *Piggyback* para a evolução das rochas que deram origem ao Grupo Cachoeirinha, no entanto, novos dados de proveniência para a parte superior da sequencia estratigráfica proposta, possui idade toniana de deposição (Hollanda et al., 2013) contrariando o modelo proposto.

Na Zona Transversal, embora o número de dados petrográficos, isotópicos e químicos relacionados ao plutonismo brasiliano permita agrupá-los segundo suas semelhanças nos esquemas de classificação propostos (por ex. Ferreira et al. 1998; Santos & Medeiros 1999; Guimarães et al. 2004; Van Schmus et al. 2011), nem sempre é possível distinguir e individualizar o ambiente geodinâmico de parte dos mesmos por se formarem a partir de fontes mistas com distintas idades e regimes tectônicos (Ferreira et al. 1998; Guimarães et al. 2011). É comum a existência de dioritos gerados a partir de fusão parcial de manto litosférico metassomatizado relacionados a vários destes grupos de granitos (Neves & Mariano 2001).

2.2. As ocorrências do sistema Fe-Ti-O na Zona Transversal

As Figs. 4 e 5 mostram os principais depósitos mineralizados em Fe-Ti encontrados dentro dos domínios da ZT. O período de colocação destes complexos é variada desde o Riaciano ao Orosiriano, Estateriano e supostamente Esteniano/Toniano.

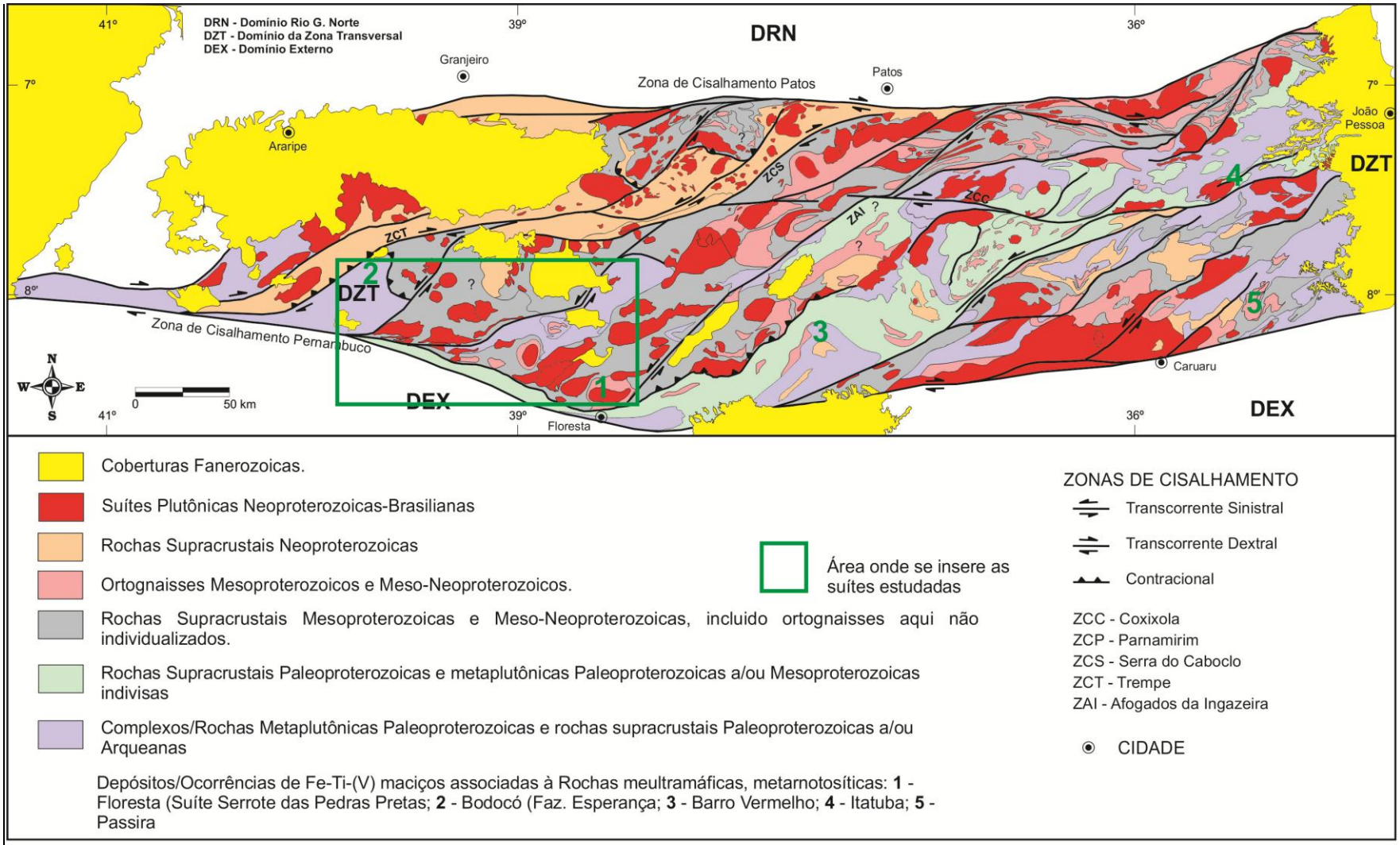

Figura 4 - Esboço geológico do Domínio da Zona Transversal, modificado de Medeiros (2004). Os depósitos de Fe-Ti estão assinalados no mapa. ? = Unidades com posicionamento geocronológico e/ou estratigráfico incerto.

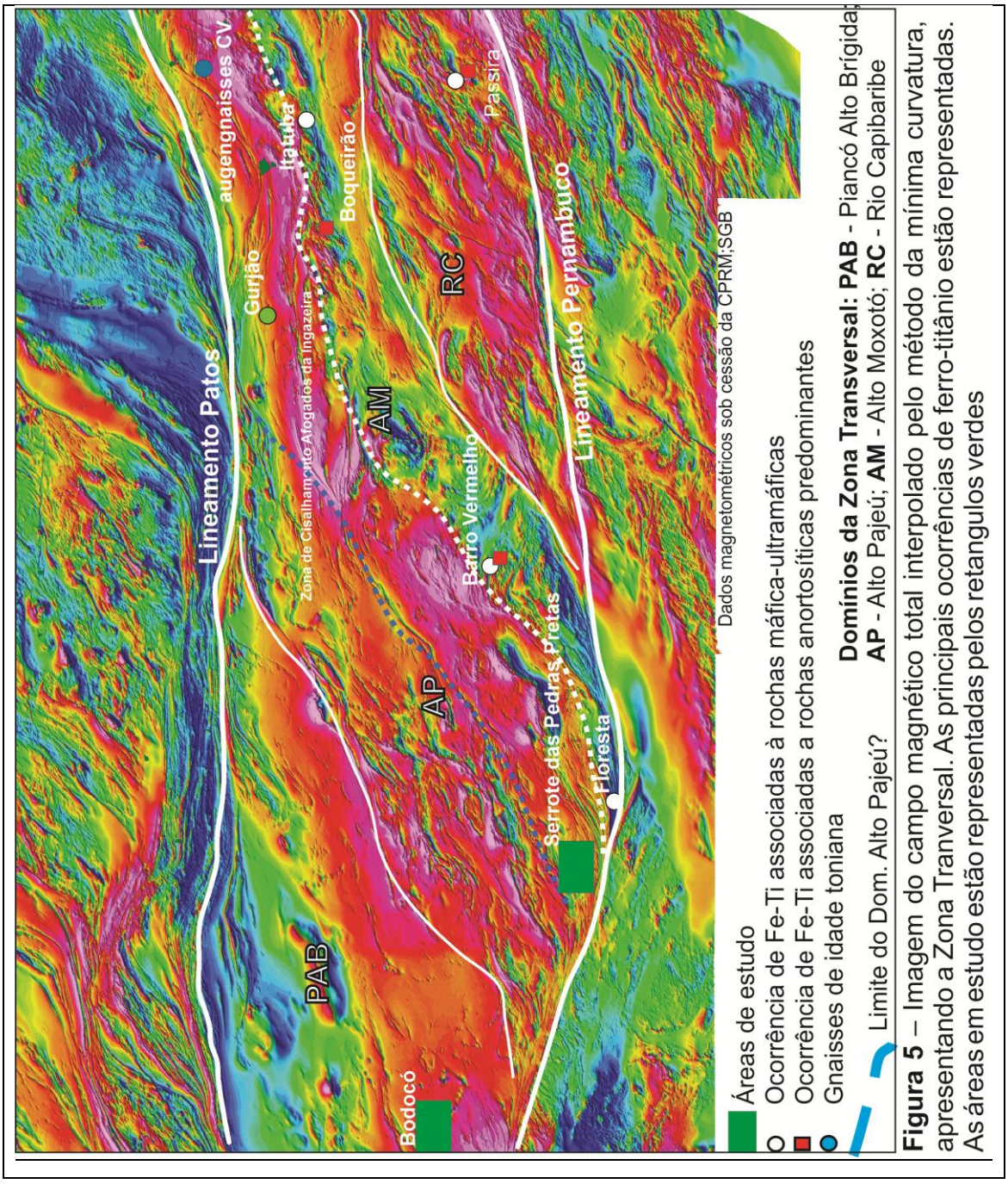

Figura 5 – Imagem do campo magnético total interpolado pelo método da mínima curvatura, apresentando a Zona Tranversal. As principais ocorrências de ferro-titânio estão representadas. As áreas em estudo estão representadas pelos retangulos verdes

Dentre as ocorrências de Fe-Ti da ZT, as de Barro Vermelho/PE ocorrem como enclaves associados a rochas gabro-anortosíticas (Melo 1998) em meio a ortognaisses tonalíticos paleoproterozóicos (Melo et al. 2002).

As ocorrências de Fe-Ti maciço associadas a rochas metamáficas de Itatuba/PB sugerem tratar-se de remanescentes de fácies eclogito apontando para uma composição predominantemente basáltica toleítica com assinatura geoquímica de arcos oceânicos (Almeida 1995; Almeida et al. 2009). Carmona (2006) encontrou pequenos corpos de rochas com afinidade anortosítica, contudo não concluiu de estas estarem associadas às

ocorrências de Fe-Ti. Este mesmo autor aventou a possibilidade dos anortositos estarem relacionadas à gênese de rochas graníticas do tipo A. Neste caso, os anortositos representariam os produtos sólidos e os granitos tipo A, os produtos líquidos derivados da fusão incongruente de um protólito da crosta inferior, durante um evento anorogênico.

A análise geocronológica de uma amostra de ortoanfibolito desta sequencia, individualizou dois grupos de idades distintas de 2.042 ± 11 Ma, interpretado como a cristalização ígnea do protólito do ortoanfibolito, e outra idade de 1.996 ± 13 Ma podendo representar um evento metamórfico durante o Riaciano (Brasilino et al. 2012; Brasilino & Miranda, no prelo; Neves et al. 2014). Santos et al. (2010b) obtiveram resultado similar em análises U-Pb SHRIMP para fácies leucocrática inclusa em rochas metamáficas onde ocorrem os ferros titanados na região de Itatuba/PB, sendo as idades de 2.086 ± 19 Ma com sobrecrescimento em 1.953 ± 25 Ma.

Ocorrências atípicas de mineralizações a Cr-Ti-Fe-(V) espinélios hospedadas em rochas metamáficas e metaultramáficas na região de Bodocó/PE possuem caráter metamórfico eclogítico de baixa temperatura associado à subducção (tipo C de Coleman 1965) junto à afinidade ofiolítica das rochas hospedeiras segundo Beurlen et al. (1992).

As ocorrências de Fe-Ti de Floresta/PE hospedadas em rochas ultramáficas da sequencia Serrote das Pedras Pretas (Veronese et al. 1985; Santos 1995) ocorrem de forma alóctone ao lado de metassedimentos do Complexo São Caetano ou como *roof pendants* no granito brasiliano Riacho do Icó (Santos 1995). A natureza toleítica-picrítica para estas rochas também possuem afinidade ofiolítica segundo Beurlen (1992). Sendo estas rochas consideradas como de provável idade toniana (Santos 1995; Santos et al. 2010a), confirmar sua natureza e idade teria importantes implicações na reconstrução dos paleocontinentes (Peri)-Rodínia e consequentemente Gondwana (Tohver et al. 2006; Fuck et al. 2008).

Pequenas mineralizações de óxidos de Fe-Ti são reportadas como associadas ao Complexo metanortosítico de Passira (Accioly, 2000) intrudidos na transição entre os períodos estateriano/caliminiano (1,7 a 1,6 Ga).

3. ARTIGO

ARTIGO

Early Tonian Floresta and Bodocó mafic-ultramafic arc cumulate-type complexes and their retrogressed high Fe-Ti eclogites: Neoproterozoic metamorphism in Central Domain, western Borborema Province, Brazil

Lages, G.A. & Dantas, E.L.

Artigo a ser submetido para publicação

Early Tonian Floresta and Bodocó mafic-ultramafic arc cumulate-type complexes and their retrogressed high Fe-Ti eclogites: Neoproterozoic metamorphism in Central Domain, western Borborema Province, Brazil

Geysson de Almeida Lages[1, 2, *], Elton Luiz Dantas[1]

[1]IG- Geoscience Institute, University of Brasilia
[2]CPRM –SUREG-RE / Geological Survey of Brazil
*Corresponding author email: geysson.lages@cprm.gov.br

ABSTRACT

Retrograde high-pressure metamorphosed Floresta and Bodocó mafic-ultramafic complexes occur as clusters of small bodies/lenses/boudins with close association with granitic/gneissic rocks and metassediments in the south limits of the Alto Pajeú domain, Borborema Province, Northeast Brazil. Ultramafic lithologies include metadunites, olivine cumulate rocks, metapyroxenites, chromitites, massive ilmenomagnetitites showing evidence of cumulus textures and mafic members include garnet amphibolites and coarse metahornblendites. The whole rock and mineral geochemistry of these complexes are akin to arc cumulate rocks especially Alaskan-type complexes which are widely considered to have formed above subduction zones.

A coarse metahornblendite from Serrote das Pedras Pretas mine were dated by U-Pb zircon (LA-ICPMS). Ages cores obtained from igneous zircons can be interpreted as representing the age of crystallisation at around 950 Ma, whereas zircon showing coarse rims with low Th/U ratios (0.008-0.038), are representative of the age of the retro-eclogitic metamorphism underwent by these rocks during Pan-African/brazilian event (concordia age of 625 ± 6 Ma). Additionally, the age of the igneous protolith is well marked in an Sm-Nd isochron in 947 ± 58 Ma (n = 18). This result is considered to be formed during magmatic crystallisation of the eclogite precursor.

Positive ε_{Nd} values between +0.2 and +4.69 suggest a depleted mantle or a source close to the chondritic reservoir during the Mesoproterozoic era for the mafic ultramafic bodies studied. The T_{DM} model ages between 1.28 to 1.6 Ga are consistent with juvenile Mesoproterozoic source or mixing between old (Paleoproterozoic) and young (Neoproterozoic) sources. The dispersion of initial ratios of $^{87}Sr/^{86}Sr$ (0.701581-0.709031) and the high fractionation of LREE relative to HREE suggest a depleted mantle source metasomatized by subduction related melts /fluids.

The mafic–ultramafic complexes and contemporary granitic and volcanic rocks, together with a possible back-arc basin constitute a Cariris Velhos marginal arc–back-arc basin system evolved between 1,000 and 950 Ma whereas FMUC and BMUC regards to a post-tectonic stage. These rocks were subsequently underwent by deformation under high pressure conditions during late Pan-African Brazilian convergence.

The economic deposits of Fe-Ti associated with ultramafic bodies and enclosed within the late Ediacaran granite in Floresta should be linked in part and combined by: early accumulation as cumulatic/intercumulus oreshoots under magmatic conditons; secondary enrichment in rutile (up to 12%) generated by mineral partition between the titanium silicate and oxide phases during the eclogitic stage; and finally, by hydrothermal interactions in ruptile-ductile conditions during granite emplacement and encapsulation of ultramafic bodies as xenoliths.

Keywords: Arc cumulate rock, supra-subduction zone, Borborema Province.

3.1. INTRODUCTION

The characterization of mafic-ultramafic rock assemblages play an important role that allows to set up and build more reliable models of convergent/divergent tectonic environments, and their petrogenesis have played crucial importance in developing plate tectonic mechanisms and crustal evolution of orogenic belts (Coleman, 1971; Gass, 1980; Moores, 1982; Dilek, 2003; Dilek & Robinson, 2003; Eyuboglu et al., 2010, 2011; Su et al., 2013).

Although Mid-Ocean Ridges provided the main sources of oceanic materials destroyed within the subduction zone (e.g. Penrose Conference in 1972; Dilek, 2003) and sometimes preserved as mafic-ultramafic suites that took part of fragments of ancient oceanic lithosphere (Gass, 1968, 1980; Coleman, 1971; Moores, 1982; Dilek, 2003; Dilek and Robinson, 2003; Eyuboglu et al., 2010, 2011; Su et al., 2013), there are some ultramafic-mafic complexes associated to orogenic belts which may represent in situ intrusions emplaced into continental basement units or ancient arc systems (Irvine, 1974; Pearce et al., 1984; Himmelberg and Loney, 1995; Eyuboglu et al., 2010, 2011).

Amongst the types of these intrusions: Uralian-Alaskan-type ultramafic–mafic complexes represent examples of island arc magmatism or shallow crustal-level in-situ intrusions injected into continental basement (Irvine, 1974; Johan, 2002; Pettigrew and Hattori, 2006; Thakurta et al., 2008; Ripley, 2009; Eyuboglu et al., 2010, 2011; Su et al., 2013). These complexes are known to be hallmarks for ophiolites, and are mostly associated with ancient suture zones evolved under different geological settings (Yellapa et al., 2014). These favorable environments to generate these probable candidates to be ophiolites are known as Suprasubduction Zone (SSZ).

Uralian-Alaskan-type intrusions occur as small-scale intrusions commonly characterized by concentric zoning often including from the core to rim: dunite and chromitite, wehrlite, clinopyroxenite, hornblendites and or gabbro, where all rocks show cumulative textures (Himmelberg and Loney, 1995; Taylor, 1967; Chen et al 2009; Tian et al. 2011). The intrusions are in most cases, distributed along narrow kilometric belts (Krause et al., 2007). They are considered to be cumulates formed by fractional crystallization of basaltic magmas in suprasubduction environment (Irvine, 1974; Farahat and Helmy, 2006; Tian et al, 2011).

This zonal structure, however, can be discontinuous, incomplete, asymmetrical, and even reverse (Himmelberg and Loney, 1995; Eyuboglu et al., 2010, 2011). Nevertheless, many of these sequences consist of a single rock-type such as peridotites, clinopyroxenites or gabbros (Eyuboglu et al. 2011) and most common hornblendites (Himmelberg and Loney, 1995).

The temporal distribution concentrate in Phanerozoic era but increasingly the number of Precambrian examples extending over the Neoarchean, Paleoproterozoic and late Neoproterozoic epochs (e.g. Pettigrew and Hattori, 2006; Farahat and Helmy, 2006; Wang et al., 2010)

The spatial distribution worldwide include, besides Urals and Alaska, other regions such as Egypt, British Columbia, USA, Turkey, Australia, Colombia, Venezuella, China (Irvine, 1974; Gray et al., 1986; James, 1971; Himmelberg and Loney, 1995; Helmy and El Mahallawi, 2003; Farahat and Helmy, 2006; Krause et al., 2007; Eyuboglu et al., 2010, 2011; Xiao et al., 2010; Wang et al. 2010; Tian en al. 2011).

Meanwhile, increases the reporting of similar small intrusions from orogenic belts hosting Ni-Cu sulfides and Ti-Fe oxides deposits has been correlated to post-orogenic extensional setting (Zhang et al., 2009, 2011; Song et al., 2011; Gao et al., 2012; Su et al., 2013; Xie et al., 2014).

Fewer Titanium deposits are found as an eclogite-type with a ferrogabbroic parental magma whereas the most common economic mineral in its association is rutile and not ilmenite (Force, 1991). Moreover, metamorphism does not enrich rocks in titanium where its contents remain approximately constant during metamorphic processes, thus, available titanium in a rock must be present in a most valuable form in order to qualify as a mineral resource (Force, 1991). Some examples of eclogitic deposits are Sunnfjord (Griffin, 1987), Piampaludo (Clerici et al., 1981) and Shubino Village deposits (Blake and Morgan, 1976).

The record of rocks of the mafic-ultramafic nature found disrupted along the Alto Pajeú domain, in the western part of the Transversal Zone, Borborema Province, is noteworthy for hosting economic Fe-Ti-V±Cu ore bodies in Floresta neighborhood and atypical occurrences of the mineralization of Cr-Ti-Fe spinels hosted on retro-metamorphic high-pressure metamafic-ultramafic rocks in Bodocó/PE (Beurlen et al., 1992). They form an important petrotectonic association as far as uncommon supposed

to be related to the subduction environment, and lack above all, more geochronological, geochemical and isotopic data.

We present in this article, unpublished LA-ICPMS U-Pb, Sr-Nd isotopic compositions of Floresta Mafic-Ultramafic Complex (FMUC – Serrote das Pedras Pretas suite) and a complete re-evaluation of available and new dataset of mineral and whole-rock geochemistry of FMUC and Bodocó mafic-ultramafic Complex (BMUC – Fazenda Esperança) with aim to set up the eclogite protoliths that provide clues for understanding tectonic architecture and Fe-Ti enrichment of some economic bodies.

3.2. GEOLOGIC SETTING

The Borborema Province (Almeida et al., 1977; 1981) started delineate its current contour when São Francisco-Congo, São Luís, West Africa and Amazonian Cratons converged to assembly of Gondwana supercontinent during the Brasiliano/Pan African orogenic cycle.

The Borborema Province has a complex tectonic framework underwent by intense magmatism (Brito Neves, 1975; Almeida et al., 1977; Ferreira et al., 1998; Santos & Medeiros 1999; Neves et al., 2000; Nascimento et al., 2000; 2008; Guimarães et al., 2004; Van Schmus et al., 2011) and several high-temperature shear zones of continental scale (Caby et al., 1991; Corsini et al., 1991; Jardim de Sá, 1994; Vauchez et al., 1995).

These events culminated in a series of deformed massifs mostly of paleoproterozoic (Siderian to Statherian) ages with small archean portions (Dantas, 1996) covered by a range of supracrustal rocks (Paleoproterozoic to Neoproterozoic periods) forming extensive regional fold belts.

This structural mosaic has many proposals of nomenclature, origin and evolution of their internal domains (e.g.: Brito Neves, 1975; 1983; Santos & Brito Neves, 1984; Jardim de Sá et al., 1992; Jardim de Sá, 1994; Van Schmus et al., 1995; Santos et al., 1999; Santos & Medeiros, 1999; Brito Neves et al., 2000; 2001a and b; 2005; Santos et al., 2002; Oliveira, 2008).

The study area is situated in the western portion of Zona Transversal or Central Domain (Fig.1), whose limits are the large E-W-striking Patos and Pernambuco transcurrent shear zones. The NE-SW striking crustal segments subdivide this domain in different tectono-stratigraphic terranes, according to distinct petrotectonic

associations, metamorphism, plutonism and geochronological signatures (Brito Neves et al., 1995; Santos, 1996; Santos & Medeiros, 1999; Neves, 2003) (Fig.2).

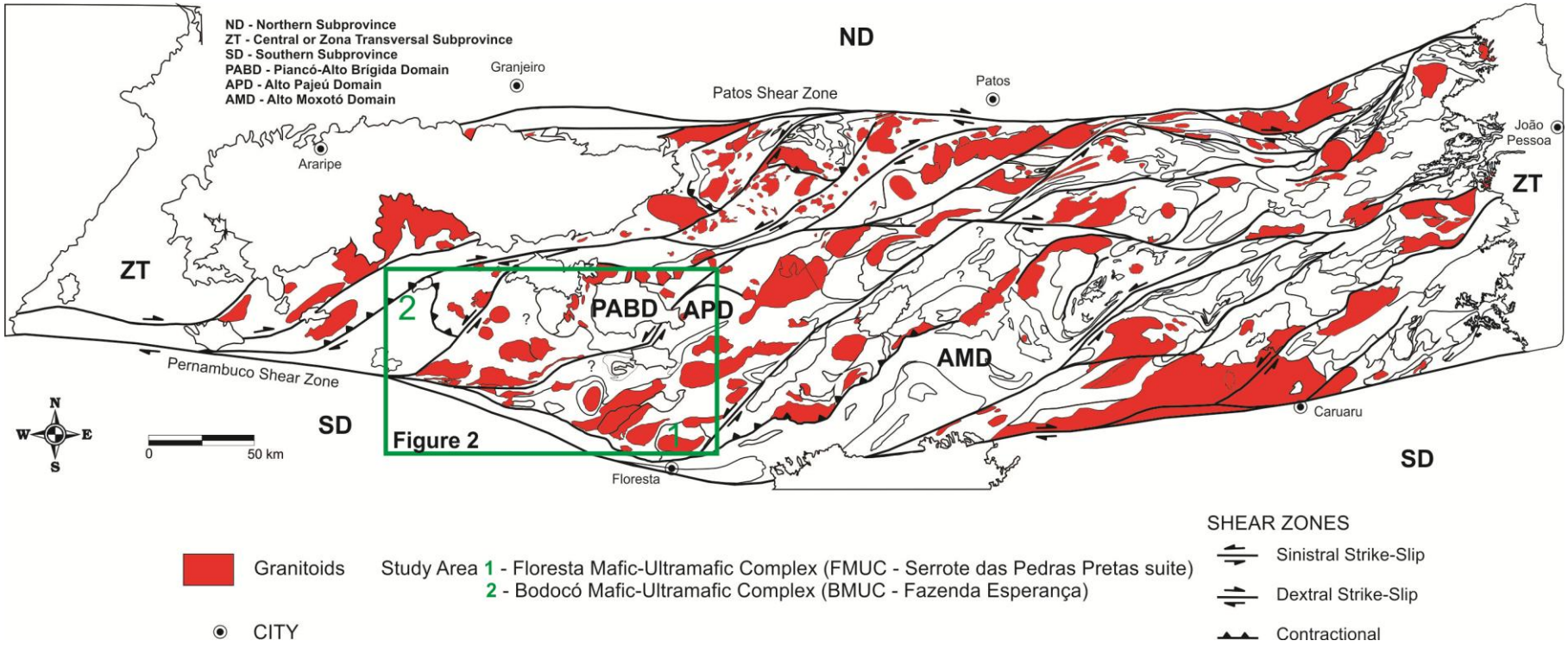

Figure 1 – Tectonic sketch highlighting Central or Zona Transversal (ZT) Subprovince position in Borborema Province and their domains Piancó-Alto Brígida and Alto Pajeú which contain mafic-ultramafic complexes of Bodocó and Floresta. Modified after Medeiros (2004).

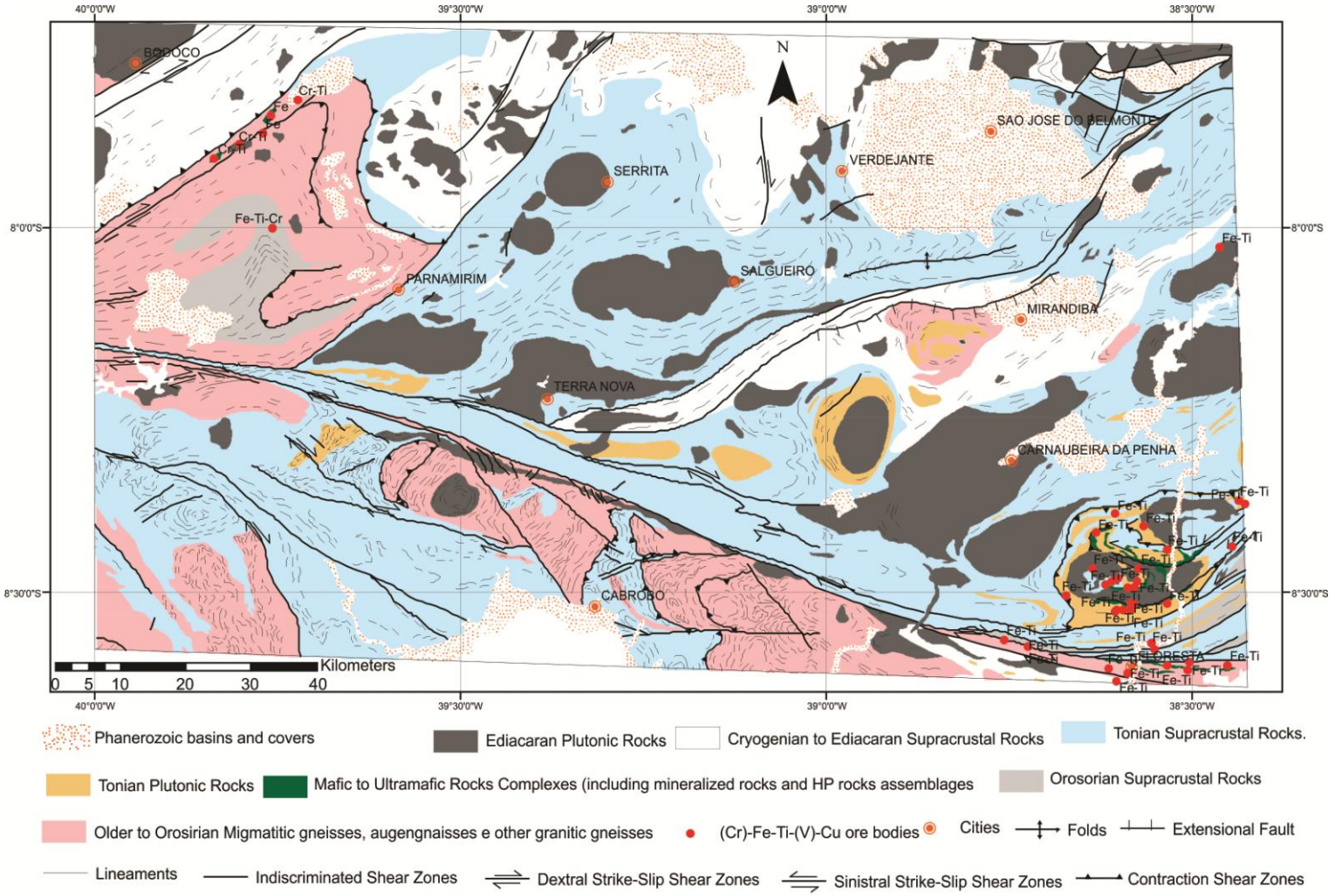

Figure 2 – Simplified regional geologic map of the study area in the Central Domain of Borborema Province showing the distribution of mafic-ultramafic complexes. Adapted and modified after Gomes and Santos (2001).

Floresta Mafic-Ultramafic Complex bodies (FMUC – Serrote das Pedras Pretras suite) (Fig. 3) occurs as clusters of small mafic to ultramafic rock sequences frequently mineralized by massive Fe-Ti-V oxides and small content of primary disseminated Ni-Cu sulfides. They often present a rounded-shaped bodies measuring less than 1.5 Km² of diameter. Folded lenses are greater than rounded-shaped "intrusions". Mineralizations are not restricted to mafic members and occur, meanwhile in ultramafic members pointing out as intercumulus textures in pyroxenites and olivine cumulates (Beurlen et al. 1992). FMUC is within the Alto Pajeú Subdomain, which consisting primarily of rocks generated during the Tonian Cariris Velhos orogenic event (Brito Neves et al. 1995; Santos 1995, 1996; Santos et al. 2010).

FMUC outcrops in metavolcano-sedimentary sequences, metagraywakes and micaschists called São Caetano Complex had their minimum age constrained by U-Pb zircon age obtained in metatuff (N of Floresta) at 995 ± 8 Ma (Santos et al., 2010). Other ages ranging from 995 to 965 Ma were found within Alto Pajeú Domain to volcanogenic and supracrustal rocks. There are a possible extension deposited during or soon after the Cariris Velhos magmatism at 932 ± 12 Ma (younger zircon, SRHIMP data -Van Schmus et al., 2011).

Tonian plutonic rocks (995-945 Ma; Santos et al., 2010) are already described and Recanto augengneiss encompasses FMUC concordantly and folded together São Caetano Complex as an outer envelope. However, main economic deposits of FMUC have as a wall-rock, the Riacho do Icó Suite and floats within it as large xenoliths. The Riacho do Icó Suite is formed by a granitic intrusion of quartz monzodiorite, granodiorite to monzogranite compositions. A U-Pb SHRIMP zircon analysis yielded an age of 608 ± 5 Ma, interpreted as the age of its crystallization (Santos et al., 2014).

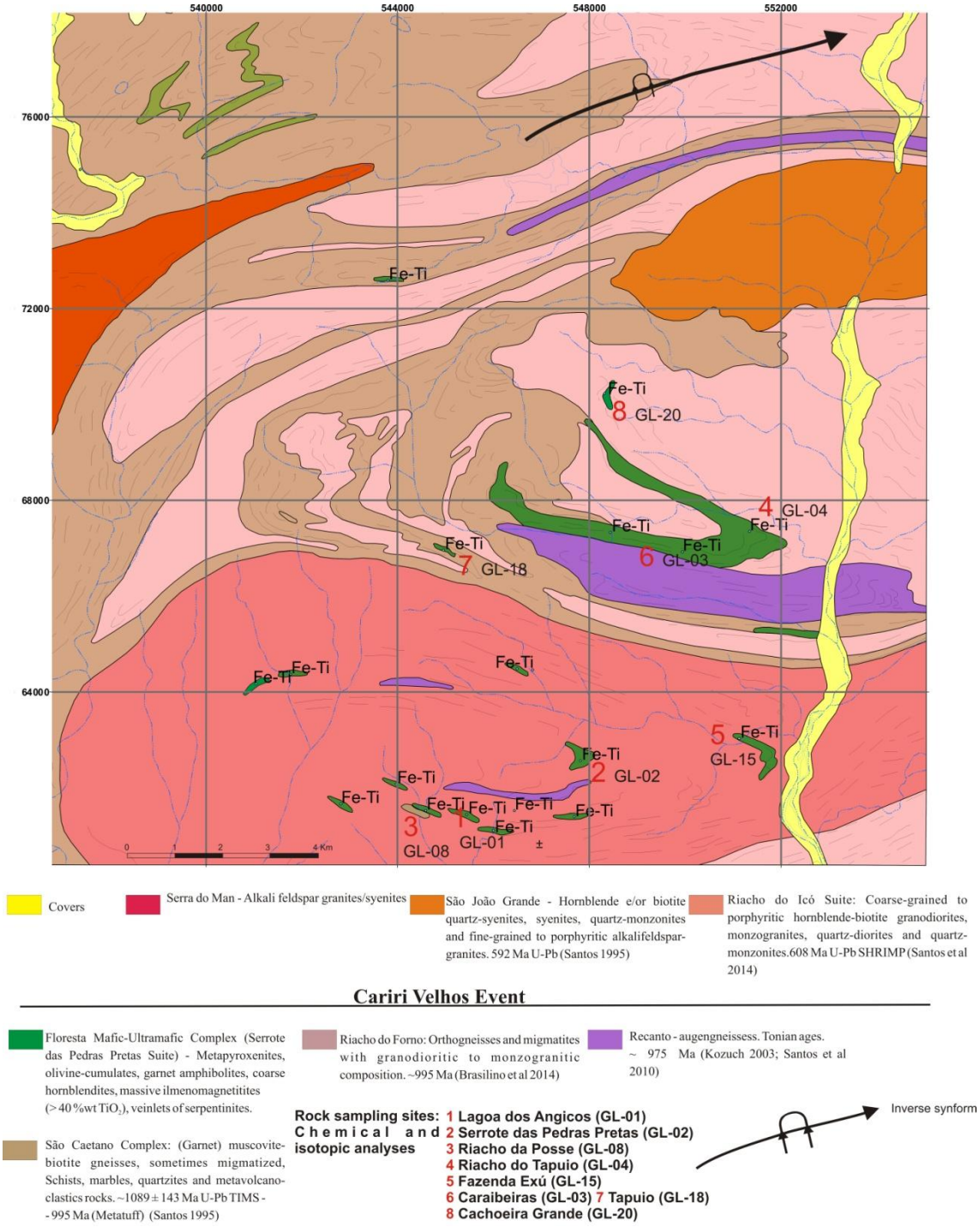

Figure 3 – Simplified geological map of Floresta Mafic-Ultramafic Complex (FMUC) showing its rock units (Serrote das Pedras Pretas suite) and sampling positions. Modified after Brasilino et al. (2014).

The Bodocó Mafic-Ultramafic Complex (BMUC – Fazenda Esperança type) (Fig.4) is inserted in Piancó-Alto Brígida basement former called Salgueiro-Cachoeirinha belt and comprises many lenses of mafic to ultramafic rocks arranged along a peripheral NW limb of a regional anticlinal. It lies in tectonic contact with

Neoproterozoic low to medium-grade metamorphic supracrustal rocks of Salgueiro Complex and Cachoeirinha Groups.

The core of the anticlinal structure called Icaiçara fragment (Medeiros et al., 1993; Santos, 1996) is compound by granite gneiss, migmatitic to banded gneiss that hosts BMUC and a psammitic-pelitic-carbonate sequence sometimes bearing-staurolite and kyanite related to Barro Complex (Mendes, 1983; Silva Filho, 1985; Medeiros et al. 1993). Available data, a Pb-Pb age in a single zircon crystal yielding 1,969 ± 9 Ma from an augen gneiss that crosscut the migmatitic gneiss can be considered to the minimum age for rocks in the core of the anticlinal (Medeiros et al. 1993). Detailed petrographic descriptions from 2 garnet-rich gabbroic members of the BMUC were carried out to ascertain eclogitic affinities (Beurlen and Villarroel 1990; Beurlen 1988; Beurlen et al. 1992).

A metarhyodacitic sheet interspersed in biotite schist (collected near the homonymous area) has provided an age at 962 Ma to the Salgueiro Complex (Brito & Cruz 2009).

Criogenian to Ediacaran age (650-625 Ma) for Cachoeirinha Group is constrained by U-Pb ages in rhyolites (Van Schmus et al. 1995; Kozuch 2003; Medeiros 2004) and recent SHRIMP U-Pb in detrital zircons reinforce an age younger than 630 Ma (Van Schmus et al. 2011)

Detailed petrographic descriptions have been already performed by (Beurlen et al., 1992; Beurlen & Villarroel, 1990; Beurlen, 1988) with emphasis on the study of thin sections, microprobe data and geochemistry from contact zones and drill core samples at Bodocó ore bodies (Fazenda Esperança - BMUC) and in Riacho da Posse inside FMUC.

In BMUC were observed eclogites, massive garnet amphibolites to banded amphibolites, metapyroxenites, tremolitites, chlorite-tremolite schists, chloritites and banded chlorite-tremolite gneisses which appear to be the result of metamorphic and deformational processes over gabbroic and pyroxenitic protoliths. Subordinated occurrences of metanorthosites appear to be interlayered with amphibolite gneisses (Beurlen et al., 1992).

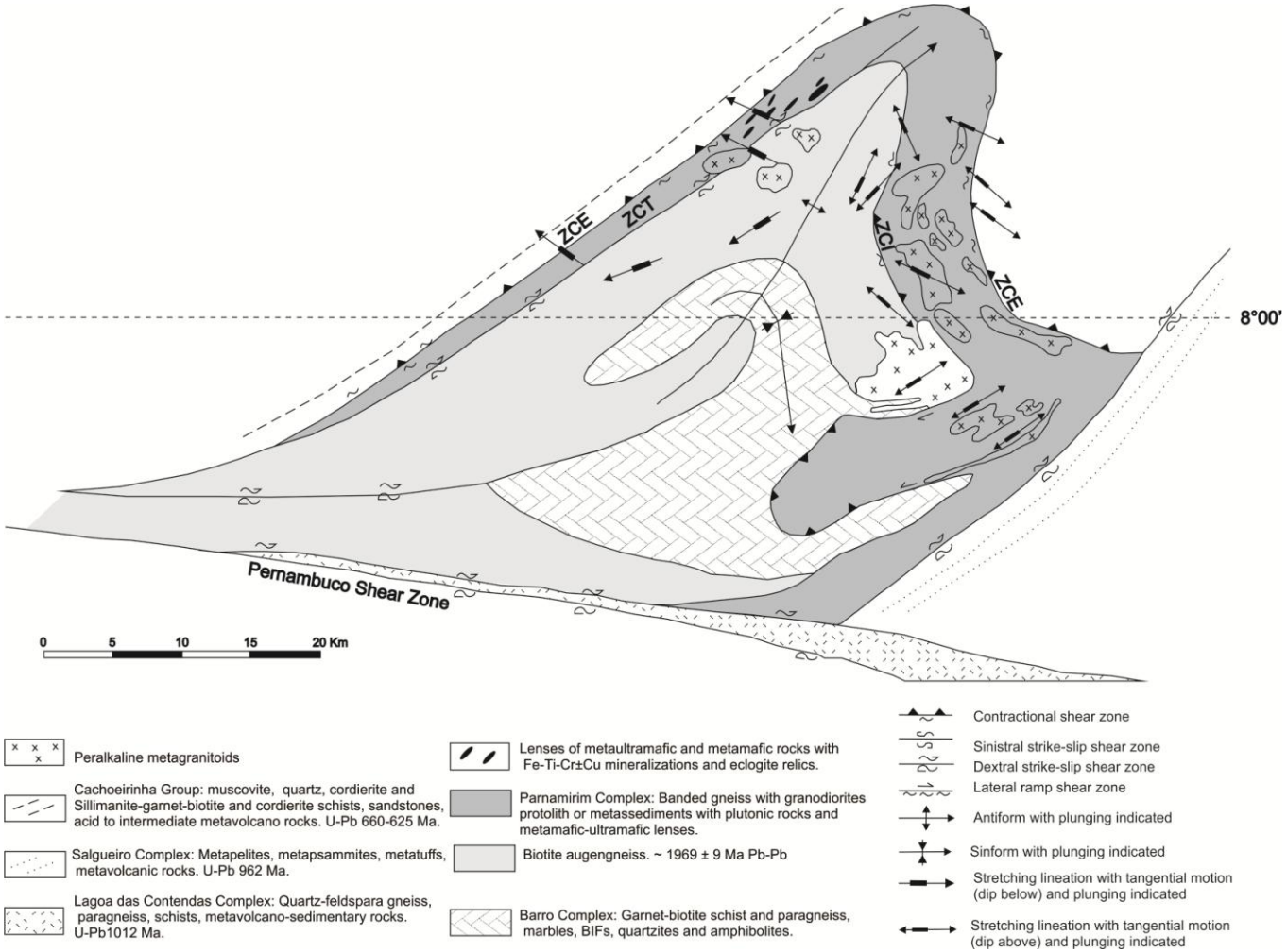

Figure 4 – Simplified geological map of Bodocó Mafic-Ultramafic Complex (BMUC) highlighting Fazenda Esperança deposits. Adapted and modified after Medeiros et al. (1993).

3.3. ANALYTICAL METHODS

U-Pb, Sm-Nd, Sr-Sr and Micropobe analyses were performed at the University of Brasilia (UnB) facilities, Brazil. Zircon, garnets, pyroxenes and amphiboles were selectively liberated using high voltage pulsed power discharges to fragment provided by SELFRAG power fragmentation equipment, besides the unmatched quality of liberation, this process requires no mechanical contact to the sample. After that, the concentrations of heavy minerals were processed by magnetic separation using a Frantz separator.

To U-Pb geochronological analyses, zircon grains were separated by hand picking using a binocular microscope. The grains were mounted on adhesive tape, enclosed in epoxy resin and polished to about half of their thickness. U-Pb analyses were performed in a mass spectrometer multi-collector Finnigan MAT-262, following the methods described by Bühn et al. (2009) and Matteini et al. (2009). For data reduction and age calculations the program PBDAT (Ludwig, 1993) and ISOPLOT-Ex (Ludwig 2001) were used. Isotopic errors were from 1σ.

Sm-Nd analyses followed the method described by Gióia and Pimentel (2000). Whole rock powders (ca. 50 mg) and leached minerals were mixed with ^{149}Sm-^{150}Nd spike solution and dissolved in savillex capsules. Sm and Nd extraction of whole-rock samples followed conventional cation exchange techniques, using Teflon columns containing LN-Spec resin (HDEHP – diethylhexil phosphoric acid supported on PTFE powder). Sm and Nd samples were loaded on Re evaporation of double filament assemblies and the isotopic measurements were carried out on a multi-collector Finnigan MAT 262 mass spectrometer in static mode.

Uncertanties of Sm/Nd and $^{143}Nd/^{144}Nd$ ratios are better than ± 0.4% (1 σ) and ± 0.005% (1 σ) respectively, based on repeated analyses of international rock standards BHVO-1 and BCR-1. $^{143}Nd/^{144}Nd$ rations were normalized to $^{146}Nd/^{144}Nd$ of 0.7219 and the decay constant used was 6.54 x 10-12. T_{DM} model ages values were calculated using the model of the DePaolo (1981). Open-source GcdKit isotopic plug-in (Janoušek et al. 2006) was used to help generate Nd evolution curves and other graphs.

Sr isotopic composition was obtained using a FINIGAN spectrometer multicolector. Total analytical blank for Sr stayed in order of 0.2 ng. The uncertainties 2σ for the $^{87}Sr/^{86}Sr$ ratios were less than 0.01%.

After polishing the thin sections and apply a carbon film, electron microprobe analyzes were performed on a Jeol JXA-8230 equipment with 5 WDS spectrometers and one EDS coupled. Analyzer crystals available (TAPJ, LIF, LIFH, PETJ, PETH, LDE1 and LDE2) allow all the chemical elements with atomic numbers greater than 4 following certain measured conditions routine analysis such: a) beam current of 1.002E-008 A; b) beam diameter of 3 μ; and c) an accelerating voltage of 15 kV. The pyroxene group was recalculated using a Visual Basic® program Winpyrox (Yavuz, 2013), the amphibole group was recalculated aided by an updated PROB-AMPH 3.0 Excel spreadsheet (Tindle and Webb, 1994). Recalculations on coexistent pairs of magnetite and ilmenite including T (°C) and $\log_{10}fO_2$ was aided by an excel spreadsheet ILMAT (Lepage 2003).

Whole rock samples were analyzed by Acme Analytical Laboratories Ltd. A small portion of the analyzes were conducted by SGS Geosol Ltd. (rock samples started at AM abbrev.). The opening method used, was the $LiBO_2$ melt and multi-acid solution and the methods of multielement analysis passed through ICP-MS, ICP-AES and X-ray fluorescence according group elements. The latest version of GCDkit 3.0 assisted in data interpretation.

Back-scattered images and EDS spots analyses were obtained in a FEI Quanta 450 SEM/EDS coupled with WD ~ 10mm and 20 kV of acceleration voltage parameters.

3.4. RESULTS

3.4.1. Mineralogy and Petrography

Our work will be focused in the FMUC (Serrote das Pedras Pretas suite) bodies considered cogenetic in relation to BMUC (Fazenda Esperança) due to their petrographic characteristics, style of mineralization and similar metamorphic trend evolution.

For this issue, about 20 occurrences related to Fe-Ti mineralizations and ultramafic-mafic rocks have been revisited and 8 were selected to perform more detailed petrographical, microprobe, geochemistry and isotopic analyses in FMUC (see Fig. 3). Samples from new outcrops within open pit mines (Serrote das Pedras Pretas – GL-02, Riacho da Posse – GL-08, Lagoa dos Angicos – GL-01, Fazenda Exú – GL-15), prospection trenchs and material accessed after the installation of a high-voltage

transmission line over Riacho do Tapuio – GL-04, are composed of fresh rocks and visible relationship between their rock assemblages and therefore, suitable for chemical, geochronological and isotopic analyses.

METADUNITES AND OLIVINE CUMULATES

In FMUC, metadunites and olivine cumulates occur frequently as mineralized olivine cumulates with net ore textured of ilmenite and magnetite intergranular (Fig. 5a and g). Disseminated Ni-Cu-Fe sulfides are interstitial involved together with Fe-Ti oxides and silicates though a post-cumulus can be suggest to sulfides in relation to Fe-Ti oxides. Serpentinized olivines (reaches up to 1 cm) in the mineralized dunites are altered to chlorites, serpentines and crystals of an acicular amphibole (cummingtonite or anthophyllite?), whereas clinopyroxenes are replaced by tremolites. The most preserved metaperidotites are in Riacho do Tapuio where olivine porphyroclasts reach dimensions greater than 1 cm. These olivines coexist in tremolitites and garnet amphibolites. In Serrote das Pedras Pretas mine occurs a massive dark green strongly serpentinized metadunite (Fig. 5b). In compacted dunites, the olivines (up to 1 cm either) are pseudomorphs generated by its breakdown remaining serpentinite/chlorite, iddingsite and a corona texture of magnetite. Thick massive ore bands of ilmenomagnetitites up to 3m (Fig. 5c) encompass a layer concordantly with these ultramafic members and thin discordant veins crosscut it.

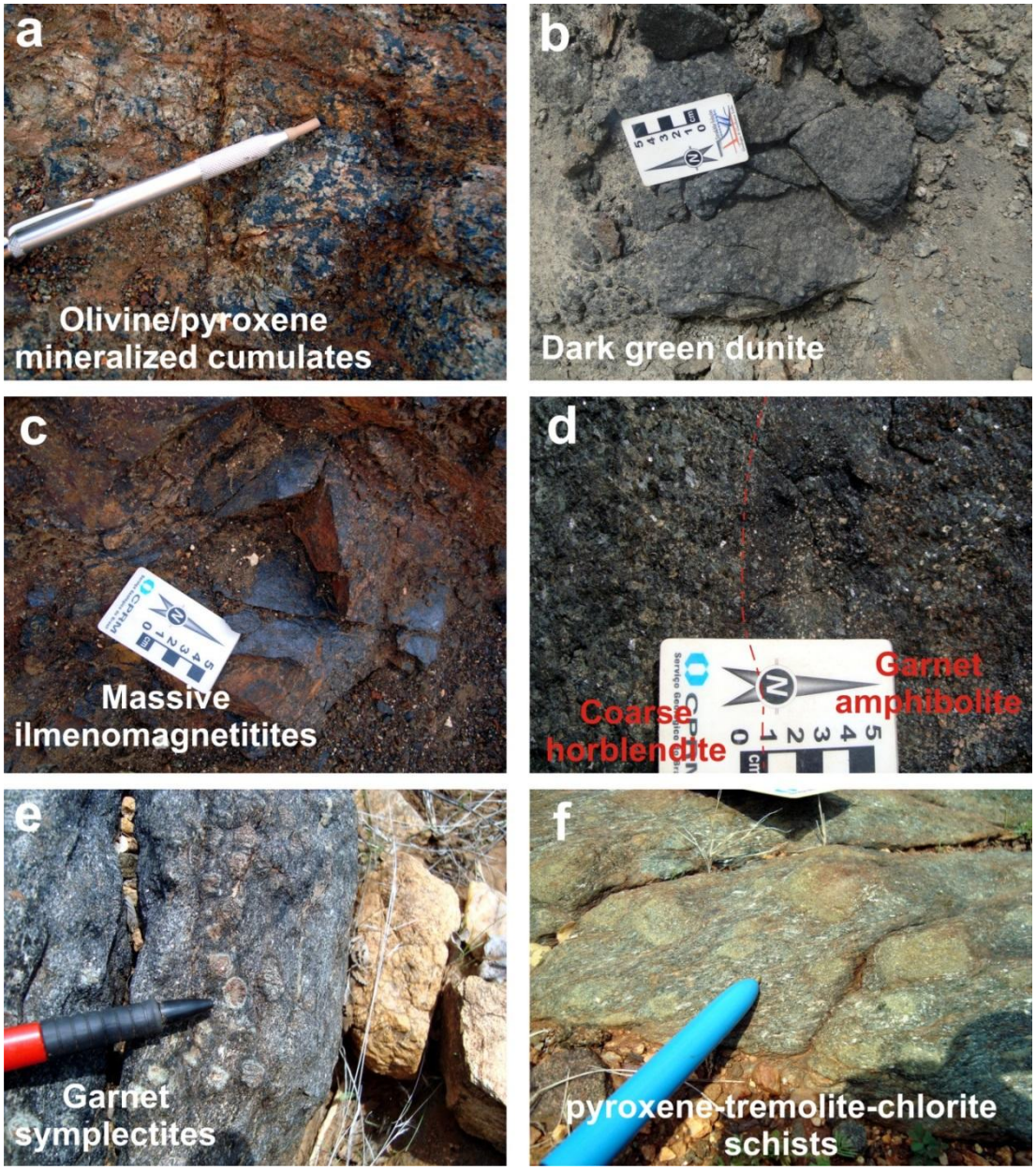
a
Olivine/pyroxene
mineralized cumulates
b
Dark green dunite
c
Massive
ilmenomagnetitites
d
Coarse
horblendite
Garnet
amphibolite
e
Garnet
symplectites
f
pyroxene-tremolite-chlorite
schists

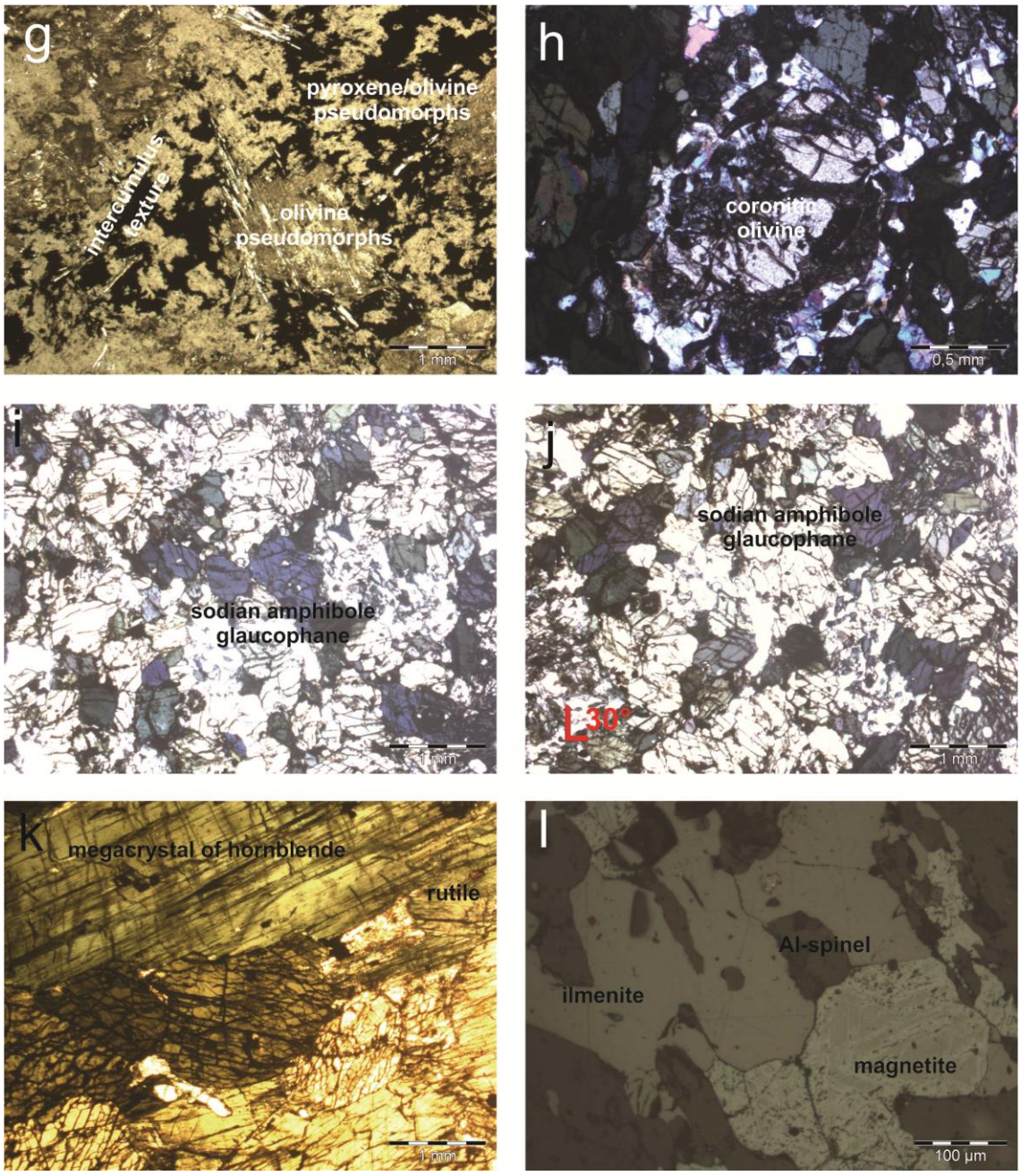

Figure 5 – Outcrop photographs of the FMUC: a) Mineralized olivine/pyroxene cumulates showing network ore texture of ilmenite+magnetite intercumulus; b) weathered compact dark green metadunite; c) massive ilmenomagnetitite occur as thick concordant bands and consist with polygonal grains of Co-V bearing magnetite and ilmenite; d) contact between coarse hornblendite and garnet amphibolite; e) centimetric garnet with coronitic feature (symplectites) in olivine garnet amphibolite; f) groundmass of tremolite-chlorite schist involving idioblastic grains of pyroxene; g) pseudomorph of olivine altered to carbonate+magnetite+talc surrounded by intercumulus in network texture of ilmenite+magnetite and silicates. Polarized light (//); h) coronitic olivine in amphibolitic matrix. Analysed light (x); i and j) characteristic pleochroism in three tones from palid to purple of sodian amphibole resemble glaucophane in polarized light and turned 30º; k) coarse idiomorphic hornblendes with rutile growth parallel to elongated crystal faces, polarized light; l) Polished section of oreshoot containing massive intergrowth between ilmenite and magnetite with presence of hercynite interstitial.

METACLINOPYROXENITES

Clinopyroxenites, tremolitites and cpx-tremolite-chlorite schists (the precursor was pyroxenites) are closely associated with olivine cumulates and preserve net textured mineralization (intergrowth between V-magnetite and ilmenite) unlike gradation wehrlite to pyroxenites are best observed in the Riacho Tapuio occurrence and consist in (olivine) clinopyroxene-tremolite-chlorite schists with pyroxenes forming idiomorfic porphyroclasts larger than 2 cm. Clinopyroxenites and wehrlites is mainly present within garnet amphibolite and metahornblendite and can also be observed with fine-grained metapyroxenites. We suppose that some metaultramafic schists surround dunites are products of metawehrlites and metapyroxenites recrystallization. “Cumulus” clinopyroxenes (augite and diopsides) are mostly altered to actinolite or tremolite (Fig. 5f).

GARNET AMPHIBOLITE

The garnetiferous amphibolites can contain up to 50 modal of garnet (reach up to 1.5 cm) in an amphibole matrix (Fig. 5d). Porphyroblastic garnets always show intense fracturing and presence of amphibole, rutile, quartz occurring as inclusions. The most voluminous amphibole is slightly oriented, with light yellow-greenish pleochroism but two other variations are observed. Symplectites are formed around garnet and are composed by intergrowths of amphibole, rutile, clinozoisite and scarce small grains of plagioclase (Fig. 5e and Fig. 6a). Coronitic olivine (Fig. 5h) occur in some members and can direct us to an olivine gabbro or even troctolite protoliths.

The "snow ball" texture and inclusions in garnet porphyroblasts record some primary minerals, such amphibole, plagioclase and clinozoisite.

Pleocroism in palid, bluish and purple tones (trichroic) is in accordance with the presence of glaucophane (Fig. 5i and j) or sodian amphiboles as compounds of one of the amphiboles, hornblende and tremolite/actnolite complete the common mineral assemblage. The granoblastic character of glaucophane remits to a origin from more a desestabilization of pyroxenes than from antigorite+albite and so belongs to a retrograde metamorphism of eclogite.

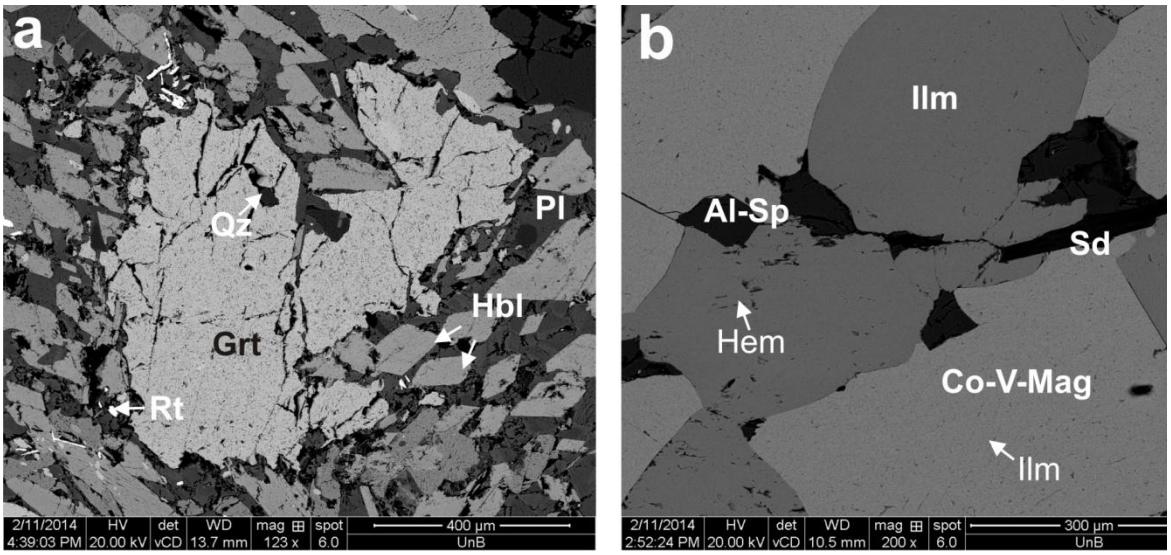

Figure 6 – Back-scattered images of rocks from FMUC: a) Sysmplectite texture exhibiting porphyroblast of fractured garnet (Grt) surrounded by mineral assemblage comprising rutile (Rt)+amphibole(Hbl)+plagioclase (Pl); b) massive Fe-Ti oxides ore with polygonal texture with Co-V bearing magnetite (Mag) and ilmenite (Ilm). Idiomorfic Al-spinel occus as hernynite-type bordering magnetite and ilmenite. There are rare hematite and ilmenite lamellae exsolutions.

COARSE METAHORNBLENDITE

Metahornblendite occupies a voluminous lithology in Riacho do Tapuio and are also considerable in Serrote das Pedras Pretas. Metahornblendites are usually associated with garnet amphibolites (Fig. 5d). It consists in idiomorfic crystals of coarse hornblende with variable pleochroism and accessory minerals such as idiomorfic rutile (more than 4%) parallel to elongated crystal faces (Fig. 5k), titanite, magnetite and interstitial fine-grained albitic plagioclase. Fine-grained amphiboles in the margins of these amphiboles are not observed, for this reason, we presumably that partly can have a cumulative origin preserved compounding a layering between precursors of garnet amphibolites probably containing plagioclase ± clinopyroxenes and hornblendites containing hornblende ± clinopyroxenes. Apparently orthopyroxene is absent and abundant plagioclase if occurred would have restricted to gabbroic member gave rise to the relicts of eclogites and now more common, garnet amphibolites.

ILMENOMAGNETITITE OR MASSIVE ORESHOOT

Three type of massive ilmenite-magnetite bands occur namely: thick lenses concordantly to the host-rocks (Fig. 5c), centimetric discordant veins commonly and parallel associated with cross fiber veins of serpentinites (chrysotile) crosscutting the third type that what exactly are the intercumulus mineralizations in Fe-Ti-V oxides

olivine ± pyroxene ± tremolite ± chlorite schists. Amounts of disseminated mineral assemblages composed of rutile+sphene or pyrrhotite+chalcopyrite+ pentlandite blebs can also be accounted.

The interstitial xenomorphic ilmenite-magnetite ores in respect to silicates suggest a cumulatic origin for the euhedral pyroxene/olivine and intercumulus nature for oxides forming a network texture. Massive coarse-grained ores form polygonal crystals of magnetite and ilmenite intergrowths (Fig. 5l) showing a complete oxidation exsolution where lamellae of ilmenite is rare in magnetite and hematite, magnetite (reduction exsolution) is virtually absent in ilmenite (Fig. 6b). Magnetite and ilmenite have approximately the same proportions in coarse massive ores. Idiomorfic grains of Al-spinel present green color as hercynite is in the margins of the ilmenites and magnetites suggest an exsolution origin or metasomatic process. Titanite occurs inside ilmenites. Rutile, siderite, sulfides and silicate ganga finish accessory minerals.

Late magmatic fluids of Riacho do Icó Suite mainly materialized in dike-like shape imposed hydrothermal alterations in mineralized ultramafic members which result in chloritite channel-filling margins in pegmatitic dikes and veins (Fig. 7a), cross-fiber veins of crysotile in sheared sites (Fig. 7b), veinlets of silicates and carbonates in stockwork texture and the most important, it culminated with the development of discordant veins and dikes of massive ilmenomagnetitites often parallel to serpentinites. This reconcentration/remmobilization of ore bands increase the grade of Fe-Ti minerals and may explain why only the ore bodies inside Riacho do Icó granites are economic until today.

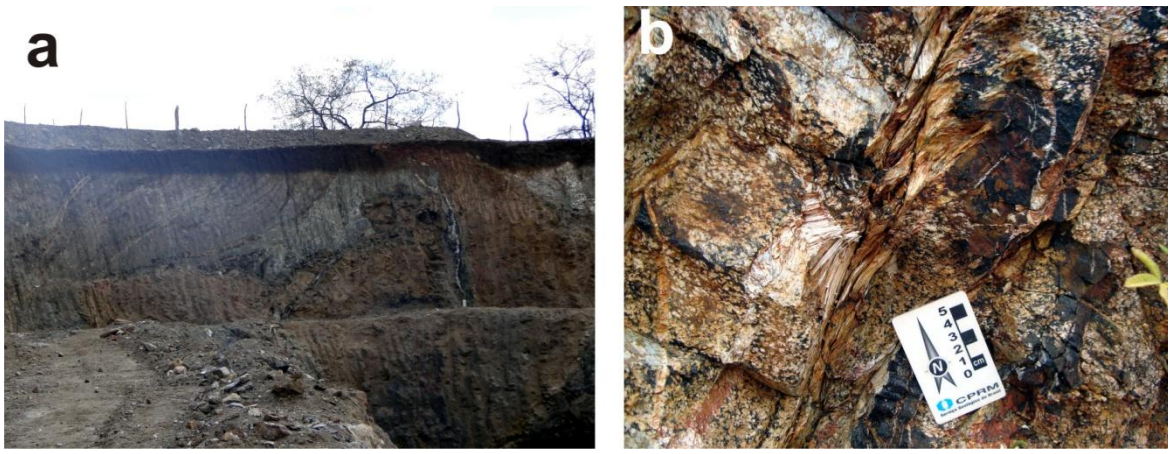

Figure 7 – Late magmatic fluids from granitic intrusion-related in FMUC: a) Metasomatic alterations caused by discharges of magmatic fluids related to pegmatoid/leucogranitoid intrusions. It is possible to notice a vertical channel-filling structure that disturb the host-rocks

represented by a chloritite/flogopitite aureole (Riacho da Posse mine); b) sheared zone with space filled by cross fiber serpentinites depleting mineralized host-rocks leaving massive Fe-Ti oxides as a restite (Serrote das Pedras Pretas mine).

Summarizing, the crystallization order from the existent ultramafic rocks may be assumed as (apatite), olivine, Fe-chromite (sulfides), clinopyroxene, magnetite, ilmenite, ± hornblende ± plagioclase, sulfides?. It looks very close to the idealized sequence appropriate to the Alaskan-type cumulates (Himmelberg and Loney, 1995). High-pressure mineral assemblage and retro-metamorphic minerals observed in thin sections of mafic and ultramafic members from FMUC are listed in Chart 1.

Chart 1 – Mineral assemblage established in thin sections from FMUC.

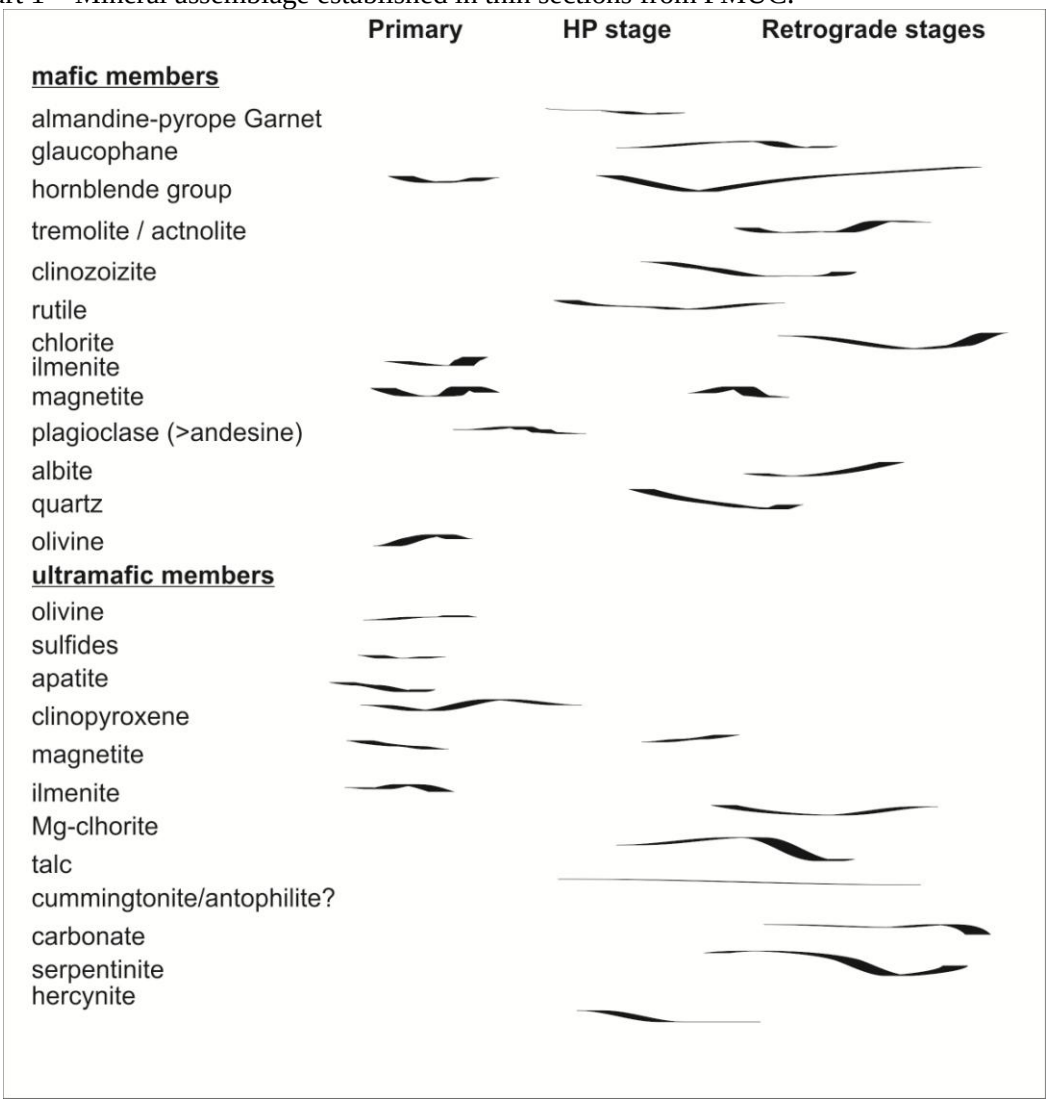

3.4.2. Mineral Chemistry

3.4.2.1. Spinel

Al-spinel commonly black and green spinel is present as an accessory phase in the massive ilmeno-magnetite ore bands from Floresta/PE and occurs at the boundary of ilmenite and vanadiferous magnetites. It is characterized by low Cr_2O_3 (0.2–0.39 wt.%), high values of Al_2O_3 (54.9–57.4 wt.%), FeO (19.64–22.24 wt.%), TiO_2 (5.5-7.4 wt.%) and V_2O_3 (0.32–0.51 wt.%). It shows a low range of Mg# ($100\times Mg/(Mg + Fe^{2+})$) between 40.7-45.7 and Cr# ($100\times Cr/(Cr + Al)$) ranges from 0.25 to 0.45 (Table 1).

Table 1 - Al-spinel composition of the Floresta mafic-ultramafic complex (FMUC)

Analyse	GL15	GL15 1 esp	GL15 2 esp	GL15 3 esp	GL15 4 esp
Type	Sp grain	Sp grain	Sp grain	Sp grain	Sp grain
Rock	Ilmenitite	Ilmenitite	Ilmenitite	Ilmenitite	Ilmenitite
Location	Faz.Exú	Faz.Exú	Faz.Exú	Faz.Exú	Faz.Exú
SiO_2	0.044	0.000	0.000	0.022	0.011
TiO_2	6.693	5.667	7.421	6.710	5.502
Al_2O_3	55.959	55.260	54.943	57.392	55.900
Cr_2O_3	0.326	0.277	0.206	0.391	0.235
FeO	21.378	21.519	22.245	19.648	20.610
Fe_2O_3					
MnO	0.063	0.154	0.187	0.121	0.131
MgO	8.677	9.624	8.570	9.287	9.741
CaO	0.000	0.000	0.000	0.000	0.000
Na_2O	0.093	0.071	0.059	0.053	0.081
K_2O	0.000	0.017	0.000	0.000	0.031
BaO	0.000	0.000	0.000	0.000	0.000
ZnO	1.585	1.763	1.694	1.341	1.739
V_2O_3	0.434	0.328	0.375	0.514	0.390
NiO	0.133	0.129	0.112	0.065	0.080
Total	95.400	94.809	95.812	95.544	94.451
Si	0.00	0.00	0.00	0.00	0.00
Ti	0.15	0.13	0.16	0.15	0.12
Al	1.94	1.91	1.90	1.96	1.94
Cr	0.01	0.01	0.00	0.01	0.01
Fe^{3+}	0.00	0.00	0.00	0.00	0.00
Fe^{2+}	0.53	0.53	0.55	0.48	0.51
Mn	0.00	0.00	0.00	0.00	0.00
Mg	0.38	0.42	0.38	0.40	0.43
#Cr	0.39	0.34	0.25	0.45	0.28
#Mg	41.98	44.36	40.71	45.73	45.73

Cr-spinel commonly Fe-chromites occur in cumulate massive bands in Bodocó/PE occurrences. Recalculated analyzes (Appendix A) reveals that the Fe-chromites has a low content of Al_2O_3 (0.64–11.96 wt.%) and MgO (0.04-8.38 wt.%); a wide range of TiO_2 (0.92-20.71 wt.%), Cr_2O_3 (15.25–34.68 wt.%) and FeO (31.43-65

wt.%). It's Cr# is between 48 and 97 (average at ~87). Mg# range from 0 to 52.8 (average at ~5).

3.4.2.2. Pyroxenes

We recompiled and recalculated all clinopyroxenes and Ca-Na pyroxenes from BMUC (database from Beurlen, 1998). The rocks analysed was pyroxenite, porphyroclastic clinopyroxene tremolitite and an eclogite (Appendix B, nomenclature scheme as proposed by IMA (Morimoto et al., 1988).

The porphyroclastic clinopyroxenes in the clinopyroxene tremolitites is mostly diopside and augite with high Mg# of 88.8 to 99.5 with the CaO-rich (21.8–24.2), low contents of TiO_2 (0.00–1.32 wt.%) and Al_2O_3 (0.00–1.68 wt.%) and Na_2O (0.00–0.69 wt.%). The pyroxenes are the only to present high Cr_2O_3 (0.23-0.54) content.

Metapyroxenite sample shows relatively low TiO_2 (0.0 wt.%, 0.14 wt.%), Al_2O_3 (0.83 wt.%, 2.09 wt.%), Na_2O (0.31 to 0.73 wt.%), and high CaO (24.15 wt.%, 25.63 wt.%) and Mg# (91.8, 100).

In the eclogite, Ca-Na omphacites were recognized (Appendix B; details in Beurlen et al., 1992) and one single crystal of augite was observed with low Al_2O_3 (4.90 wt.%), Na_2O (1.34 wt.%) and high MgO (14.8 wt.%).

Their Mg number (100Mg/[Mg + Fe^{2+}]) varies between 80.45 and 95.98. They are also characterized by relatively high TiO_2 (0.51–2.03 wt.%), Cr_2O_3 (0.22–1.92 wt.%), low Na_2O (0.20–0.65 wt.%), MnO (0.03–0.29 wt.%) and variable amounts of Al_2O_3 (1.60–4.97 wt.%), inasmuch almost all spots present a core to rim variation in SiO_2 and Al_2O_3.

3.4.2.3. Amphiboles

Hornblende group minerals (hbl) are the most abundant mineral displaying a wide range composition in BMUC and FMUC (Table 2 and Appendix C). Secondary Hbl inherit precursory compositions of clinopyroxenes and occur mainly as tremolite or actnolite (in case of eclogites and pyroxenites), predominantly magnesium-Hbl, and tschermakitic hornblende. Some relics as inclusions or in snow-ball texture can be primary hbl and include ferroan pargasite but also include Fe-tschermakite (hornblende) and Mg-hbl (updated classification scheme (Leake et al., 1997, 2004).

Table 2 - Classification scheme for amphiboles from FMUC

Sample number	GL04A	GL4A 1	GL4B	GL4B	GL4B	GL4B
Rock type	metahornblendite			garnet amphibolite		
analyse	4a	1	1	5b	9c	9d
Location			inclusion			
SiO_2	48.60	48.14	41.31	43.93	46.09	44.45
TiO_2	0.77	0.65	0.65	0.65	0.70	0.63
Al_2O_3	9.65	9.36	14.89	13.85	11.28	12.67
FeO	12.36	11.97	18.77	17.86	16.72	17.75
MnO	0.23	0.16	0.20	0.24	0.13	0.27
MgO	14.08	14.56	7.31	8.15	9.95	8.94
CaO	10.61	10.15	11.72	11.95	11.87	11.81
Na_2O	2.30	2.14	1.56	1.60	1.39	1.57
K_2O	0.19	0.18	0.47	0.51	0.42	0.44
NiO	0.08	0.10		0.00	0.00	0.05
Total	99.07	97.58	97.02	98.97	98.64	97.79
Si	6.86	6.83	6.24	6.49	6.74	6.54
Al^{iv}	1.14	1.17	1.76	1.51	1.26	1.46
Al^{vi}	0.46	0.40	0.89	0.90	0.69	0.74
Ti	0.08	0.07	0.07	0.07	0.08	0.07
Fe^{3+}	0.65	0.92	0.39	0.13	0.22	0.32
Fe^{2+}	0.81	0.50	1.98	2.07	1.83	1.87
Mn	0.03	0.02	0.03	0.03	0.02	0.03
Mg	2.96	3.08	1.65	1.80	2.17	1.96
Ni	0.01	0.01	0.00	0.00	0.00	0.01
Ca	1.60	1.54	1.89	1.89	1.86	1.86
Na	0.63	0.59	0.46	0.46	0.39	0.45
K	0.03	0.03	0.09	0.10	0.08	0.08
Total	17.27	17.16	17.44	17.45	17.33	17.39
Amphibole group	Ca	Ca	Ca	Ca	Ca	Ca
$Mg/(Mg+Fe^2)$	0.78	0.86	0.45	0.46	0.54	0.51
Amphibole names	Mg-Hbl**	Mg-Hbl	Fe-tschermakite	Fe-tschermakitic Hbl	Mg-Hbl	Mg-Hbl

No. of oxygens = 23 ** Abbrevs. Hbl - Hornblende;

The most Mg-rich hornblendes are close (Mg # ~ 1) in the amphibolites with range between 0.43-1. Hornblendes have high contents of CaO (6.26 - 12.65), Na_2O (0.66 – 2.93), MgO (6.42 – 20.24) and variable content between TiO_2, Al_2O_3 (with a positive correlation in eclogite symplectites) and SiO_2.

Fe-tschermakitic hornblende and (Ferri)-barroisite (Na-Ca group) identified in symplectites from eclogite (BMUC; BO-436) and grains from garnet-amphibolite (FMUC; RP-614) support an alleged retrograde phase from an eclogite facies where high-Al tschermakitic hornblendes are derived from omphacites in the early stages of retrograde metamorphism. In the case of barroisite amphiboles, its commonly associated to a blueschist metamorphic facies.

3.4.2.4. Magnetite

The magnetites from a sample of cumulate massive ilmeno-magnetitite in Floresta orebodies (Table 3; GL-15 - Fazenda Exu; UTM 551130; 9063033) are vanadiferous bearing magnetite with low TiO_2 (0.11-0.49 wt.%). Fe_2O_{3t} and V_2O_3 ranging from 82.87-85.96 and 1.82-2.1 wt .%., respectively. They exhibit low contents of Al_2O_3 ~ 0.4 and Cr_2O_3 ~ 0.35. The mol of uvölspinel range from 0.37 to 1.70 % revealing a low occurrence of lamellae exsolutions of ilmenite where the polygonal array of coexistent pairs of ilmenite and magnetite suggest recrystallization and perhaps segregation from these exsolutions.

Table 3 - Composition, T (°C) and $\log_{10} fO_2$ based on coexistent pairs of magnetite and ilmenite

	Massive ore Fe-Ti oxide Floresta (Faz. Exú)																					
Mt-Ulv-Ilm set	(granular/intergrowths)		(in exsolution lamellae)		(granular/intergrowths)		(granular/intergrowths)		(granular/intergrowths)		(granular/intergrowths)		(granular/intergrowths)		(granular/intergrowths)		(granular/intergrowths)		(granular/intergrowths)		(granular/intergrowths)	
Mineral	Magnetite	Ilmenite	Magnetite	Ilmenite	Magnetite	Ilmenite	Magnetite	Ilmenite	Magnetite	Ilmenite	Magnetite	Ilmenite	Magnetite	Ilmenite	Magnetite	Ilmenite	Magnetite	Ilmenite	Magnetite	Ilmenite	Magnetite	Ilmenite
Analysis #	GL15 1m	Gl15 1 il	GL15 1a m	GL15 1a il	GL15 2 m	GL15 2 il	GL15 3 ma	Gl15 3 il	GL15 4 ma	GL15 4 IL	GL15 5 ma	Gl15 5 il	GL15 6 ma	GL15 6 IL	GL15 7 ma	Gl15 7 il	GL15 8 ma	GL15 8 IL	GL15 9 ma	Gl15 9 il	GL15 10 m	GL15 10 IL
SiO_2	0.38	0.01	0.44	0.04	0.36	0.02	0.43	0.00	0.38	0.01	0.50	0.00	0.44	0.01	1.36	0.02	0.56	0.02	0.56	0.04	0.52	0.01
TiO_2	0.39	48.63	0.40	49.00	0.22	49.43	0.30	49.46	0.11	49.67	0.16	49.86	0.28	50.09	0.49	49.50	0.12	49.43	0.14	49.61	0.20	49.52
Al_2O_3	0.31	0.05	0.25	0.01	0.33	0.00	0.31	0.02	0.29	0.04	0.25	0.00	0.36	0.00	0.81	0.01	0.29	0.04	0.38	0.02	0.36	0.02
Cr_2O_3	0.37	0.09	0.41	0.07	0.37	0.08	0.37	0.03	0.38	0.10	0.32	0.03	0.40	0.03	0.36	0.07	0.38	0.04	0.33	0.07	0.37	0.09
FeO_T	85.92	45.38	85.96	45.12	85.66	45.77	83.44	45.29	84.28	45.22	85.29	45.09	85.53	44.48	82.87	45.30	83.82	45.17	85.35	45.28	85.11	45.22
Fe_2O_3	61.78	7.49	61.69	7.05	61.85	7.40	59.92	6.53	60.90	6.43	61.30	6.17	61.41	4.89	57.42	6.24	60.10	6.66	61.34	6.42	61.10	6.58
FeO	30.33	38.64	30.45	38.78	30.01	39.11	29.52	39.42	29.47	39.43	30.13	39.54	30.27	40.08	31.20	39.69	29.74	39.18	30.15	39.51	30.13	39.30
MnO	0.00	0.93	0.03	0.93	0.06	0.92	0.00	0.91	0.03	0.90	0.00	0.97	0.04	0.98	0.02	0.92	0.00	0.97	0.00	0.92	0.00	0.97
MgO	0.17	2.31	0.18	2.43	0.19	2.44	0.13	2.31	0.12	2.42	0.11	2.39	0.13	2.23	0.16	2.20	0.10	2.40	0.19	2.38	0.15	2.38
CaO	0.09	0.00	0.07	0.00	0.05	0.02	0.04	0.00	0.05	0.02	0.06	0.00	0.05	0.00	0.06	0.00	0.08	0.00	0.06	0.00	0.08	0.00
Na_2O	0.01	0.00	0.07	0.04	0.12	0.00	0.01	0.02	0.06	0.00	0.07	0.02	0.02	0.01	0.01	0.01	0.05	0.00	0.01	0.02	0.00	0.04
K_2O	0.00	0.02	0.01	0.00	0.00	0.00	0.00	0.01	0.01	0.00	0.01	0.00	0.00	0.00	0.01	0.01	0.00	0.02	0.00	0.00	0.00	0.00
ZnO	0.02	0.06	0.00	0.09	0.03	0.10	0.07	0.05	0.03	0.03	0.00	0.08	0.00	0.04	0.00	0.02	0.00	0.04	0.07	0.00	0.00	0.04
V_2O_3	2.01	0.99	2.10	0.96	2.07	0.88	1.96	0.87	1.90	0.88	2.10	0.85	2.05	0.90	1.82	0.89	2.15	0.88	2.15	0.89	2.04	0.86
NiO	0.05	0.00	0.10	0.02	0.03	0.00	0.04	0.00	0.02	0.03	0.01	0.00	0.09	0.00	0.01	0.08	0.10	0.00	0.10	0.00	0.00	0.04
Total	95.53	99.12	95.77	99.34	95.31	100.31	92.73	99.58	93.37	99.86	94.71	99.87	95.15	99.21	93.37	99.58	93.29	99.65	95.14	99.79	94.59	99.75
Si	0.02	0.00	0.02	0.00	0.01	0.00	0.02	0.00	0.02	0.00	0.02	0.00	0.02	0.00	0.06	0.00	0.02	0.00	0.02	0.00	0.02	0.00
Ti	0.01	0.92	0.01	0.92	0.01	0.92	0.01	0.93	0.00	0.93	0.00	0.93	0.01	0.94	0.01	0.93	0.00	0.93	0.00	0.93	0.01	0.93
Al	0.01	0.00	0.01	0.00	0.02	0.00	0.01	0.00	0.01	0.00	0.01	0.00	0.02	0.00	0.04	0.00	0.01	0.00	0.02	0.00	0.02	0.00
Fe^{+3}	1.85	0.14	1.85	0.13	1.86	0.14	1.85	0.12	1.87	0.12	1.86	0.12	1.85	0.09	1.75	0.12	1.85	0.13	1.85	0.12	1.85	0.12
Cr	0.01	0.00	0.01	0.00	0.01	0.00	0.01	0.00	0.01	0.00	0.01	0.00	0.01	0.00	0.01	0.00	0.01	0.00	0.01	0.00	0.01	0.00
Fe^{+2}	1.01	0.81	1.01	0.81	1.00	0.81	1.01	0.82	1.01	0.82	1.02	0.82	1.01	0.84	1.06	0.83	1.02	0.82	1.01	0.82	1.01	0.82
Mn	0.00	0.02	0.00	0.02	0.00	0.02	0.00	0.02	0.00	0.02	0.00	0.02	0.00	0.02	0.00	0.02	0.00	0.02	0.00	0.02	0.00	0.02
Mg	0.01	0.09	0.01	0.09	0.01	0.09	0.01	0.09	0.01	0.09	0.01	0.09	0.01	0.08	0.01	0.08	0.01	0.09	0.01	0.09	0.01	0.09
V	0.06	0.02	0.07	0.02	0.07	0.02	0.06	0.02	0.06	0.02	0.07	0.02	0.07	0.02	0.06	0.02	0.07	0.02	0.07	0.02	0.07	0.02
Calc. Methods:	Mol % Usp	Mol % Ilm	Mol % Usp	Mol % Ilm	Mol % Usp	Mol % Ilm	Mol % Usp	Mol % Ilm	Mol % Usp	Mol % Ilm	Mol % Usp	Mol % Ilm	Mol % Usp	Mol % Ilm	Mol % Usp	Mol % Ilm	Mol % Usp	Mol % Ilm	Mol % Usp	Mol % Ilm	Mol % Usp	Mol % Ilm
Stormer (1983)	1.24%	92.42%	1.27%	92.87%	0.71%	92.61%	0.99%	93.45%	0.37%	93.55%	0.53%	93.81%	0.91%	95.08%	1.70%	93.74%	0.40%	93.30%	0.44%	93.56%	0.65%	93.40%
Geothermobarometer by Andersen and Lindsley (1985)																						
XUsp & XIlm from:	Temp (°C)	$\log_{10} fO_2$	Temp (°C)	$\log_{10} fO_2$	Temp (°C)	$\log_{10} fO_2$	Temp (°C)	$\log_{10} fO_2$	Temp (°C)	$\log_{10} fO_2$	Temp (°C)	$\log_{10} fO_2$	Temp (°C)	$\log_{10} fO_2$	Temp (°C)	$\log_{10} fO_2$	Temp (°C)	$\log_{10} fO_2$	Temp (°C)	$\log_{10} fO_2$	Temp (°C)	$\log_{10} fO_2$
Stormer (1983)	573	-18.26	568	-18.58	545	-18.83	550	-19.26	506	-20.15	518	-20.10	522	-21.04	571	-19.08	512	-19.87	513	-20.01	532	-19.54

*Recalculated Iron and Total; Cation prop. (Carmichael 1967); N°. Of Oxygen 4 - magnetite 3 - Ilmenite

3.4.2.5. Garnet

Poor Cr granoblastic garnet from a garnet amphibolite (GL-04B – Riacho do Tapuio; Table 5) in Floresta mafic-ultramafic complex has composition of almandine$_{52.09\text{-}55.24}$, pirope$_{10.69\text{-}14.27}$, grossular$_{26.73\text{-}29.91}$ and sperssatite$_{2.83\text{-}7.58}$. Millimetric xenoblastic terms in symplectite intergrowth shows depletion on pirope$_{7.65}$ mol with incipient replacement of Mg to Mn. These garnets have an ubiquitous inclusions of quartz, rutile and amphibole.

Table 4 - Analyses of garnet from garnet amphibolite (Riacho Tapuio).

ANALYSIS	GL4B 1	GL4B 1a	GL4B 1a	GL4B 4	GL4B 6
Position	core	core	symp	core	core
SiO_2	37.86	38.41	38.33	38.76	38.76
TiO_2	0.05	0.07	0.08	0.13	0.12
Al_2O_3	19.24	19.46	19.21	19.22	19.47
Cr_2O_3	0.00	0.04	0.04	0.00	0.01
FeO	25.86	24.94	25.34	25.74	25.07
MnO	2.62	2.92	3.71	1.30	3.48
MgO	3.03	2.76	1.97	3.72	3.13
CaO	9.93	11.03	11.15	10.03	10.27
Na_2O	0.06	0.02	0.03	0.02	0.05
K_2O	0.02	0.00	0.00	0.01	0.00
V_2O_3	0.06	0.04	0.02	0.06	0.04
NiO	0.00	0.08	0.00	0.01	0.00
TOTAL	98.72	99.77	99.88	99.01	100.39
Si	3.04	3.05	3.06	3.09	3.06
Ti	0.00	0.00	0.00	0.01	0.01
Al	1.82	1.82	1.81	1.80	1.81
Cr	0.00	0.00	0.00	0.00	0.00
Fe^{3+}	0.09	0.06	0.07	0.01	0.06
Fe^{2+}	1.65	1.59	1.62	1.71	1.60
Mn	0.18	0.20	0.25	0.09	0.23
Mg	0.36	0.33	0.23	0.44	0.37
Ca	0.85	0.94	0.95	0.86	0.87
End member *					
almandine	54.17	52.15	53.05	55.24	52.09
pyrope	11.92	10.69	7.65	14.27	12.01
grossular	26.73	29.60	29.91	27.46	27.34
spessartine	5.85	6.43	8.18	2.83	7.58
andradite	1.29	1.03	1.09	0.08	0.86

*mol % Fe^{3+} Total cations = 8. Total oxygens = 12.

3.4.2.6. Ilmenite and rutile

Ilmenites form an equigranular mosaic with magnetite in massive and net-texture orebodies with a high modal ratio. They have TiO_2 in the range of 48.6–51.5 wt.%, FeO of 44.4–45.9 wt.%, and V_2O_5 of 0.34–0.98 wt.% (Table 5). All the analysed titanites and a unique rutile spot show homogeneous compositions (Table 5). The mol of ilmenite > 92.42 % confirm the nature devoid of exsolutions. Rutile is the second voluminous Ti resources and can reach modal proportions exceeding 4% up to 12%.

3.4.2.7. Plagioclase and epidote

Plagioclases are absent in the dunites/olivine cumulates, coarse hornblendites, massive and net textured ore bodies and are present only as part of symplectites in garnet amphibolite from samples analysed in Floresta.

An individualized small grain and a symplectite intergrowth have similar anorthite (An) numbers at ~ 40 close to andesine composition. A single grain found in a hornblendite sample has an albitic/oligoclase composition with (Ab) number at 85.98 and could represent a retromorphic component.

The epidotes found occur as symplectites together with quartz, rutile and scarce plagioclase surrounding garnets and are compatible with clinozoisite composition (Table 5). They have high FeO at ~ 8% and Al_2O_3 ranging between 24.63 – 24.77 which a wide replacement of Al by Fe^{3+} depicts substitutions present in the monoclinic members.

3.4.3. Bulk-Rock Chemistry

In order to determine the geochemical characteristics of the studied metamafic-ultramafic rocks (FMUC and BMUC), representative samples were analyzed for their major (#48), trace and rare earth elements concentrations (#42) being 22 new analyses and 26 recompiled from Beurlen (1988). The results are shown in Table 6 and Appendix D with main findings summarized below.

Table 5 - Plagioclase,epidote, rutile and titanites composition of the Floresta mafic-ultramafic complex (Riacho do Tapuio)

Sample	Rock type	Mineral	Location	SiO_2	TiO_2	Al_2O_3	Cr_2O_3	FeO	MnO	MgO	CaO	Na_2O	K_2O	Total	An	Ab
GL04A 2	Metahornblendite	plagioclase	grain	65.98	0	19.892	0	0.098	0.007	0	3.022	10.411	0.041	99.868	13.79	85.98
GL4B 5a	Garnet amphibolite	plagioclase	grain	58.775	0	24.423	0.016	0.391	0	0.01	8.714	7.081	0.036	99.659	40.40	59.40
GL4B 6 cor	Garnet amphibolite	plagioclase	symplectite	60.202	0	24.354	0	0.089	0.032	0	8.597	7.087	0.071	100.665	39.97	59.63
GL4B 2 cor	Garnet amphibolite	clino/zoisite	symplectite	40.351	0.226	24.771	0.068	8.036	0.069	0.059	23.958	0.001	0	97.692		
GL4B 4a cor	Garnet amphibolite	clino/zoisite	symplectite	39.471	0.155	24.638	0.048	8.08	0	0.11	23.413	0	0.017	96.364		
GL4B 6a cor	Garnet amphibolite	clino/zoisite	symplectite	39.913	0.059	24.64	0.001	8.218	0.214	0.03	24.018	0	0.011	97.198		
GL4B 2 cor	Garnet amphibolite	titanite	symplectite	31.604	37.617	1.112	0	0.315	0.014	0.022	29.028	0.015	0	100.354		
GL4B 4c cor	Garnet amphibolite	titanite	symplectite	31.278	37.236	1.078	0.048	0.391	0	0.004	29.163	0.004	0	99.657		
GL4B 7a	Garnet amphibolite	titanite	grain	32.413	36.362	1.141	0	0.413	0.001	0.024	29.275	0.001	0	99.972		
GL04A 5a	Metahornblendite	rutile	grain	0.004	96.593	0	0	0.397	0	0	0.055	0.011	0.006	98.148		

Table 6 - Whole-rock chemistry data for Rocks of FMUC

Sample	Locality	Rock type	SiO_2	TiO_2	Al_2O_3	Fe_2O_3	MnO	MgO	CaO	Na_2O	K_2O	P_2O_5	Cr_2O_3	LOI	Sum	Ni	Co	V	Cu	Pb	Zn	Rb	Cs	Ba	Sr	Ga	Ta	Nb	Hf	Zr	Y	Th	U	La	Ce	Pr	Nd	Sm	Eu	Gd	Tb	Dy	Ho	Er	Tm	Yb	Lu
AM-446D	Mirandiba	Peridotite	33	6.97	12.9	23.1	0.36	11.4	8.48	1.13	0.27	0.015		1.84	99.47																																		
GL-02D	Pedras Pretas	Dunite	34.88	7.45	13.42	20.9	0.23	10.17	8.59	1.42	0.39	<0.01	<0.01	1.36	98.77	131	82	70	10.9	2.7	86	3.6	0.15	20	58.6	11.3	0.54	1.69	0.22	10	1.53	3.4	<0.1	4.3	1.7	0.16	0.8	0.16	0.28	0.19	<0.05	0.16	<0.05	0.09	<0.05	0.19	0.04
GL-08D	Riacho da Posse	Olivine cumulate	43.43	9.89	2.67	20.93	0.26	21.6	0.24	0.02	<0.01	<0.01	0.12	2.21	101.3	571.1	122.4	26	86.2	1	93	0.5	0.62	<5	3.4	6.1	0.57	3.01	0.48	18.3	1.12	1.1	0.9	6.4	1.3	0.07	0.4	0.1	<0.05	0.08	0.012	0.07	<0.05	0.09	<0.05	0.1	0.04
GL-04.M.C	Riacho Tapuio	Metapyroxenite	44.47	1.45	7.53	12.89	0.17	20.21	7.36	0.56	0.07	0.16	0.198	4.4	99.58	1050	98.1	174	55.0	0.2	29	0.5	<0.1	4	49.0	11.8	0.9	14.4	2.2	86.4	12.7	0.8	0.1	9.0	21.5	3.01	14.3	3.20	0.91	3.16	0.48	2.68	0.50	1.41	0.18	1.20	0.14
GL-04.M.D	Riacho Tapuio	Metapyroxenite	46.11	2.27	11.65	12.19	0.20	8.94	14.92	2.10	0.29	0.34	0.079	0.5	99.63	198	67.8	292	131.0	0.4	20	9.2	1.8	202	499.8	17.5	1.3	21.3	4.4	154.9	23.2	1.7	0.4	21.1	45.1	6.10	27.5	6.16	2.14	6.00	0.91	4.67	0.89	2.20	0.26	1.82	0.23
GL-04.M.A	Riacho Tapuio	Metahornblendite	42.75	2.98	12.80	16.48	0.23	10.15	9.68	2.80	0.35	0.28	0.050	1.1	99.66	146	74.0	332	1.8	0.3	36	3.3	0.4	38	274.4	19.2	1.8	31.3	4.8	178.1	26.8	2.1	0.3	24.8	53.9	6.91	31.0	6.84	2.05	7.18	1.04	5.45	1.08	2.68	0.37	1.97	0.32
GL-08.M.A	Riacho da Posse	Metahornblendite	40.49	3.19	13.21	18.33	0.21	9.62	10.81	1.64	0.49	0.46	0.023	1.1	99.61	92	82.3	692	2.0	4.1	24	6.7	1.7	33	60.0	25.4	5.8	30.0	10.2	342.9	57.9	11.6	2.5	26.5	63.2	7.66	32.3	8.69	2.80	10.60	1.75	10.95	2.17	6.51	0.90	6.47	0.87
GL-02.M.A	Pedras Pretas	Metahornblendite	39.11	6.27	12.48	18.46	0.17	9.39	11.10	1.33	0.53	0.04	0.009	0.7	99.62	161	107.3	897	7.2	1.6	26	14.7	1.8	57	124.7	18.2	0.5	4.6	1.2	22.3	12.4	1.4	1.8	8.9	36.4	6.66	33.0	8.51	3.97	7.41	0.82	3.15	0.41	1.01	0.12	0.95	0.10
AM-445E	Mirandiba	Metahornblendite	33.9	14.9	3.02	25	0.27	11.2	10.4	0.57	0.11	0.032		-0.24	99.16																																		
AM-448A	Mirandiba	Metahornblendite	43	2.62	13.4	15.3	0.2	8.44	16	0.65	0.23	0.317		0.07	100.2																																		
GL-08E	Riacho da Posse	Metahornblendite Garnet	48.77	1.35	15.2	12.13	0.15	10.48	10.83	2.51	0.68	0.06	0.07	1.12	103.4	98.6	60.7	163	40.8	8.5	80	23	1.98	57	211.1	14.9	2.67	3	1.74	63.2	17.43	4.2	0.4	6.6	11.9	1.1	6	1.9	0.81	2.8	0.39	3.15	0.55	1.9	0.18	1.7	0.34
GL-08.M.B	Riacho da Posse	Hornblendite Garnet	43.26	2.01	15.75	13.56	0.22	8.77	11.80	1.94	0.85	0.23	0.018	1.3	99.70	87	65.2	328	34.6	5.3	26	38.4	4.0	109	202.4	20.5	0.5	7.6	3.9	129.9	35.8	4.2	0.8	15.5	37.4	4.72	24.2	5.75	1.94	6.84	1.14	6.78	1.29	4.01	0.55	3.76	0.52
GL-04.M.B	Riacho Tapuio	Hornblendite Garnet	48.51	2.57	13.56	13.77	0.20	6.48	11.18	1.45	0.38	0.26	0.016	1.3	99.68	57	93.9	380	84.4	0.8	29	6.7	0.7	26	305.0	19.0	0.6	8.3	4.6	156.8	31.4	1.5	0.2	12.2	29.0	4.22	20.8	5.46	1.93	6.28	0.99	6.00	1.19	3.62	0.51	3.11	0.49
GL-02.M.B	Pedras Pretas	Hornblendite Garnet	38.85	6.26	14.08	19.23	0.23	6.85	11.36	1.52	0.50	0.09	0.013	0.7	99.68	111	94.6	726	5.6	2.0	18	15.3	2.3	74	196.3	16.3	0.6	9.0	1.3	46.4	24.1	1.2	1.2	7.9	27.9	4.95	27.3	8.10	3.42	9.10	1.24	5.94	0.94	2.16	0.28	1.83	0.26
AM-456A	Mirandiba	Hornblendite Garnet	43.8	1.77	11.9	15.4	0.35	7.65	16.1	1.37	0.2	0.185		0.1	98.83																																		
AM-446C	Mirandiba	Hornblendite	36.7	6.36	13.5	20.5	0.25	9.61	9.88	1.4	0.59	0.028		1.69	100.5																																		
GL-08.M.C	Riacho da Posse	Massive Fe-Ti ore	1.07	44.52	0.42	49.84	0.47	5.16	0.03	<0.01	<0.01	0.03	0.398	-2.7	99.24	283	167.1	3633	16.2	0.5	28	0.7	0.2	12	2.6	5.2	1.5	16.1	2.2	80.7	0.6	<0.2	<0.1	0.7	1.0	0.16	0.7	0.14	0.06	0.22	0.04	0.23	0.06	0.10	0.05	0.31	0.10
GL-02.M.C	Pedras Pretas	Massive Fe-Ti ore	0.40	40.98	0.22	49.89	0.43	4.06	<0.01	<0.01	<0.01	0.01	0.324	-3.1	93.26	107	105.1	2933	57.2	0.2	21	0.7	0.1	3	0.9	7.5	1.0	11.0	1.9	53.0	0.5	<0.2	<0.1	0.6	0.5	0.13	0.6	0.12	0.05	0.24	0.03	<0.05	0.05	0.09	0.04	0.22	0.06
GL-15	Faz.Exú	Massive Fe-Ti ore	0.75	19.6	2.91	74.33	0.39	1.89	<0.01	<0.01	<0.01	<0.01	0.13	<0.01	100.1	183.3	146.5		8.3	1	4	0.7	<0.05	45	1.5	30.8	0.45	4.6	0.84	16.4	0.94	3.1	0.37	5.7	8.2	0.8	2.6	0.4	0.21	0.39	<0.05	0.66	<0.05	<0.05	<0.05	0.2	<0.05
GL-20	Cachoeira Grande	Massive Fe-Ti ore	0.84	17.43	3.28	76.82	0.31	1.28	<0.01	<0.01	<0.01	<0.01	0.04	<0.01	100.1	222.2	101.7		23.3	1.4	49	<0.2	<0.05	47	<0.5	37.9	0.3	5.56	1.51	31.1	0.21	1.4	0.93	2.3	4.1	0.4	1.1	0.3	<0.05	0.13	<0.05	0.11	<0.05	<0.05	<0.05	0.3	<0.05
AM-446B	Mirandiba	Massive Fe-Ti ore	0.56	47	<0.1	49.9	0.47	3.85	0.12	0.14	<0.01	0.018		-3.08	98.98																																
GL-20a	Cachoeira Grande	Massive Fe-Ti ore	0.44	44.6	0.16	54.5	0.49	2.28	0.09	0.11	<0.01	0.011		-3.12	99.56																																

The control of lithology and fractional crystallization of cumulus minerals is perceived by the existence of some systematic trends among the major element oxides showed in Fig. 8. A suggestive control fractionation of olivine and clinopyroxenes is revealed by Al_2O_3 displaying a negative correlation with MgO and CaO exhibiting a positive correlation in the metahornblendite/amphibolites whereas fractionation of Fe–Ti oxides seem to be significant as revealed by an expanded plot of major element TiO_2 x MgO (Fig. 8).

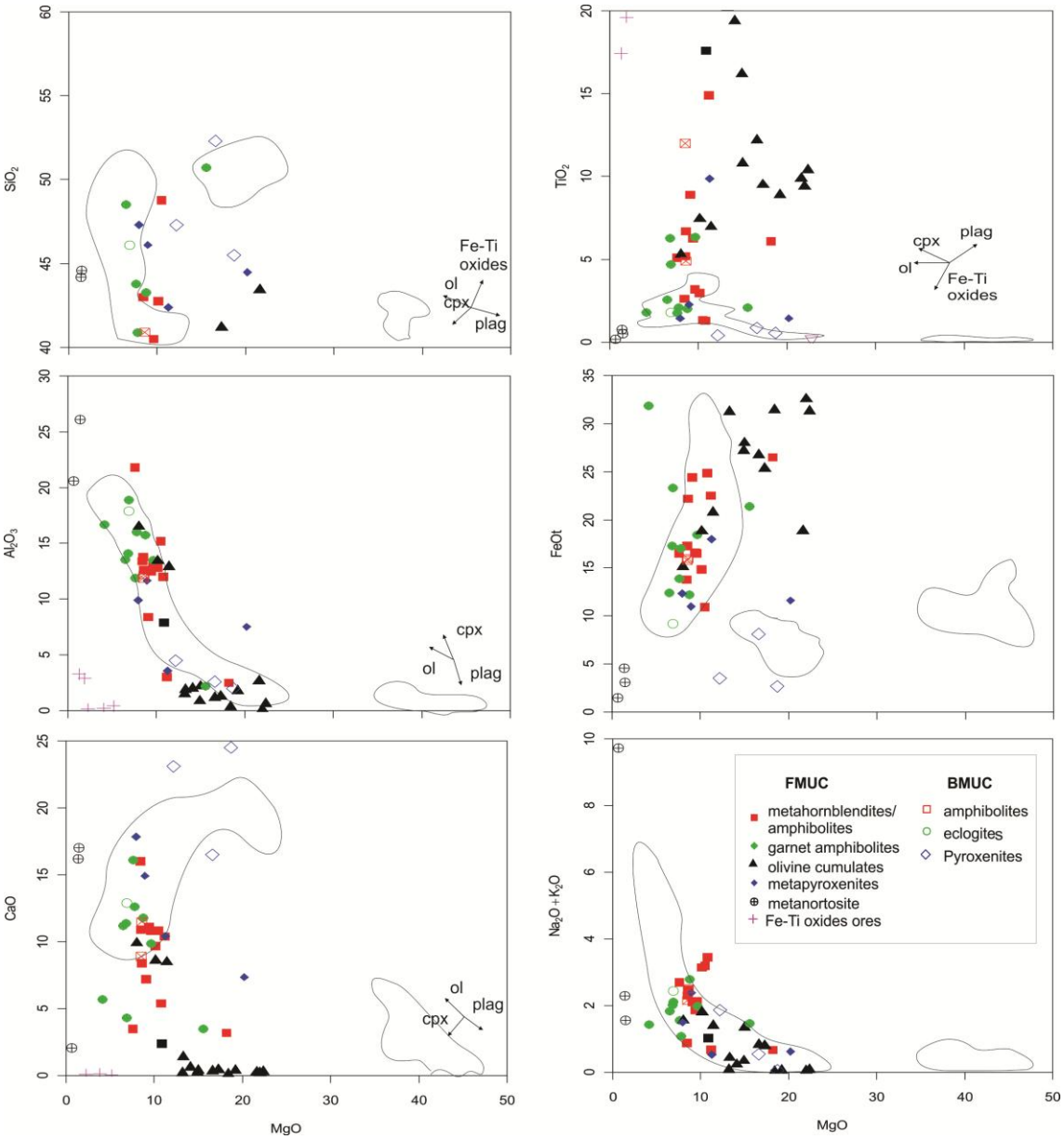

Figure 8 – Variation diagrams of major oxides vs. MgO index plots showing major fractional indices (the mineral trends are from Shaw et al., 2003; Alaskan-type fields are extracted from Wang et al. (2010).

On the AFM diagram, the metapyroxenites plot in the arc-related ultramafic cumulate field meanwhile the olivine cumulates follow a parallel trend to MF side (Fig.

9) given that magnetite/ilmenite mineralizations (up to 39 wt.% FeO_t; 25 wt.% TiO_2; Table 9). The majority of amphibolites and gabbroic rocks fall into the arc-related mafic cumulate field.

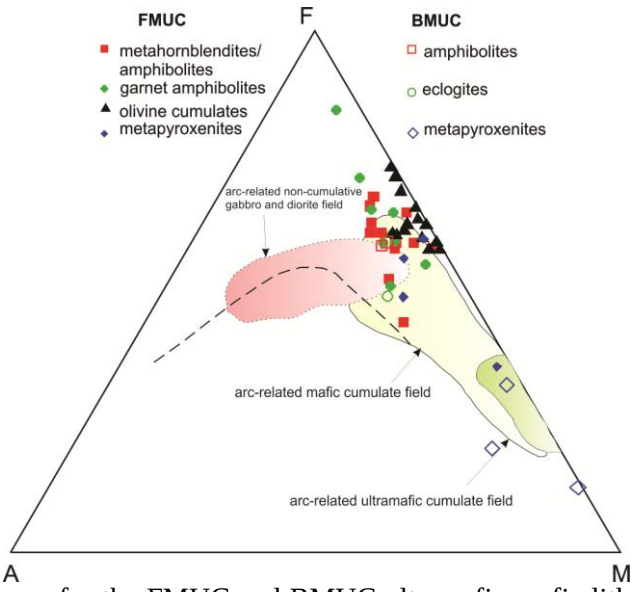

Figure 9 – AFM diagram for the FMUC and BMUC ultramafic-mafic lithologies with fields of Arc-related cumulate ultramafic–mafic rocks and Arc-related gabbro and diorites field from Beard (1986), after Eyuboglu et al. (2011).

The Al_2O_3 content rises from less than 2.67 wt.% in the olivine cumulates and 2–11.6 wt.% in the metaclinopyroxenites to values between 2.5 wt.% and 21.8 wt.% in the metahornblendites/garnet amphibolites. Olivine cumulates also have low CaO concentrations of less than 1.4 wt.%, whereas the clinopyroxenites contain the highest CaO concentrations (8.9–20.2 wt.%). The TiO_2 content is highest in the olivine cumulates (5.3–25.3 wt.%), decreases in the clinopyroxenite (0.41–2.27 wt.%) and (1.3–14.9 wt.%) in the metahornblendites/amphibolites.

The peridotites include high concentrations of Ni (131–2000 ppm), Cr (49–2016 ppm), Co (82–400 ppm) and Cu (10.9–1120 ppm), and low concentrations of Rb (0.5–64 ppm) and Sr (3.4–58.6 ppm). The pyroxenites have Ni (42–1050 ppm), Cr (58–2809 ppm), Co (11–98.1 ppm) and concentrations of Rb (0.5–<10 ppm) and high Sr (15–499 ppm).

The high Ni, Cr, Co, TiO_2 and the MgO contents of the analyzed metaultramafic–mafic rocks and systematic compositional variations imply that differentiation of olivine, pyroxene, Cr-spinel and Fe–Ti oxides exerted an important control in the cumulate phases (e.g. fractionation and accumulation of olivine is suggested by negative correlation between Ni and Co with SiO_2 – not show).

The TiO_2 content of the samples of massive ore bands (FMUC) analyzed by XRF show similar values between 40.8 to 44.6 wt.% (minimum 24.45% of Ti) for the deposits of Serrote das Pedras Pretas, Riacho da Posse e Riacho da Cachoeira Grande between 49.84 to 54.05 wt.% of Fe_2O_3 and Vanadium analyses by ICP-MS ranging to 2933-3633 ppm (minimum 0.29% of V for the samples).

On the primitive mantle-normalized spiderdiagrams and chondrite-normalized rare earth element diagrams, the pyroxenites and amphibolites/metahornblendites have similar distribution patterns (Fig. 13a, b, c and d) where both rock groups are slightly enriched in LILE and HFSE with respect to primitive mantle. A part of the amphibolite group seems to inherit the pyroxenites pattern probably reflecting a total substitution/redistribution by coarsening/static recrystallization from pyroxenes to amphiboles. The chondrite-normalized patterns of pyroxenites and amphibolitic/metahornblendites rocks display slight enrichment in LREE relative to HREE, a typical characteristic of subduction-related arc magma (Eyuboglu et al., 2011) and similar to the REE slope pattern experienced in IAB (Island arc basalts - Kelemen et al., 2003) (Fig. 10a and b), however, they do not show negative Nb, Zr, Ti in all samples. Garnet amphibolites and metahornblendites plot near IAB, OIB average and far from N-MORB average basalts.

The metapyroxenites exhibit uniformly LREE enriched chondrite-normalized REE similar to Alaskan-type field (Fig. 10c) and are less enriched than amphibolites. On the primitive mantle-normalized diagram, the metapyroxenites exhibit regular trace elements patterns (Fig. 10d), and commonly are characterized by Pb, Sr, Zr and Y troughs.

The patterns of the peridotites are comparable to the Alaskan-type peridotites, except for their smoother slopes in the MREE and HREE (Fig. 10e). They show a characteristic “U” shape pattern similar to harzburgites and wehrlites from these type of complexes. In Fig. 10f, the peridotite spider diagram show a well-marked positive Pb anomaly and a high fluid mobile elements (Cs, Rb, Th and U) which should reflect fluid percolation during the superimposed subduction process.

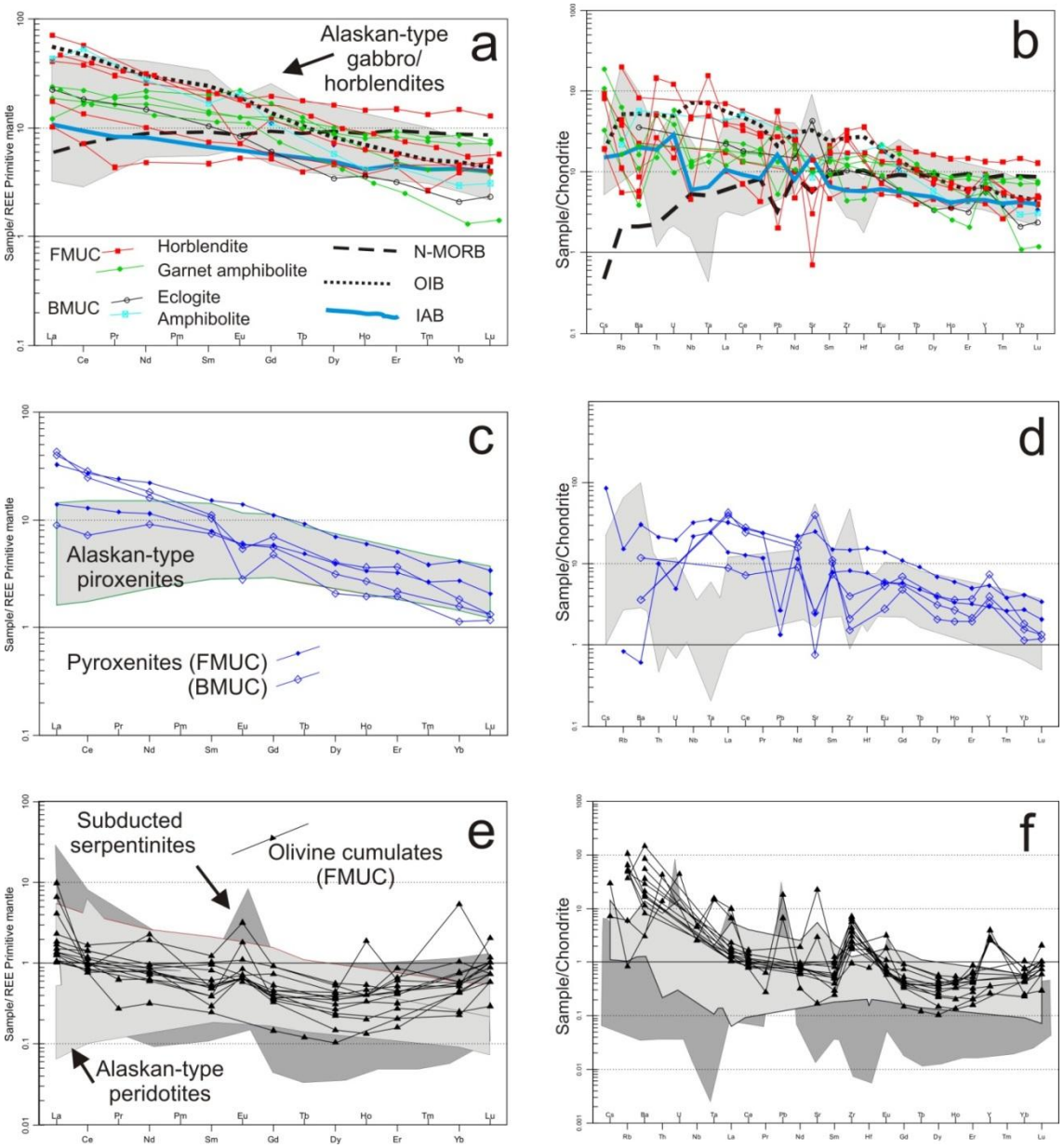

Figure 10 – Chondrite-normalized REE patterns and primitive mantle normalized trace-element patterns for the Bodocó and Floresta mafic–ultramafic rocks.Primitive mantle and chondrite normalizing values are from McDonough and Sun (1995). The data for the Alaskan-type field are from Himmelberg and Loney (1995). N-MORB average rocks are from Hofmann (1998), IAB average data are from Kelemen et al. (2003) and OIB are from Sun and McDonough (1989). Data for subducted serpentinites are from Deschamps et al. (2013)

The usage of relative concentrations of immobile elements is useful to determine tectonic environment for the formation of mafic and ultramafic rocks (e.g. Pearce, 1975; 1982; 2008; Shervais, 1982; Beard, 1986; Thanh et al., 2014).

On the Nb/Yb vs. Th/Yb diagram, most gabbroic, amphibolitic and eclogitic samples plot within the arc array field. There is, however, a minor tendency of one sample toward the MORB array (Fig. 11a). It may suggest that protoliths have been derived from a mantle source metasomatized (enriched magma) by subduction-related

fluids (Pearce, 2008). These data in combination with the LREE-enriched patterns for FMUC and BMUC suggest an arc-setting. The Cr vs. Y plot (Fig. 11b) also present many samples in Island arc tholeiite (IAT) source suggesting the rocks were derived in an island arc setting.

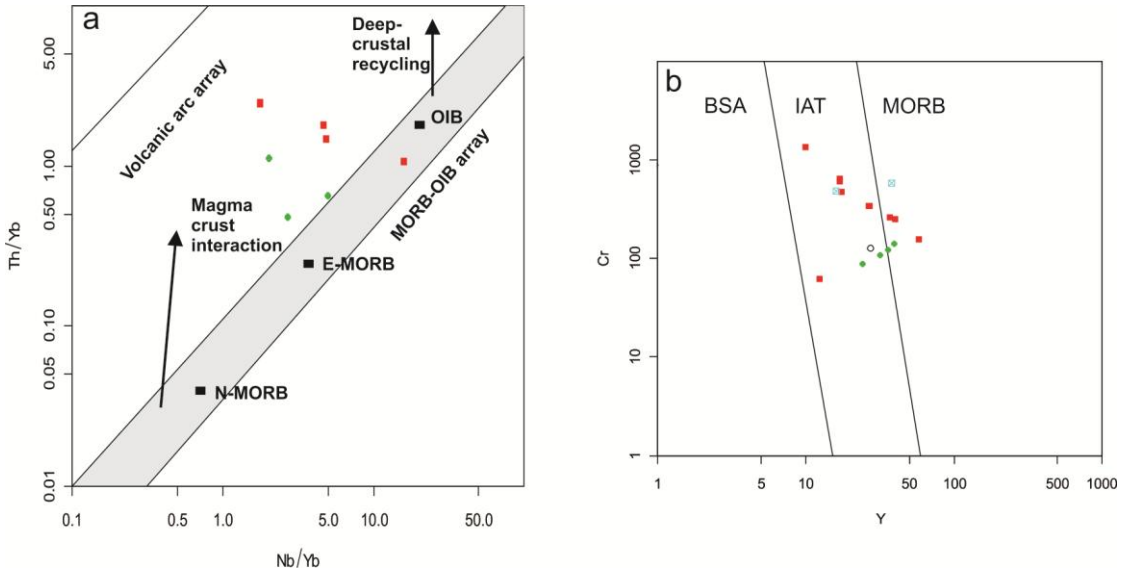

Figure 11 – a) Diagram of Nb/Yb vs. Th/Yb for gabbroic, amphibolitic and eclogitic rocks from FMUC and BMUC (after Pearce, 2008); b) Cr (ppm) vs. Y (ppm) discrimination diagram (after Pearce, 1982) BSA: basalts of shoshonite affinity, IAT: island arc tholeiite and MORB: Mid-ocean ridge. Same symbols on Fig. 8.

Many ratios correlation possibly indicate magma mixing between MORB (low Ba/La, Ce/Pb and La/Yb) and arc basalt (high Ba/La, Ce/Pb, Zr/Nb and La/Yb) (Sun and McDonough, 1989; Thanh et al., 2014) (Table 7). This mixture perhaps can direct us to a back-arc tectonic setting.

Table 7 - Average trace element ratios in the analyzed mafic rocks. Table extracted and adapted after Thanh et al. (2014) and shown for comparison.

Ratio	Location and tectonic setting					
	FMUC	Cao Bang (a)	N-MORB (b)	Indonesian arc (c)	Mariana (d)	Aleutian (e)
Ta/Nb	0.06-0.19	0.076–0.089	0.06	0.07–0.13	0.06–0.1	0.06–0.39
Zr/Nb	4.34-18.89	12.56–20.87	31.76	14–23	37–86	21–145
Ce/Pb	4.58-179.67	1.81–6.52	25	3–7	3.5–13.4	3.16–34.39
Th/Yb	0.48-1.79	1.52–3.57	0.04	1–4	0.1–0.5	0.03–0.51
Th/Nb	0.06-0.55	0.81–1.77	0.05	0.45–1.12	0.4–0.8	0.08–0.83
Ba/La	0.44-9.57	4.00–22.19	2.52	23–36	22–60	5.2–51.45
Ba/Th	2.84-118.82	9.06–64.41	52.5	63–177	187–674	47–708
Sr/Nd	1.86-21.69	3.42–15.52	12.33	16–44	18.4–49.4	13–62
(La/Sm)N	0.61-2.28	2.2–2.8	0.59	1.92–3.57	0.8–1.7	0.4–1.6

(a)Thanh et al. (2014); (b)Sun and McDonough (1989); (c)Handley et al. (2007), (d)Elliott et al. (1997) and (e)Class et al. (2000) apud Thanh et al. (2014)

3.4.4. Isotopic Data

3.4.4.1. Zircon LA-MC-ICP-MS U-Pb geochronology

Zircon grains were separated from a coarse metahornblendite sample (GL-02_SPP) collected from Serrote das Pedras Pretas mine within FMUC. These zircon grains are prismatic in shape formed by two distinct phases, older cores that can be homogeneous or growth zoned, locally, with traces of earlier resorption and recrystallization and coarse metamorphic rims are generally homogeneous, and are separated from cores by irregular interfaces indicative of corrosion (Fig. 12a). These textures are common to that displayed in zircons from eclogite and high-grade metamorphic rocks as granulites (Corfu et al., 2003).

The cores of zircon grains from the metahornblendite have high Th/U values that range between 0.132 and 0.834 and define a Discordia age at upper intercept at 945 ± 78 Ma (Table 8; Fig. 12b), that we interpreted as to have developed during magmatic crystallization of the mafic-ultramafic sequence FMUC.

Table 8 - LA-ICPMS U-Th-Pb results for zircons from metahornblendite within FMUC (Serrote das Pedras Pretas Mine), western Borborema

		Ratios								Apparent Ages						
Samples Spots	Th/U	$\frac{^{206}Pb}{^{204}Pb}$	$\frac{^{207}Pb}{^{206}Pb}$	±1σ	$\frac{^{207}Pb}{^{235}U}$	±1σ	$\frac{^{206}Pb}{^{238}U}$	±1σ	ρ	$\frac{^{207}Pb}{^{206}Pb}$	(Ma)	$\frac{^{207}Pb}{^{235}U}$	(Ma)	$\frac{^{206}Pb}{^{238}U}$	(Ma)	Conc. (%)
GL-02_SPP																
cores																
004-Z1N	0.83	13089	0.06961	0.27	1.4070	0.84	0.146601	0.79	0.94	917	6	892	5	882	6.52	99
006-Z2N	0.50	50601	0.07459	0.40	1.4052	0.89	0.136623	0.79	0.87	1058	8	891	5	826	6.11	93
008-Z3N	0.35	51013	0.07323	0.36	1.5439	0.93	0.152919	0.86	0.91	1020	7	948	6	917	7.36	97
009-Z3M	0.34	2358	0.07100	0.80	1.2402	1.46	0.126686	1.22	0.85	957	16	819	8	769	8.85	94
010-Z4N	0.35	125864	0.07734	0.27	1.7740	0.93	0.166370	0.89	0.95	1130	5	1036	6	992	8.18	96
013-Z4M	0.13	56254	0.07146	0.88	1.0979	2.33	0.111431	2.15	0.92	971	18	752	12	681	13.92	91
028-Z15N	0.38	76188	0.07730	0.33	1.3844	0.87	0.129888	0.81	0.92	1129	6	882	5	787	5.99	89
038-Z20N	0.23	58133	0.07696	0.26	2.1941	0.89	0.206781	0.85	0.95	1120	5	1179	6	1212	9.42	103
040-Z21N	0.54	237702	0.07470	0.26	1.6684	0.76	0.161979	0.72	0.93	1061	5	997	5	968	6.46	97
COMP_006-Z6N	0.42	86207	0.07214	1.32	1.4943	1.75	0.150236	1.14	0.64	931	28	928	11	902	9.64	97
COMP_010-Z12N	0.23	10414	0.06852	0.82	1.0478	1.59	0.110910	1.36	0.85	825	18	728	8	678	8.76	93
COMP_012-Z31N	0.45	37481	0.07301	0.91	1.5507	1.41	0.154041	1.08	0.75	956	19	951	9	924	9.29	97
COMP_017-Z23N	0.46	125064	0.06956	0.34	1.3645	0.77	0.142265	0.69	0.88	856	7	874	4	857	5.52	98
COMP_018-Z33N	0.22	61409	0.07308	0.56	1.5399	0.93	0.152825	0.75	0.77	958	12	946	6	917	6.41	97
rims																
005-Z1B	0.04	6896	0.06246	0.79	0.9218	1.70	0.107048	1.50	0.88	690	17	663	8	656	9.37	99
007-Z2B	0.01	21174	0.06404	0.56	0.8131	1.07	0.092081	0.92	0.84	743	12	604	5	568	4.98	94
019-Z10B	0.04	6103	0.06611	1.34	0.8583	2.40	0.094158	1.99	0.83	810	28	629	11	580	11.05	92
020-Z11B	0.02	4616	0.06310	0.92	0.8533	1.35	0.098084	0.98	0.72	711	20	626	6	603	5.62	96
023-Z12B	0.02	20870	0.06364	0.93	0.8986	1.46	0.102409	1.12	0.76	730	20	651	7	629	6.71	97
025-Z13B	0.01	7820	0.06128	1.19	0.8601	1.82	0.101796	1.37	0.75	649	26	630	9	625	8.16	99
027-Z14B	0.01	20281	0.06164	0.92	0.8666	1.18	0.101958	0.75	0.59	662	20	634	6	626	4.46	99
029-Z15B	0.01	5178	0.06077	0.87	0.8433	1.45	0.100645	1.16	0.79	631	19	621	7	618	6.86	100
036-Z18B	0.01	5477	0.06331	1.16	0.8254	1.64	0.094556	1.16	0.70	719	25	611	8	582	6.48	95
037-Z19	0.04	6569	0.06672	1.47	1.0445	1.90	0.113549	1.20	0.62	829	31	726	10	693	7.89	95
046-Z25B	0.01	96949	0.06355	0.60	0.9481	1.10	0.108203	0.92	0.82	727	13	677	5	662	5.79	98
048-Z26B	0.02	7713	0.06645	0.92	0.8566	1.64	0.093498	1.37	0.82	821	19	628	8	576	7.53	92
049-Z27B	0.01	7843	0.06598	1.08	0.9081	1.63	0.099816	1.22	0.74	806	23	656	8	613	7.16	93
inheritance																
COMP_011-Z30N	0.26	162785	0.12426	1.90	5.6729	3.15	0.331103	2.51	0.80	1968	35	1927	27	1844	40.33	96
COMP_021-Z27N	0.43	130943	0.11016	0.82	3.3566	1.03	0.220994	0.62	0.54	1750	15	1494	8	1287	7.18	86
COMP_022-Z34N	0.44	129607	0.11146	0.88	3.3241	1.59	0.216292	1.33	0.83	1771	16	1487	12	1262	15.24	85

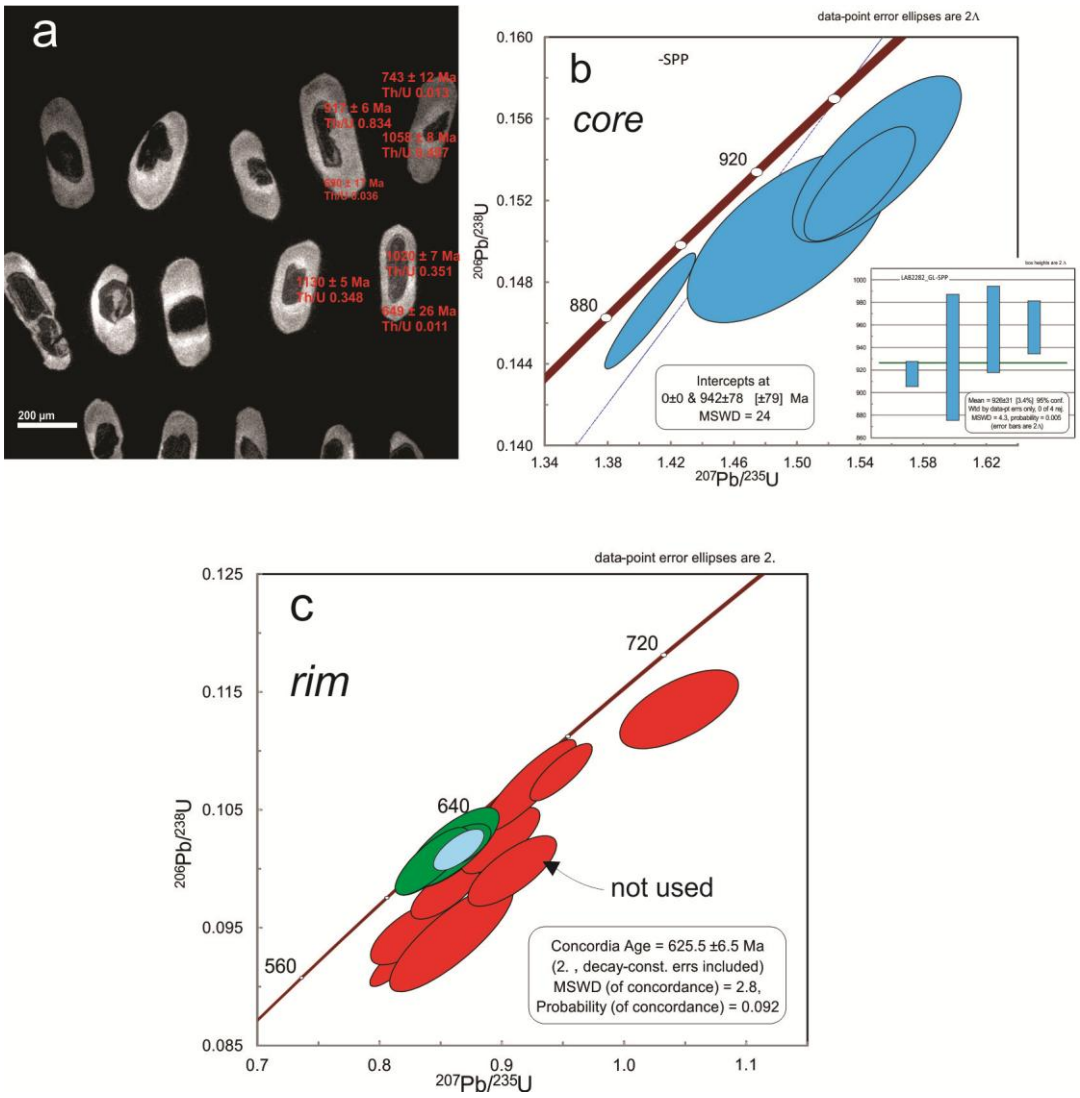

Figure 12 – LA-ICPMS U-Pb analyses of zircons from FMUC (Serrote das Pedras Pretas mine): a) Back-scattered image of prismatic older cores homogeneous to growth zoned, locally with traces of earlier resorption and recrystallization and coarse metamorphic homogeneous rims; b) Concordia age (upper intercept) at 945 ± 78 Ma obtained from the most concordant core grains; c) Concordia age at 625 ± 6 Ma obtained from rim os zircon grains.

Data points of zircon rims, which metamorphic margins have systematically low Th/U values ranging between 0.008 and 0.038, yield a concordant age at 625 ± 6 Ma (Table 8; Fig. 12c), which we interpreted as the age of high-grade metamorphic event (possible high-pressure metamorphism or first stages of retrograde metamorphism).

Three xenocrystals denote an inheritance at ca. 1.9 Ga that is not exposed as basement in this area.

3.4.4.2. Sr-Nd Isotopes

We choose five representative localities to sampling rocks wherein three of them (Serrote das Pedras Pretas – GL-02; Riacho da Posse – GL-08; Lagoa dos Angicos - AM-445) within the Riacho do Icó granite and Tapuio – GL-04 and Caraibeiras – (AM-448 and AM-456) folded along to São Caetano Schists. The coordinates and whole-rock Sr and Nd isotopic system compositions of the Floresta mafic–ultramafic complex are presented in Table 9.

The $^{147}Sm/^{144}Nd$ ratios of the coarse metahornblendites are 0.1306 to 0.1569, garnet amphibolites values range from 0.1429 to 0.31106, massive Fe-Ti oxides cumulates are between 0.1625 and 0.1718, peridotites (olivine cumulates) is equal to 0.2281 to 0.2452 and metapyroxenites 0.1373 and 0.1620. These values represent typical ratios obtained for mafic and ultramafic rocks of primitive arc and oceanic crust fragments. Some values of Sm/Nd ratio are close of the chondritic value of Sm/Nd at 0.1967 (DePaolo and Wasserburg, 1976).

Table 9 - Sm-Nd and Sr-Sr data obtained for FMUC rocks

Sample	Rock/Mineral	Location	UTM N	UTM E	Sm	Nd	$^{47}Sm/^{144}Nd$	$^{143}Nd/^{144}Nd$	±2σ	εNd(0)	εNd(t) t = 945 Ma	T_{DM}	Rb	Sr	$^{87}Sr/^{86}Sr$	±2σ	$^{143}Nd/^{144}Nd_i$	$^{87}Sr/^{86}Sr_i$
GL02(M)A	metahorblendite	Serrote das Pedras Pretas	547817	9062566	9,000	34,671	0.1569	0.512516	0.000001	-2.38	2.66	1.40					0.511499	
GL 02(M)B	garnet amphibolite	Serrote das Pedras Pretas			7,756	24,548	0.191	0.512636	0.000012	-0.05	0.68						0.511398	0.706062
GL 02(M)C	Fe-Ti-V cumulus	Serrote das Pedras Pretas			0.032	0.111	0.1718	0.512487	0.000012	-2.94	0.2	2.00					0.511373	
GL-02A	metahorblendite	Serrote das Pedras Pretas			8,902	31,361	0.1716	0.512537	0.000009	-1.97	1.21	1.80	15	124.7	0.71256	0.00001	0.511425	0.707949
GL2B	garnet amphibolite	Serrote das Pedras Pretas			3,920	11,960	0.1981	0.512648	0.000007	0.2	0.02		15	196.3	0.70911	0.00001	0.511364	0.706062
GL2E	olivine cumulate	Serrote das Pedras Pretas			0.639	1,574	0.2452	0.513064	0.000004	8.31	2.18						0.511475	
AM-446C	metahorblendite	Serrote das Pedras Pretas			7.96098	33.961	0.14170	0.512433	0.000021	-4.00	2.66	1.28					0.511555	
AM-446D	garnet amphibolite	Serrote das Pedras Pretas			1.00862	1.9601	0.31106	0.513411	0.00002	15.08	1.25						0.511482	
GL 04(M)A	coarse horblendite	Riacho Tapuio/Arapuá	551344	9067350	7,095	31,599	0.1357	0.512328	0.000007	-6.04	1.67	1.38					0.511448	
GL 04(M)C	tremolitite	Riacho Tapuio/Arapuá			3,037	12,414	0.1479	0.512386	0.000005	-4.92	1.26	1.50					0.511427	
GL 04(M)D	pyroxenite	Riacho Tapuio/Arapuá			6,408	28,083	0.1379	0.512353	0.000008	-5.56	1.88	1.38					0.511459	
GL-04A	metahorblendite	Riacho Tapuio/Arapuá			6,357	29,423	0.1306	0.512317	0.000008	-6.25	2.1	1.32	3.3	274.4	0.70436	0.00001	0.51147	0.70389
GL-04B	garnet amphibolite	Riacho Tapuio/Arapuá			5,618	20,576	0.1651	0.512673	0.000012	0.69	4.69	1.15	6.7	305	0.70989	0.00001	0.511603	0.709031
GL-04C	pyroxenite	Riacho Tapuio/Arapuá			3,149	11,748	0.162	0.512495	0.000017	-2.79	1.6	1.60	0.5	49	0.70379	0.00001	0.511445	0.703391
GL-04D	pyroxenite schist	Riacho Tapuio/Arapuá			6,454	28,410	0.1373	0.512347	0.000011	-5.68	1.84	1.38	9.2	499.8	0.70364	0.00001	0.511457	0.702921
GL 08(M)A	metahorblendite	Riacho da Posse	544582	9061535	9,814	38,368	0.1546	0.512452	0.000013	-3.63	1.7	1.51					0.51145	
GL 08(M)C	Fe-Ti-V cumulus	Riacho da Posse			0.034	0.126	0.1625	0.512501	0.000014	-2.67	1.66	1.59					0.511448	
GL-08A	metahorblendite	Riacho da Posse			15,077	67,538	0.1349	0.512298	0.000006	-6.64	1.19	1.43	6.7	60	0.71173	0.00001	0.511424	0.707362
GL-08B	garnet amphibolite	Riacho da Posse			5,483	19,486	0.1701	0.512656	0.000008	0.36	3.72	1.33	38	202.4	0.709	0.00001	0.511553	0.701581
AM-445E	olivine cumulate	Lagoa dos Angicos	546436	9061525	1.44712	3.835	0.2281	0.512976	0.000013	6.59	2.8						0.511562	
AM-448A	garnet amphibolite	Caraibeiras road			5.53793	23.432	0.1429	0.512439	0.000038	-3.89	2.63	1.29					0.511553	
AM-448D	metahorblendite	Caraibeiras road	549944	9066921	3.23183	14.324	0.1364	0.512401	0.000013	-4.63	2.68	1.26					0.511555	
AM-456A	garnet amphibolite	Caraibeiras	549195	9067122	3.87138	16.132	0.1451	0.512424	0.000006	-4.17	2.07	1.36					0.511524	

An external Sm-Nd whole-rock isochron of eighteen samples from the FMUC (cogenetic sequence) yields an age of 947 ± 58 Ma (MSWD = 2.0) with initial ε(t)= +1.8 (Fig. 13a), interpreted and adopted here as the possible age of the protoliths of mafic-ultramafic complex.

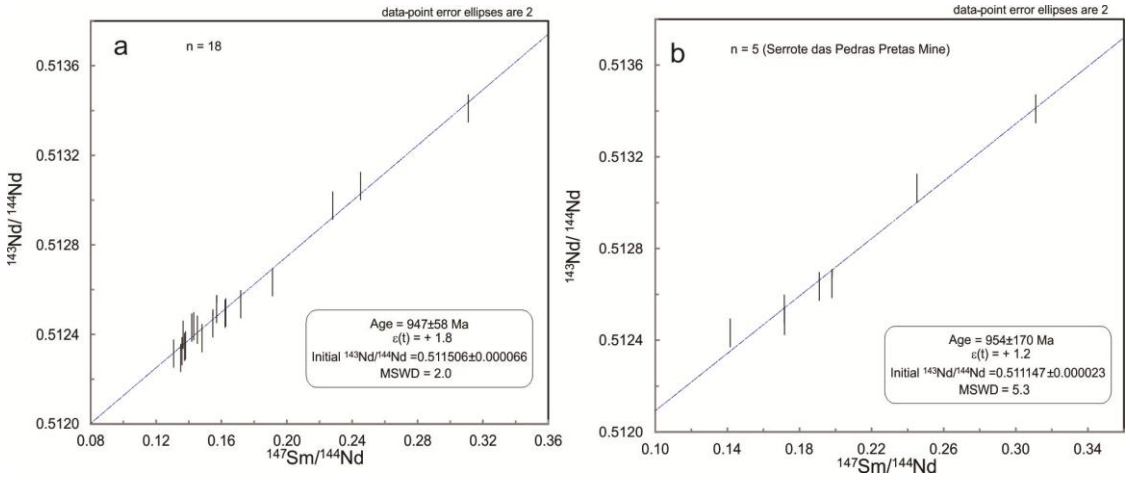

Figure 13 – a) External whole-rock Sm-Nd isocrhon age of 18 samples of FMUC yield an apparent age at 947 ± 58 Ma (MSWD 2.0) and ε(t) parameter: +1.8; b) whole-rock Sm-Nd isocrhon age of 7 samples of lithological facies of Serrote das Pedras Pretas mine yield an apparent age at 954 ± 170 Ma (MSWD 5.3) and ε(t) parameter: +1.2.

The Sm-Nd isochron age obtained is quite similar from that obtained by U-Pb method considering error ranging. Another isochron was obtained using seven analyses considering only the lithological facies from Serrote das Pedras Pretas Mine yielding an apparent age of 954 ± 170 Ma (Fig. 13b) that overlaps the full ishochron considering the errors. Despite of, and considering the large uncertainty of the age obtained, these ages are constrained by U-Pb coupled together with errors overlapping both methods. Hence, whether this age is correct some hypothetical scenarios will be proposed in the following sections.

The initial isotopic ratios are calculated based on 945 Ma (Table 9). The $(^{143}Nd/^{144}Nd)_I$ ratios of the FMUC mafic–ultramafic rocks range from 0.511364 to 0.511603 and $\varepsilon Nd_{(945\ Ma)}$ values are in the range of +0.2 – +4.69. Their T_{DM} values range with the majority between 1.16 and 1.6 Ga (except one sample) suggesting that their protoliths were derived from a juvenile Mesoproterozoic asthenospheric source or a mixing between Paleo and Neoproterozoic sources.

The initial ratio, expressed by positive parameter $\varepsilon Nd_{(t)}$ (+1.8) obtained in the isochron diagram (Fig. 13a) and the Nd isotopic growth diagram (Fig. 14) reveals that

the original magma is slightly contaminated with older crustal rocks and seem to have no affected by metamorphism processes. The $\varepsilon Nd_{(t)}$ are consistent with derivation close to chrondritic reservoir and from depleted mantle, which suggest similarities between these rocks and tholeiites of island arcs or MORB.

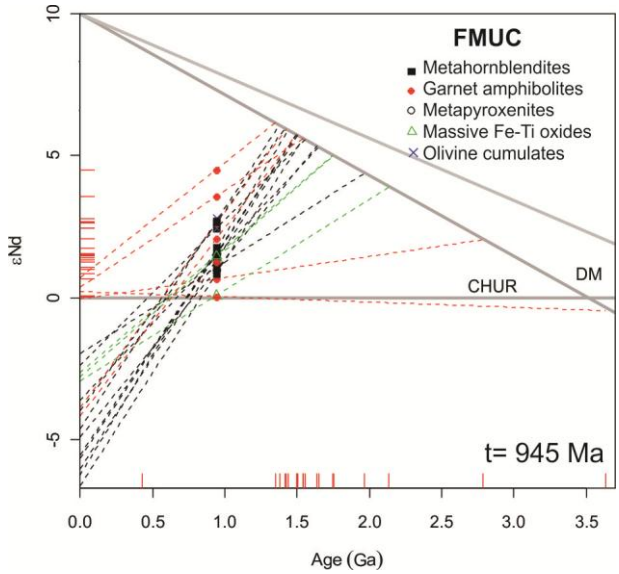

Figure 14 – Nd evolution diagrams of FMUC from isochron Sm-Nd age obtained at 945 Ma.

The Sr-Sr isotopic compositions show marked variation in the different rock types of the FMUC. Metahornblendites samples have the highest and more scattered $^{87}Sr/^{86}Sr$ values of 0.70436 to 0.712564 corresponding a $(^{87}Sr/^{86}Sr)i$ value of 0.70389 to 0.707949. Garnet amphibolites have consistent values of $^{87}Sr/^{86}Sr$ of 0.70989 to 0.70911 and $(^{87}Sr/^{86}Sr)i$ values of 0.701581 to 0.709031. Metapyroxenites samples show lower $^{87}Sr/^{86}Sr$ values of 0.70364 to 0.70379 and $(^{87}Sr/^{86}Sr)i$ values of 0.702921 to 0.703391.

These combined data suggest a isotopically enriched mantle reservoir close to EM-II (more enriched, especially in $^{87}Sr/^{86}Sr$).

3.5. DISCUSSION

3.5.1. Petrogenesis and Tectonic Settings

Ultramafic rocks when related with orogenic belts may be classified as alpine-type (including ophiolite rock assemblages) or Alaskan-type intrusions (Irvine, 1974; Farahat and Helmy, 2006). The historical terminology of Taylor (1967) refers to ultramafic-mafic complexes developed in orogenic belts, especially distinguished by their igneous tectonic setting, characteristic structures, mineralogy and sometimes by

their host-mineralization (Burg et al., 2009; Eyuboglu et al., 2010; Himmelberg and Loney, 1995; Irvine, 1974; Pettigrew and Hattori, 2006) which could be take part as products from arc magma or arc–root complexes (Irvine, 1974; Taylor, 1967; Brügmann et al., 1997; Debari and Coleman, 1989; Ishiwatari and Ichiyama, 2004; Farahat and Helmy, 2006; Zaccarini et al., 2008). They are related to the subduction environment and arc accretion (Taylor 1967; Irvine 1974; Pettigrew and Hattori, 2006; Su et al., 2012) and comprise cumulate rocks which may form as part of oceanic or continental arcs (Loucks, 1990; Eyuboglu et al. 2010).

Petrologically, the complexes are commonly composed of dunite, wehrlite, olivine clinopyroxenite, hornblende clinopyroxenite, hornblendite and hornblende gabbro (Himmelberg and Loney, 1995; Irvine, 1974; Johan, 2002; Farahat and Helmy, 2006; Su et al. 2012). However, It is more common to observe incomplete sequences, sometimes, one only lithology is present (Irvine, 1974; Himmelberg and Loney, 1995).

The ultramafic cumulates tend to show adcumulated textures and lack interstitial minerals with chromite concentrating in dunites, nevertheless, it can form irregular veins and even stratiform segregations (Irvine, 1974; Himmelberg and Loney, 1995; Johan, 2002; Thakurta et al., 2008; Ripley, 2009; Su et al., 2012).

Proper petrologic features present in these complexes and considered consistent with arc environment are cumulative clinopyroxene, presence of hornblende and frequent absence of orthopyroxene and plagioclase (Eyuboglu et al., 2010; Helmy and El Mahallawi, 2003; Johan, 2002; Pettigrew and Hattori, 2006; Ripley, 2009, Su et al. 2014). Magnetite and ilmenite are common minerals and their modal abundance can range between ~15 and 20% (Taylor 1967; Irvine, 1974; Himmelberg and Loney 1995). Also, Mg-rich olivine, Ca-rich clinopyroxene, high Fe–Cr chromite, and calcic hornblendes with a broad compositional spectrum (Irvine, 1974; Rublee, 1994; Helmy and El Mahallawi, 2003; Su et al., 2012; Farahat and Helmy, 2006) characterize the minerals of Alaskan-type complexes.

Supported by petrological data, we suggested studied ultramafic and mafic rocks are remarkably similar to subduction-related arc cumulates, analogous to Alaskan type complexes (Irvine, 1974; Himmelberg and Loney, 1995; Helmy and El Mahallawi, 2003; Farahat and Helmy, 2006; Eyuboglu et al., 2010).

Among the features obtained from the data can be correlated, we highlight:

PETROGRAPHY

The preference of Ti mineralizations for ultramafic rocks in the FMUC area resembles that at BMUC as well as similarities of mineral assemblages (abundance of garnet and rutile, the absence of plagioclase and bluish pleochroism of the amphiboles could be ascribed to desestabilization of former omphacites (Beurlen, 1988; Beurlen and Villarroel, 1990; Beurlen et al., 1992).

In despite of intense recrystallization observed, it is pointing out that in drill holes profiles and fragments of uplifted blocks in the Riacho da Posse open pit and in particular from Serrote das Pedras Pretas outcrops, outline as a possible protoliths: a cumulative rock assemblage starting with a metadunite core (olivine cumulates with Fe-Ti oxides intercumulus and later Ni-Cu sulfides) gradating to a transitional phase composed by recrystallization of these dunites forming tremolitites to chlorite-tremolite schists and clinopyroxene-tremolite-chlorite schists with variable amounts of olivine may also possibly belong from wehrlites and pyroxenites facies. Hbl-gabbros (probably a previous plagioclase-rich phase that originated garnet amphibolites) and a rim of coarse to pegmatitic hornblendites therefore considered a coarsening recrystallization of the amphiboles of the symplectites and with partial resorption of the garnets and plagioclase. We suppose it can compose a separate lithology given that the previous mineral assemblages are devoid of free abundant plagioclase, presence of decussed euhedral amphiboles, the absence of intertistial fine-grained amphiboles and abrupt contacts between garnet amphibolites and coarse to pegmatitic hornblendites or even reflect a compositional cumulative layering. Apparently, orthopyroxene inexists and abundant plagioclase if occurred would have restricted to gabbroic member that gave rise to the relicts of eclogites. The crystallization order from the existent rocks may be assumed as (apatite), olivine, Fe-chromite, clinopyroxene, magnetite, ilmenite, ± hornblende ± plagioclase, sulfides. It looks very close to the idealized sequence appropriate to the Alaskan-type cumulates (Himmelberg and Loney, 1995).

CLINOPYROXENE CHEMISTRY

a) Ca enrichment, high Mg number and variable Al_2O_3 contents of the clinopyroxenes from cumulate facies and amphibolites have similar behavior to those of clinopyroxenes from arc-related cumulates/Alaskan-type mafic–ultramafic rocks (Himmelberg and Loney, 1995; Farahat and Helmy, 2006; Pettigrew & Hattori, 2006; Krause et al., 2007; Wang et al. 2010; Eyuboglu et al., 2010; 2011) and it plots in the

composition field of the clinopyroxene from Alaskan-type complexes and arc-related cumulates (Fig. 15). Calcic composition and variable Al_2O_3 and TiO_2 contents of the clinopyroxenes and evidence of crystal accumulation such as scarce graded layers (Farahat and Helmy, 2006) are distinguish features from alpine-type, ophiolites and layered intrusions;

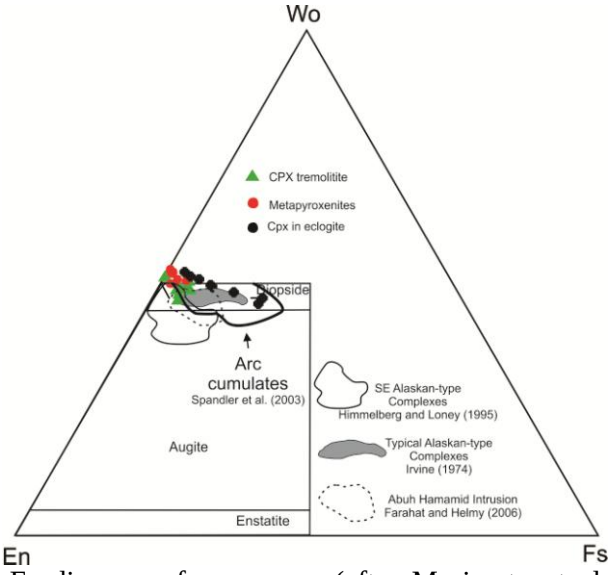

Figure 15 – En-Wo-Fs diagram of pyroxenes (after Morimoto et al., 1988) from BMUC. Shown for comparison the range of pyroxene compositions in Gabbro Akarem intrusion (Helmy and El Mahallawi, 2003), SE Alaskan Complex (Himmelberg and Loney, 1995) and typical Alaskan-type complex (Irvine, 1974). Arc cumulate complexes field are from Spandler et al. (2003). Modified after Abd El-Rahman et al. (2012).

b) The $A1_2O_3$ content of clinopyroxene shows a marked enrichment with differentiation (Hilmmeberg and Loney, 1995). Loucks (1990) demonstrated that the trend of the Al^{iv}/TiO_2 ratio in clinopyroxene in arc cumulates is distinct from trend in rift-related tholeiites. This discrimination diagram is presented in Fig. 16a with the data from BMUC following arc cumulate trend and plots near arc cumulate field and Alaskan-type complexes. One single grain (rim) plots outside the compositional field where at low Al^{IV} and TiO_2 concentrations, the island-arc and MORB-trends are similar. However, the Ural/Alaskan-type distinguishes from MORB-magma by their enriched trace element pattern in parental magma (Krause et al., 2007).

Similar characteristics can be observed in Fig. 16b with Al_2O_3 x SiO_2 diagram. The trend of alumina enrichment with differentiation also has been attributed to reflect crystallization of clinopyroxene from progressively more hydrous melts characteristic of arc magmas and high-alumina basaltic magma at convergent plate settings (Murray, 1972; Conrad and Kay, 1984; Loucks, 1990; Himmelberg and Loney, 1995);

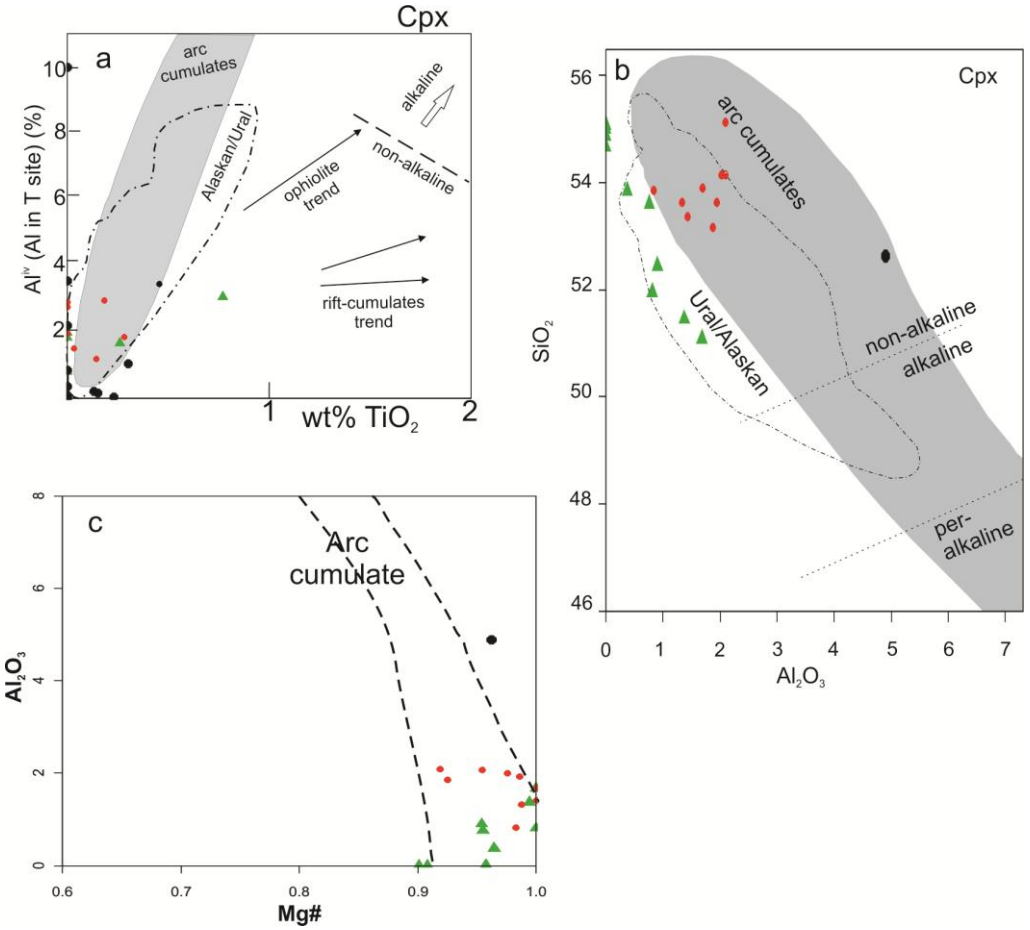

Figure 16 – Clinopyroxene compositions of the BMUC. a) Alz refers to the percentage of Al in the tetrahedral sites ($100\times^{IV}Al)/2$ diagram of Loucks (1990); b) the Al–Si discrimination diagram of Le Bas (1962) after Pettigrew and Hattori (2006).The gray area for arc cumulates are by Loucks (1990). Area with dash–dot lines are Alaskan/Ural type ultramafic intrusions along subduction zones (Pettigrew and Hattori, 2006). The term non-alkaline by Le Bas (1962); c) Plots of Al_2O_3 vs. $Mg/(Mg + Fe^{2+})$. The compositional range for arc cumulate is from Debari and Coleman (1989). Rock type symbols are the same as those used in Fig. 15.

d) High Wo (Fig. 15) and Cr_2O_3 (up to 0.54 wt.%) content of clinopyroxenes from BMUC cumulate rocks support that they are similar to products stemmed from near-liquidus crystallization of water bearing basaltic magma (e.g. Sisson and Grove, 1993; Pettigrew and Hattori, 2006; Eyuboglu et al., 2011);

e) The negative correlation generated by the increase in Al_2O_3 with decreasing $Mg/(Mg + Fe^{2+})$ in clinopyroxenes (Fig. 16c) is consistent with a crystallization trend of H_2O bearing subduction-related magma, being typical of Alaskan-type complexes (Wang et al., 2010).

SPINEL CHEMISTRY

a) Chromites display a Fe-enrichment trend (Fig. 17a) ranging from Fe-Chromite to Cr-magnetites. According to Farahat and Helmy (2006), this increasing of Fe^{3+} is reported from spinels of the Alaskan-type complexes and absent from other igneous complexes such as ophiolites or layered intrusions demonstrated that the continuity in compositions from chrome-spinel to magnetite in Alaskan-type complexes reflects a combination of trapped liquid reaction and oxidation. In the same diagram, the chromites plot near and parallel to the island arc and Alaskan-type fields and far away of the ocean island and MORB-type basalt fields.

Cr-spinels from the Bodocó chromitites overlap the field defined for Alaskan-type complexes from the Ural Mountains (Krause et al., 2007) and SE Alaskan complexes (Barnes and Roeder 2001) and also plot near to the Island arc basalt field (Fig. 17b).

On Fig. 17c, spinel compositions stared at inside the designated fields of Southeast Alaskan-type complex (Jan and Windley, 1990; Salem et al., 2012). It still plot far away from stratiform complexes and ophiolite fields.

Due to the high TiO_2 and low Al_2O_3 values, the chromites plot parallel to the island arc field, where a opposite behavior is observed to mid-ocean ridge basalt and Ocean island basalt fields in Al_2O_3 versus TiO_2 diagram (Fig. 17d). Magnetites exhibit similar behavior and spinel plot away from diagram;

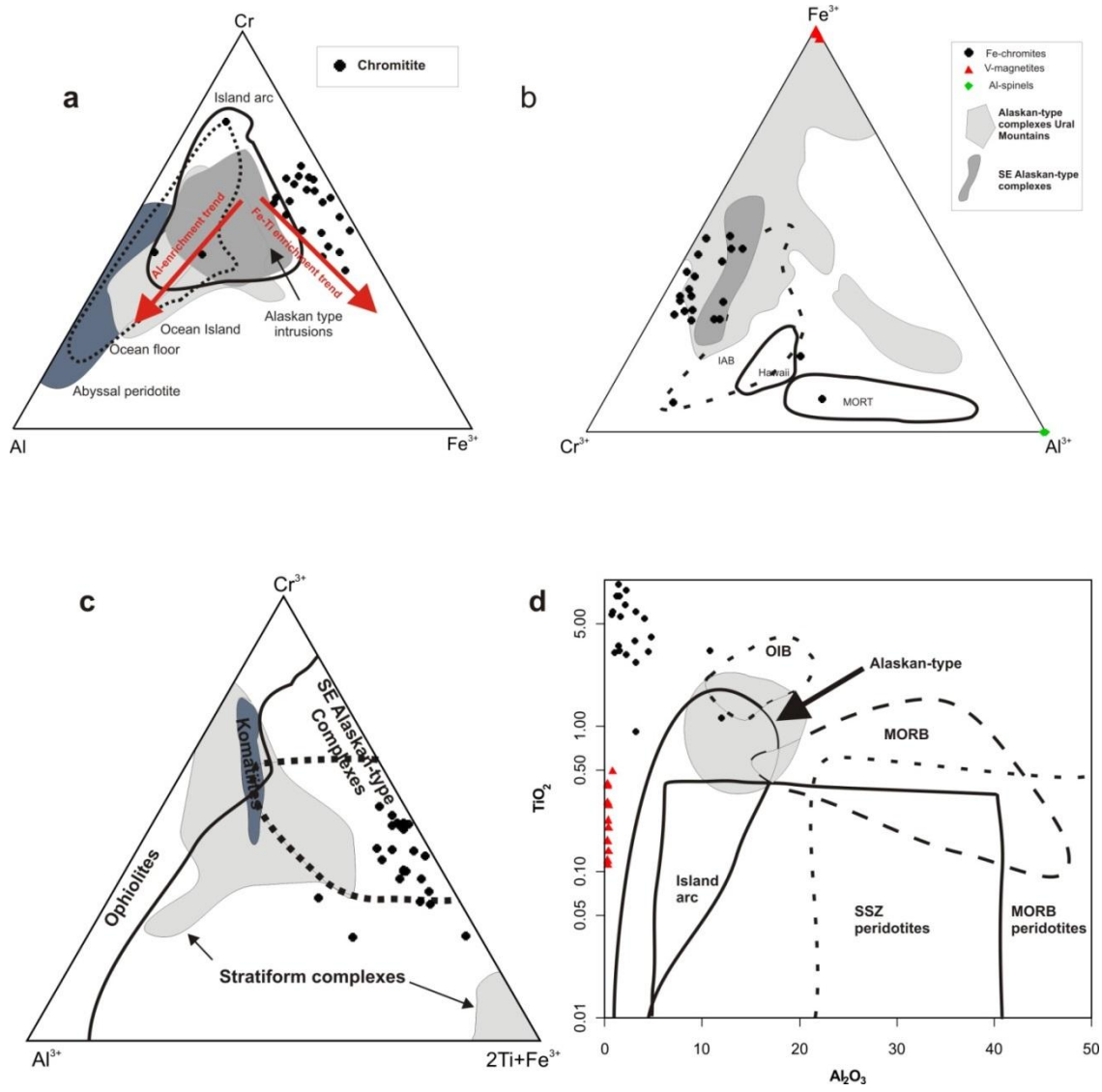

Figure 17 – Variations of trivalent diagrams of a) Cr–Al–Fe^{3+} for spinels in the Bodocó chromitites demonstrating Fe enrichment trend. The defined fields are from Barnes and Roeder (2001) after Wang et al. (2010); b) Plot of chromites from the Bodocó chromitites complex and Vanadium bearing magnetites and Al-spinels from Floresta occurrences. Also shown the fields for chromites from island-arc basalts (IAB), Hawaii tholeiites (Hawaii), and mid-ocean-ridge tholeiites (MORT) after Tian et al. (2011). Field of Alaskan-type complexes Ural Mountains is from Krause et al. (2007) and SE Alaskan-type complexes are from Barnes and Roeder (2001); c) plot of Cr-spinels from Bodocó chromitites. Fields of ophiolites, komatiites, Stratiform complexes and SE Alaskan-type complexes are from Jan and Windley (1990), after Salem et al. (2012); d) Al_2O_3 versus TiO_2 tectonic discrimination diagram showing the parallel relationship between the Bodocó chromites and Floresta magnetites and the island-arc field. Alaskan-type field after Himmelberg and Loney (1995). Fields for arc volcanic rocks, supra-subduction zone (SSZ) peridotites, ocean island basalts (OIB), and MORB basalts and peridotites are from Kamenetsky et al. (2001), modified after Farahat (2008).

b) Agroupment of Fe^{+3} enrichment and high Fe^{3+}# and Mg# spinel compositions. The parent magma of Alaskan-type complexes tend to show a Fe^{3+}-enrichment of the primary spinel attributed to the oxidized nature of arc magma (Barnes and Roeder,2001; Ahmed et al., 2008). The existence of Fe^{3+}# and high Mg# in spinels from a same

sample is a secondary feature attributed to initial spinel unmixing (Figs. 18a and b) (Ahmed et al., 2008);

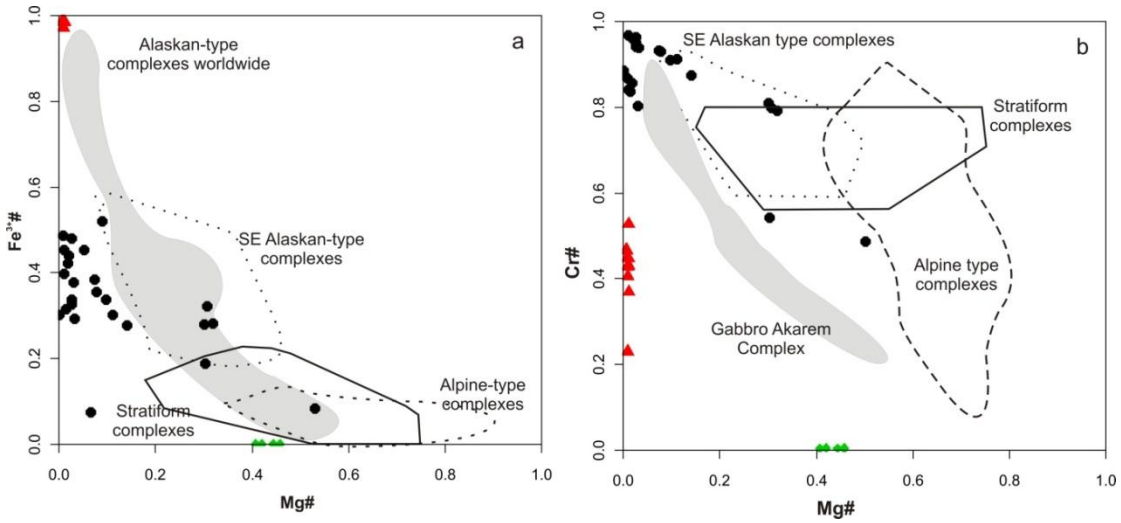

Figure 18 – a) Fe^{3+}# ($100Fe^{3+}/(Fe^{3+}+Cr+Al)$) x Mg# ($100Mg/Mg+Fe^{2+}$) and b) Fe^{3+}# ($100Cr/(Cr+Al)$) x Mg# ($100Mg/Mg+Fe^{2+}$) variation diagrams of spinels from BMUC and FMUC ultramafic roks. Discriminating fields of Alpine-type complexes, stratiform complexes and South East (SE) Alaskan-type complexes (Irvine, 1967) and Alaskan-type complexes worldwide (Barnes and Roeder, 2001) and Gabbro Amkaren (Helmy and El Mahallawi, 2003) are presented for comparison, modified after Ahmed et al. (2008). The large red symbols are the estimated initial compositions (Rock symbols are the same in Fig. 17).

c) Primary titanium-vanadium magnetite is a common accessory in Alaskan-type complexes (Himmelberg and Loney, 1995).

AMPHIBOLES

a) Wide compositional range and negative correlation between Si and Na+K contents from hbls of BMUC and FMUC (Fig. 19). The compositional range of these hbls are similar to those ones from most Alaskan-type complexes (e.g. Himmelberg & Loney, 1995; Pettigrew and Hattori, 2006; Su et al., 2012; amongst others);

b) The high Mg# and the TiO_2 content of some hornblendes reinforce the suggestion of a primary magmatic origin;

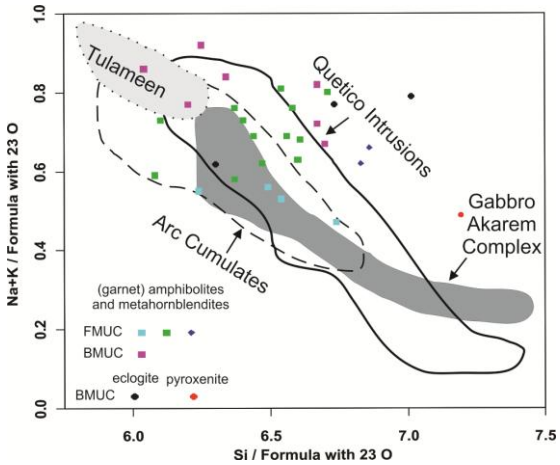

Figure 19 – Hornblende compositions in the BMUC and FMUC mafic–ultramafic complex plotting Si versus Na+K contents (23 oxygens). The fields of the Alaskan-type complexes are from Quetico, Pettigrew and Hattori (2006); Tulameen, Rublee (1994) and Gabbro Akarem, Helmy and El Mahallawi (2003). Arc cumulates field is defined by Beard and Barker (1989), modified after Su et al. (2012).

WHOLE-ROCK CHEMISTRY

Cumulates rocks, where there is no direct access to the melt composition, the trace element concentrations e distribution in minerals are useful to monitoring the fractionation of silicate melts, in order to understand the origin and evolution of parental melts (Krause et al., 2007).

Generally, the subduction related magma are characterized by high contents of LILE and LREE relative to HFSE and HREE respectively, and Nb, Ta, Zr, Hf and Ti negative troughs. Moreover, this can be associated with hydrous minerals such as hornblende and biotite (Pearce, 1982; Ringwood, 1990; Hawkesworth et al., 1991; Pearce and Robinson, 2010; Eyuboglu et al., 2011).

The FMUC and BMUC cumulate ultramafic and mafic members (Figs. 13a, b, c, d, e and f) in chondrite and primitive mantle normalizations, are slightly enriched in LILE and LREE, depleted in HFSE and HREE, and show high positive (cumulate phases) to slight negative (mafic phases) Eu anomaly, high Pb anomaly (cumulate phases), moderate negative Hf, Zr anomalies (peridotites and pyroxenites) and any conspicuous Nb, Ta and Ti negative anomalies.

The introduction of fluids from subducted oceanic lithosphere (including sediments) may be responsible for the enrichment in LILE and LREE (Ringwood, 1990; Hawkesworth et al., 1991).

The presence of ilmenite as a cumulus phase may explain the enrichment in Nb, Ta and Ti (Green and Pearson, 1987). Eyuboglu et al. (2011) also attributes the absence

of Nb, Ta and Ti negative anomalies in some Alaskan-type intrusions to phases such as ilmenite and rutile. Xiong (2006) suggest the enrichment of these elements is a result of melting of rutile-bearing hydrous eclogite.

Furthermore, positive Eu anomaly in peridotites, which is typical of cumulate rocks, whereas in the gabbroic rocks, there are a lack of any conspicuous positive Eu anomaly and a minor tendency to small negative Eu anomaly in gabbroic members indicate that fractional crystallization was not a major process controlling magma evolution suppressing fractional crystallization of plagioclase and Fe-Ti oxides in the parental magma. These combined evidences may explain the absence of the negative Nb, Ta, Ti and Eu anomalies (Pettigrew and Hattori, 2006; Eyuboglu et al., 2011).

Another suggestion of a subduction-related origin in their petrogenesis is a strong positive Pb anomaly with respect to the neighbouring trace elements in peridotites and some gabbroic members. These Pb anomalies are present in Alaskan-type peridotites and are coeval and better marked in subducted serpentinites and mantle wedge than in abyssal serpentinites that have experienced melt/rock interactions (Deschamps et al., 2013).

3.5.2. Parental Magma and Mantle Source

We suggest a high-Ti ferropicritic melt following a tholeiitic differentiation trend as parental magma for FMUC and BMUC formed from a possible lithospheric mantle enriched by subduction related component based on the following evidences:

a) In FMUC and BMUC, Cr-spinel, olivine and clinopyroxene are early phases to crystallize. Intercumulus minerals consist of pyroxene, magnetite, ilmenite and hornblende. The high Mg# of clinopyroxene (> 88) and Mg-hornblendes suggest high-Mg features in the primary liquid. According to Su et al. (2014), the high-Mg features in silicate minerals can be attributed to crystallization of magnetite and ilmenite which host large amounts of Fe. The modal abundance of magnetite and ilmenite in the FMUC and BMUC can reach up to 20% in peridotites. The Ti content in chromites and Fe-Ti oxides as an earlier intercumulus phases call for a high-Ti ferropicritic magma composition;

b) The tholeiitic nature involved in the formation of the BMUC and FMUC is accounted for the clinopyroxene compositions showed in Fig. 20a and 20b of Ti + Cr vs Ca and Ti vs Al diagrams in the clinopyroxenes of the BMUC. They plot in the field of

orogenic basalts and tholeiitic affinity. It should be noted we excluded clinopyroxenes from the eclogite were probably affected by reequilibration;

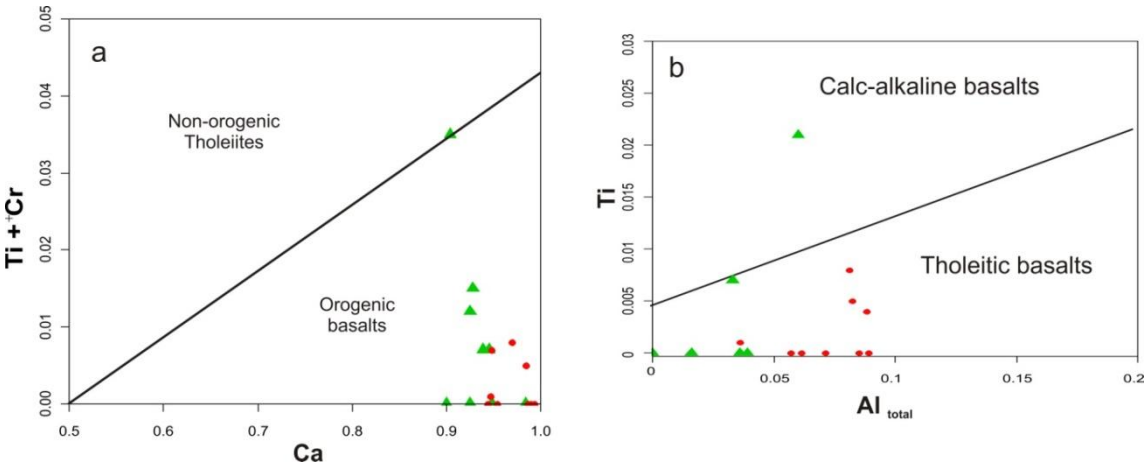

Figure 20 – a) Ti + Cr vs. Ca and b) Ti vs. Al(total) plots of clinopyroxene compositions from BMUC. The various fields are based on clinopyroxene phenocrysts in basalts (after Leterrier et al.,1982).

c) Picritic or olivine tholeiite melt is in accordance as the parent magmas of Alaskan-type intrusions (Irvine, 1974) with hydrous (Loucks, 1990) and arc tholeiite affinity (Helmy and El Mahallawi, 2003);

d) Many world-class Fe-Ti oxide deposits in the Panxi district (China) is assigned to a ferropicritic parental magma generated by the interaction of plume and the lithospheric mantle, with the latter enriched in eclogitic component related to subduction (Hou et al., 2012). We don't have evidences to a plume acting during the generation of FMUC and BMUC but it is worth mentioning that some REE patterns show similar enrichment to a OIB source.

e) The εNd values (+0.2 to +4.69) and the slightly enrichment in light REEs are in agreement with a lithospheric mantle source initially depleted and most probably, the sources of these rocks include lithospheric mantle enriched by subduction related processes such as recycled ocean crust and a small amounts of subducted sediments or recycling of melt-impregnated oceanic lithosphere.

f) The variations of Sr–Nd isotopes (Fig. 21) suggest an isotopically enriched mantle reservoir close to EM-II (more enriched, especially in $^{87}Sr/^{86}Sr$) and they may be originated by recycled ocean crust and small amount of subducted sediment or recycling of melt-impregnated oceanic lithosphere (Zindler and Hart, 1986; Wilson, 1989). The wide Sr isotopic variation points to an oceanic trend, which has been widely interpreted

as a subduction signature (e.g.,Rollinson, 1993; Su et al., 2014). These evidences above, indicate the derivation of their parental magmas from a depleted mantle source has undergone metasomatism in a subduction setting.

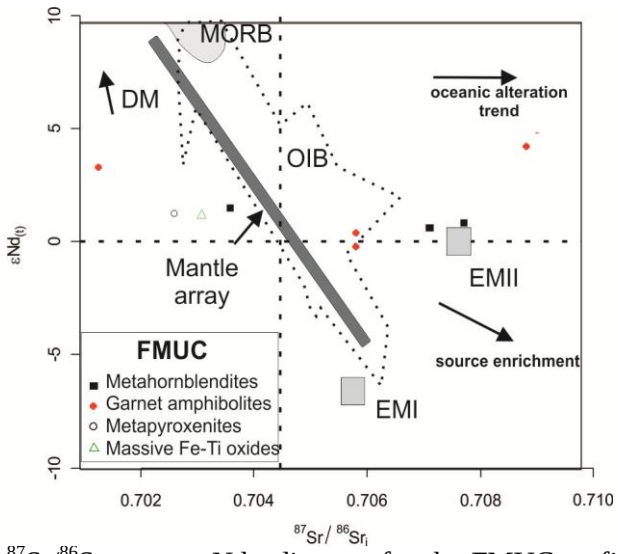

Figure 21 – a) Initial $^{87}Sr/^{86}Sr$ versus $\varepsilon Nd_{(t)}$ diagram for the FMUC mafic–ultramafic complex showing the Sr and Nd isotope compositions. MORB field is from Zimmer et al. (1995). OIB field is from White and Duncan (1996). EMI and EMII are from Hart (1988). εNd(t) = 0 and $(^{87}Sr/^{86}Sr)i = 0.705$ are values of bulk silicate Earth (Zindler and Hart, 1986). Modified after Cai et al. (2012).

This signature of the Nd–Sr system and hydrous minerals such as primary hornblende (preserved within garnet snow-ball textures, inclusions and probably in the coarse metahornblendites) strengthens an analogous to subduction-related arc cumulates (Irvine, 1974; Himmelberg and Loney, 1995; Helmy and El Mahallawi, 2003; Farahat and Helmy, 2006; Eyuboglu et al., 2010).

To evaluate the crustal contamination of the parental magma, we can signalize that the scarcity of relics of orthopyroxene in the peridotites indicates crustal contamination of parental magma can be negligible. The positive Eu anomaly in peridotites and some samples from the main BMUC and FMUC is consistent with their cumulate textures and also suggest insignificant crustal contamination. In contrast, some slightly negative Eu anomaly from grabbroic members, T_{DM} model ages > 1.6 Ga in two samples and inheritance of zircon aged at ~1.9 Ga may attest to an involvement of a crustal source in the genesis.

A robust criterion to try identifying if a system fractionation remain closed is the $(^{143}Nd/^{144}Nd)_I$ vs. 1/Nd diagram (Macdonald et al., 2000; Chavagnac, 2004) (Fig. 22a) in which the studied samples generally display a similar characteristic (line passing in

0), except for samples GL-02(M)C and GL-08(M)C that correspond to the discordant lenses of massive Fe-Ti oxide ore shoots. In the diagram of $(^{143}Nd/^{144}Nd)_I$ vs. Nd (Fig. 22b), the samples plot near a horizontal array $(^{143}Nd/^{144}Nd)_I$ = 0.51142) with a little dispersion for the garnetiferous samples GL-04B and GL-08B which probably correspond to the garnet fractionation during metamorphism. Therefore the effect of crustal contamination according to the Sm–Nd isotopes system is quite limited.

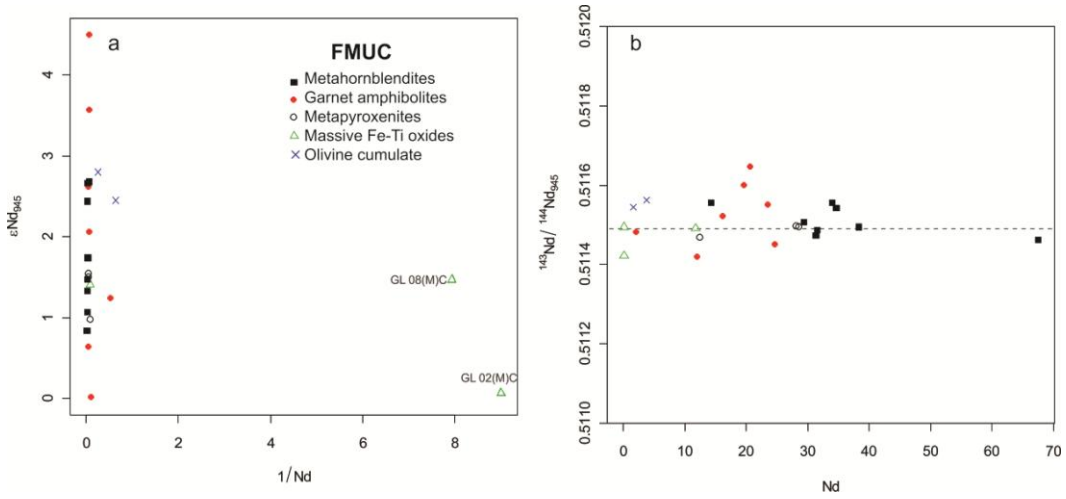

Figure 22 – a) $(\varepsilon Nd)_i$ vs. 1/Nd (from Macdonald et al., 2000; Chavagnac, 2004) and (b) $(^{143}Nd/^{144}Nd)_i$ vs.Nd (modified from Hawkesworth et al., 1999) diagrams for evaluating crustal contamination.

3.5.3. Metamorphism

The metamorphic conditions in the FMUC and BMUC mafic-ultramafic complexes may be stablished by following evidences:

A similar metamorphic evolution for both may be established based on almost identical paragenetic and textural sequences formed during the retrograde metamorphism (Beurlen et al., 1992): a pre-eclogitic mineral assemblage formed by olivine ± Cr-spinel ± clinopyroxene ± magnetite ± ilmenite ± apatite ± sulfides? ± plagioclase? ± hornblende?; a high pressure stage (omphacite preserved in BMUC – Beurlen et al., 1992) ± rutile ± (clino)zoizite ± garnet with a consistent bulk composition similar to garnets from eclogites within glaucophane schists and a small portion with a granulitic trend (Figs. 23a and b) and a retrograde stage with the formation of symplectitic amphibole-plagioclase intergrowths, sodic-calcic amphibole

growth (Fe-glaucophane, barroisite to sodian Mg-hornblendes) and recrystallization of amphibole.

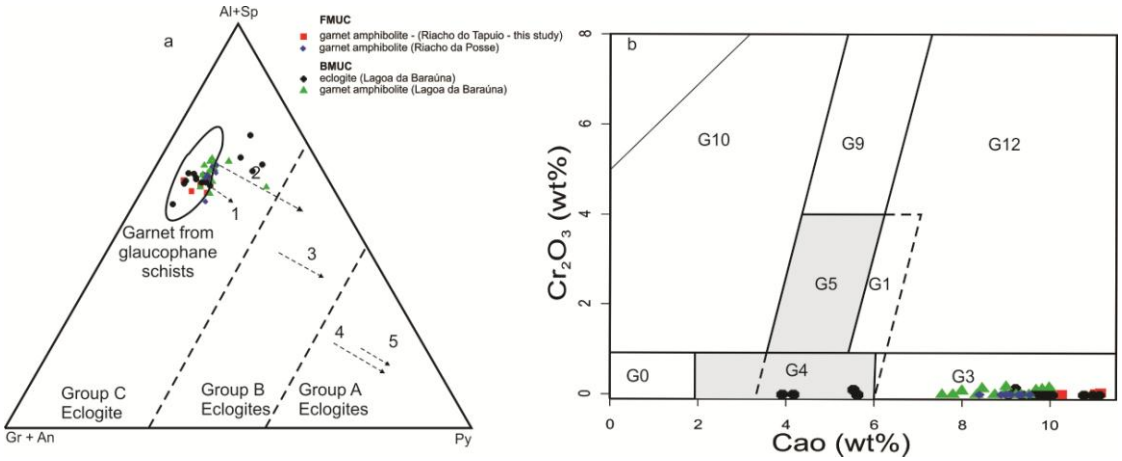

Figure 23 – a) Triangular diagram for garnet end members for garnets in eclogites and related rocks (Coleman et al., 1965). Dotted lines is for the following averages: 1 – garnets from amphibolites, 2 – garnets from chanockites and granulites, 3 – garnets from eclogites occurring in gneissic or migmatite metamorphic terrains, 4 – garnets from eclogites associated in kimberlites pipes, 5 – garnets from eclogites within ultramafic rocks such as dunite and peridotite; b) Cr_2O_3 vs. CaO diagram of Grütter et al. (2004) with G-number nomenclature of the classification scheme: G0 – unclassified, G1- low-Cr megacrysts, G3 - eglogitic, G4 and G5 - pyroxenitic, websteritic and eclogitic, G9 – lherzolitic, G10 – harzburgitic and G12 – wehrlitic.

According to Beurlen et al. (1992), high pressure metamorphism is supported for BMUC based on the jadeite content of omphacite/clinopyroxenes, the Fe/Mg partitioning between omphacite/clinopyroxene and garnet, the Si activity in phengite, and the Na content of amphiboles in retrograde symplectites in gabbroic members, suggesting a progressive metamorphic evolution up to C-type eclogites at 13 kbar/525 °C, followed by a retrograde path of medium P/T ratio, to the greenschist facies.

Sodian amphibole similar to glaucophane (found in thin sections from FMUC; GL-04) and almandine-pyrope garnets ressemble blueschist metamorphic conditions. Tschermakitic amphibole and Fe-barroisite found in the coronas surrounding the garnets from BMUC and as grains in FMUC (Table 2 and Appendix C) can be attributed to the early stages of the retrograde metamorphism derived from omphacites (Deer et al., 1966) and relics of blueschist metamorphic facies, respectively.

Thus, beside the similar retrogressed high-pressure metamorphic evolution, FMUC and BMUC are correlated by their high Ti/Fe ratios in massive ores associated to ultramafic rocks, the same gabbroic intercalations composed of only garnet and amphibole with the same mineral compositions and lacking plagioclase but rich in

rutile (Beurlen et al., 1992; Beurlen and Vilarroel, 1990; Beurlen and Lira, 1988; Beurlen, 1988; this study).

3.5.4. Subsolidus Exsolution of the Fe–Ti Solid Solutions

A measurement of temperature and O_2 fugacity was obtained using coexisting magnetite and ilmenite in a sample of massive Fe-Ti oxides lense from the Faz. Exú occurrence. The ilmenite–magnetite geothermobarometry based on the geothermometer of Anderson and Lindsley (1985) aided by Ilmat program (Lepage, 2003) helped to calculate oxygen fugacities and possible Fe–Ti oxide blocking temperatures of subsolidus equilibration. Calculated temperatures and oxygen fugacities are listed in Table 3 and plotted in temperature vs.−logfO_2 diagram (Fig. 24a).

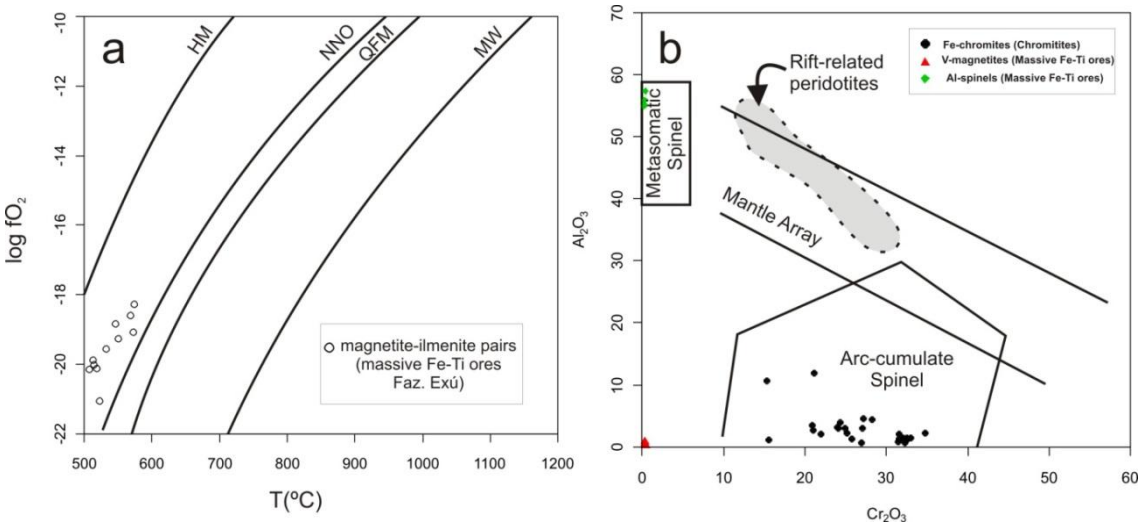

Figure 24 – a) O-fugacity and temperature determined for the massive Fe-Ti ore in FMUC based on magnetite–ilmenite coexistents pairs. HM trajectory for haematite-magnetite buffer, NNO for nickel–nickel-oxide, FMQ for quartz–fayalite–magnetite, WM for wüstite–magnetite (Eugster and Wones, 1962); b) Al_2O versus Cr_2O_3(wt.%) diagram of Franz and Wirth (2000) (after Seo et al., 2013).

The calculated oxygen fugacities obtained from the ilmenite–magnetite coexistent couples vary from ~$10^{-21.04}$ ~$10^{-18.26}$ and plot as high as the nickel–nickel-oxide (NNO) curve similar to that required for arc cumulates/Alaskan-type complexes (Himmelberg & Loney, 1995). The blocking temperatures of subsolidus equilibration range from 573 to 506 °C. Note that these blocking temperatures obtained on the basis of the magnetite–ilmenite intergrowths are much lower than the early crystallization temperatures of ilmenite and magnetite from Alaskan-type intrusions ranged above 815°C (Himmelberg and Loney, 1995). It should be noted, however, due to sub-solidus

cation exchange and re-equilibration during high pressure metamorphism and new fluids influx driven by subduction related process or by granitic intrusion (Riacho do Icó suite wall-rock), the calculated temperatures should be taken as minimum temperatures for these modifications and no for crystallization due to the difficulty of reconstructing the original composition of the minerals subject to a large margin of error.

For clarity's sake, the ulvöspinel contents in the magnetite, calculated using the method of Stormer (1983), are below 1.7 mol%. This is in accordance with almost absence of fine trellis intergrowths in magnetite crystals. The endmember component (X_{Ilm}) of the analyzed ilmenite is almost pure (> 92.41% mole ilmenite). These textural features show magnetite lost almost all amount of Ti to its surroundings through solid-state diffusion, contributing to the formation of a newly granular ilmenite enhancing the quality of the ore. Moreover, the presence of intersticial Al-spinels surrounding magnetite and ilmenite attest complete exsolution by lowering temperature and they plot as to be of metasomatic origin (Fig. 24b). These changes seem doesn´t take affected Fe-chromites outside of granites (BMUC in this case) remain unscathed plotting along Arc cumulates spinels and far from Rift-cumulates spinel (Fig. 24b).

The occurrence of cumulus magnetite and ilmenite as the oxide phases suggest magma was rich in Fe_2O_3 and H_2O from which the ultramafic rocks crystallized. Considering these oxides crystallized after clinopyroxene, but before the supposed hornblende, the oxidation conditions of the magma at the time of crystallization were similar to that reported for arc-basalt ultramafic xenoliths (Conrad and Kay, 1984) that have mineral assemblages similar to Alaskan-type ultramafic rocks (Himmelberg and Loney, 1995) at least as high as the NNO buffer (Helz, 1973).

Recapitulating, ilmenite growth pass to be an unfavorable phase in the eclogitic rocks where rutile is the most common accessory (Force, 1991). Thus, we can not discard the late magmatic fluids as a mechanism for the enrichment of protore mineralization inside the granite as suggested by fluid/rock interactions present in the mines (Figs. 7a and b). Perhaps this may explain why only the deposits within the Riacho do Icó Suite have economic value.

We suggest some Fe-Ti ore lenses and ultramafic protore probably re-equilibrated under new water/fluid content and oxygen fugacity conditions growing their Ti/Fe (modal ilmenite/magnetite) ratios substantially during possible stemmed

fluids from Riacho do Icó granitic intrusion. Previously, secondary enrichment was given that by rutile growth (up to 12%) during high pressure/low temperature metamorphism.

3.6. GEODYNAMIC SIGNIFICANCE AND CONCLUSIONS

Crystallization age for the FMUC (also known as Serrote das Pedras Pretas suite) yielded ca. 950 Ma with $\varepsilon Nd_{(t)}$ of +1.8 confirming an accretionary juvenile event with Cariris Velhos age where the nature of this kind of intrusion is quite younger to a supposed arc environment in the same age either (eg. Kozuch, 2003). Preferentially, similar Alaskan-type emplacement occur close to the end of subduction, prior to accretion-collision terranes (Pettigrew and Hattori, 2006; Su et al., 2012).

A closer and analogous Mesoproterozoic (~980–960 Ma) continental arc (Poço Redondo tonalitic gneisses) developed on the south margin of the Paleoproterozoic Pernambuco-Alagoas Block and post-tectonic Serra Negra granite intruded in this arc close to ~950 Ma (Oliveira et al., 2010) corroborate with the possibility that these ultramafic-mafic complexes refer to the end of subduction or post-tectonic intrusion related to this tonian event.

Similar post-orogenic intrusions occur along CAOB (Central Asian Orogenic Belt) frequently hosting Ni-Cu sulfides mineralizations (Xie et al., 2014) whereas giant Fe-Ti-V oxides layers occur in the lower and middle parts of relatively small mafic-ultramafic intrusions interpreted as a product of interaction between mantle plume with a subduction component (eg. Giant Hongge Fe-Ti-V oxide deposit – Bai et al., 2012).

FMUC rocks could be originated by igneous accumulation from hydrous magma probably at shallow depth due to the high amounts of ilmenite and magnetite as early cumulus phases and it being emplaced along a major fault zones. In contrast, the content of Ni-Cu sulfides should remit to a deeper level of the arc where it could remain as a magma chamber crystallized at the base of an arc system. Cu-Ni sulfide disseminations can indicate a lower oxidation state in Archean and Neoproterozoic arcs whereas in Phanerozoic arcs, Pt-Fe alloy is more common, reflecting highly oxidized conditions (Helmy et al., 2014).

It happened contemporaneously or shortly after the cessation of deposition of sedimentary and volcanoclastic sequences in the southwesternmost part of the terrane, considering elderly ages obtained to volcanic and gneissic rocks in this part (~995 Ma –

Santos et al., 2010; Brasilino et al., 2014). During active subduction, these sediments could accumulated probably in a back-arc basin forming the São Caetano sequence, whereas with crust thickness relatively shallow in this stage, the emplacement of these subduction-related ultramafic–mafic intrusions occurred in a remnant portion of the arc (older). The volcanic front would be situated in north part where younger ages were recorded (975-920 Ma for volcanogenic sequence and granitic protoliths starting at ~ 960 Ma – Kozuch, 2003).

BMUC accumulate in the border of the Paleoproterozoic continental basement Icaiçara Fragment (see Geologic Setting section) surrounded by similar sedimentary sequences. Today, this recognized alloctonous fragment, could be formed through accretion of a microcontinent or part of a disrupted continental margin. BMUC and FMUC may represent the subduction-related magmatism, either prior than short after (post-orogenic) to the juxtaposition of the juvenile arc with one of these candidates: Pernambuco-Alagoas massif or Alto Moxotó Terrane .

Santos et al. (2010) suggest that Rodinia was drifting ‘‘westward” between 1,000 and 900 Ma, and that the Cariris Velhos tectonic regimes developed as part of a continental margin arc–back-arc system developed on a Paleoproterozoic crust of the leading edge. This assumption is based on a hypothetical reconstruction of the “western” margin of Rodinia at ca. 1,000 Ma putting together Borborema-Central Africa-Saharan region attached to the Congo-Sao Francisco cratons (Li et al., 2008; Fuck et al., 2008). Furthermore, it is still difficult to reconstruct where the arc docked due to strong tectonic overprint imposed by large amounts of transcurrent displacements during Pan-african-brazilian deformation and metamorphism (650–500 Ma).

Arc affinity of metasedimentary rocks in the central and north–northeastern parts of the Alto Pajeú domain is attested by geochemical signatures of metamorphosed greywackes, lithic sandstones, and arkoses characteristic of derivation from a island arc and/or continental arc sources (Sales et al., 2011) and sources mixed with volcanogenic derivates of mafic and intermediate igneous rocks (Santos, 1995; Kozuch, 2003; Medeiros, 2004; Santos et al., 2010). The chondrite-normalized spiderdiagrams obtained for volcanic rocks of both assemblages in Riacho do Gravatá and from the southwestern part of the Alto Pajeú terrane are somewhat similar to those of medium and high-K calc-alkaline series of continental magmatic arcs (Santos, 1995; Kozuch, 2003; Medeiros, 2004).

Summarizing, U-Pb data for felsic volcanic rocks of the Cariris Velhos event in the Alto Pajeú terrane suggest a range of volcanism spanning about 30 million years, from ca. 995 to ca. 965 Ma (Santos et al., 2010).

Moreover, other elements such augen-gneisses and migmatitic facies have the majority of samples classified as calk-alkaline to high-K calck-alkaline character compatible both with continental arc or syn-to-late collisional signatures (Jardim de Sá, 1994; Santos, 1995; Santos e Medeiros, 1999; Kozuch, 2003; Medeiros, 2004; Santos et al., 2010). These metaplutonic rocks show more precise results falling in the interval 960–925 Ma, generally younger than the ages for metavolcanic rocks (Brito Neves et al., 1995; Kozuch, 2003; Santos et al., 2010).

The purpose of some authors of a back-arc or fore-arc basin developed as an adjunct to a zone of subduction (Santos, 1995; Kozuch, 2003; Sales et al., 2011) is coeval with the geochemical patterns of the non-cumulative metamafic rocks from FMUC similar of a tholeiitic series mixing between arc and MORB/back-arc setting (see bulk-rock chemistry section).

According to Cai et al. (2012), the opening of a back-arc basin caused by roll-back of the subduction zone would bring an extension of the arc lithosphere and uplift the asthenosphere into contact with the mantle wedge. This induces extensive partial melting of the mantle materials to form oceanic crust if the arc crust is not very thick. Similar features are expected caused by spreading seafloor mid-ocean ridges for back-arc basins (Crawford et al., 1981; Jarrard, 1986; Cai et al., 2012).

Preserved relics of oceanic crust of Monte Orebe (Moraes, 1992) formed between São Francisco Craton and Pernambuco-Alagoas block far less than 200 km of BMUC and 380 km of FMUC suggest a development of a new young oceanic floor between the intervening Borborema Province and the São Francisco Craton at ca. 820 Ma (Caxito et al., 2014).

In the western Gondwana amalgamation, relics of eclogitic rocks range at c. 615 Ma (Amaral, 2010; Santos et al., 2014; Araújo et al., 2014a) and high pressure granulites (613-589 Ma; Amaral et al., 2012) were found in Ceará Central Domain which roughly align with other HP and UHP rocks in Africa also dated at c. 620–610 Ma (Bernard-Griffiths et al., 1991; Affaton et al., 2000; Jahn et al., 2001; Araújo et al., 2014a) defining a large Himalayan-scale collisional orogeny (Araújo et al., 2014a and b) converging craton blocks and consuming a large ocean along the Transbrasiliano Lineament. In the eastern part of Central Domain, this metamorphic peak at c. 620 Ma

have already associated with high-T conditions of 640–750°C and 6–8 kbar (Neves et al., 2012).

High-pressure metamorphism is recorded in BMUC whereas retrogressed phases resembles in FMUC outcrops. U-Pb zircon age on the metamorphic overgrowth rims with low Th/U ratios (0.008-0.038) on FMUC rock samples yield a Pan-african/brazilian age of 625 ± 6 Ma which is compatible either with metamorphic peak of the eclogitic stage than retroeclogitic stage as well (the dated sample is a sodian rutile-bearing metahornblendite).

We argue that these retrogressed eclogitic rocks took place in this context, representing part of the western Gondwana marking the closure of a branch of a neoproterozoic ocean basin between and along southern and southwestern borders of Alto Pajeú, Piancó-Alto Brigida belts, Alto Moxotó and Pernambuco-Alagoas domains probably correlating eastward to the Central African fold belt (Van Schmus et al., 2008). In the meantime, according to Santos et al. (2010), Cariris Velhos rocks do not seem to extend from the Alto Pajeú terrane into the northern part of the West African fold belt. Coeval rocks have been reported farther east in eastern Chad (de Wit et al., 2005 apud Santos et al., 2010). Arc-related magmatism at c. 608 Ma (Riacho do Icó Suite) suggests this subduction last until this epoch. Diachronically, it was followed by remaining west to eastward thickening of the crust, with inversion of the ediacaran Cachoeirinha basin in a detachment fault system preserving low-grade metamorphic sediments over exhumed high pressure rocks of BMUC including arc cumulates and kyanite-bearing sediments with the development of thrust related foliation in the vicinity of the contact of these.

In relation of FMUC, a uplift was undergone by capture of parts of these rocks as xenoliths within of Riacho do Icó Suite at 608 Ma which accelerate the replacement of the high pressure mineral assemblage to amphibolite/greenschist-facies conditions by isothermal decompression and re-hydratation favored abundant symplectites and growth of hornblende.

In the search of possible mechanisms to explain how the arc cumulate peridotites reached the subduction channel and what is its relationship with granitic rocks of Riacho do Icó and Icaiçara gneissic rocks. We found similar processes happened in ultramafic cumulates from subarc mantle (Rio San Juan Complex, Dominic Republic; Abbott et al., 2007; Hattori et al., 2010a), mantle wedge peridotites (Sulu Belt, China;

Xie et al., 2013) and garnet bearing ultramafic rocks of Sanbagawa metamorphic belt, Southwest Japan (Hattori et al., 2010b).

Mantle wedge peridotites may be dragged down to the subduction channel by the corner mantle flow for a later exhumation (Hattori et al., 2010a; b; Xie et al., 2013).

In the beginning of a subduction event, the overlying plate and subducting plate are not fully decoupled (Xie et al., 2013). With the progressive hydration of the mantle wedge, the overlying plate is thinned by thermal flux and might have been responsible for the thermal erosion of the arc root/subarc mantle counting with a vigorous mantle corner flow to drag the subarc mantle peridotite into the subduction channel (Arcay et al., 2007; Hattori et al., 2010a).

The buoyancy of granitic rocks can result in the decoupling of blocks from the subducted lithosphere due to their density instability (Li and Gerya, 2009). Thus, peridotites incorporated from the mantle wedge would may be easily exhumed together with the upward movement of granitic rocks in return flows in the subduction channel (Hattori et al., 2010a; Xie et al., 2013). Consequently, they would not be subducted to a deep levels in the subduction channel (Xie et al., 2013).

In summary, these mafic-ultramafic complexes joined together contemporany granitic and volcanic rocks constituting an hypothetical marginal arc–back-arc basin system evolved between 1000 and 920 Ma. The Arc cumulates complexes were emplaced ca. 950 Ma in the roots of the arc or ascend as a magma conduits/ small magma chambers in a possible neighbooring back-arc or post-tectonic geodynamic setting. Arc accretion probably stopped between 950-820 Ma. This relatively long-life of Cariris Velhos arc is probably responsible for the vast crustal growth in this area but this architecture still unclear due to scarce detail studies.

The onset of a new subduction process driven by westward convergence could cause thermal erosion and delamination dragging arc root pieces into the subduction channel. A short loop of these rocks in the eclogitic condition (< 14 Kbar) reached the metamorphic peak at ca. 625 Ma from which it was exhumed with granitic and sediment materials by upward movements.

High Ti/Fe ratios are attributed first to the early stages of accumulation from an enriched source. In part from titanium partitioning between silicate and oxide phases with enrichment up to 12% in rutile minerals at eclogitic conditions. After that, by hydrothermal magmatic fluids stemmed by means such as processes of exsolutions within granitic wall-rock, specifically in FMUC economic ore bodies.

3.7. ACKNOWLEDGEMENTS

This study represents a partial fulfillment of the requirements to obtain the master degree title by Geysson de Almeida Lages at the University of Brasilia - UnB. We would like to thank CPRM-Geological Survey of Brazil for financial support and UnB by the use of their isotopic facilities.

3.8. REFERENCES

Abbott Jr., R.N., Broman, B.N., Draper, G., 2007. UHP magma paragenesis revisited, olivine clinopyroxenite and garnet-bearing ultramafic rocks from the Cuaba Gneiss, Rio San Juan Complex, Dominican Republic. International Geology Review 49, 572–586.

Abd El-Rahman, Y., Helmy, H. M., Shibata, T., Yoshikawa, M., Arai, S., & Tamura, A. 2012. Mineral chemistry of the Neoproterozoic Alaskan-type Akarem Intrusion with special emphasis on amphibole: Implications for the pluton origin and evolution of subduction-related magma. Lithos, 155, 410–425.

Affaton, P., Kröner, A. and Seddoh, K.F., 2000. Pan-African granulite formation in the Kabye Massif of northern Togo (West Africa): Pb–Pb zircon ages.Int. J. Earth Sci.,88, 778–790.

Ahmed, A.H., Helmy, H.M., Arai, S., Yoshikawa, M., 2008. Magmatic unmixing in spinel from late Precambrian concentrically-zoned mafic–ultramafic intrusions, Eastern Desert, Egypt. Lithos 104, 85–98.

Almeida, F. F. M., Brito Neves, B.B. Fuck, R.A. 1977. Províncias estruturais brasileiras. In: SIMPÓSIO DE GEOLOGIA DO NORDESTE, 8, Campina Grande. Atas do... Campina Grande: SBG. Núcleo Nordeste, p.363-391.

Almeida F.F.M.de, Hasui Y., Brito Neves B.B., Fuck R.A. 1981. Brazilian structural provinces: an introduction. Earth-Sci.Reviews, 17:1-21.

Amaral, W.S., 2010. Analise geoquímica, geocronológica e geotermobarométrica das rochas de alto grau metamórfico adjacentes ao arco magmático de Santa Quitéria, NW da Província Borborema.PhD thesis, Universidade Estadual de Campinas, 210p.

Amaral, W.S., Santos, T.J.S., Wernick, E., Nogueira Neto, J.A., Dantas, E.L. and Matteini, M., 2012. High-pressure granulites from Cariré, Borborema Province,

NE Brazil: tectonic setting, metamorphic conditions and U–Pb, Lu–Hf and Sm–Nd geochronology. Gondwana Res., 22, 892–909.

Andersen, D.J., Lindsley, D.H., 1985. New (and final!) models for the Ti-magnetite/ilmenite geothermometer and oxygen barometer. Abstract AGU 1985 Spring Meeting Eos Transactions. American Geophysical Union. pp. 66–416.

Araujo, C.E.G. De, Rubatto, D., Hermann, J., Cordani, U.G., Caby, R., Basei, M.A.S., 2014a. Ediacaran 2,500-km-long synchronous deep continental subduction in the West Gondwana Orogen. Nat. Commun. 5, 1–8.

Araújo, C. E. G., Weinberg, R. F., & Cordani, U. G. 2014b. Extruding the Borborema Province (NE-Brazil): a two-stage Neoproterozoic collision process. Terra Nova, 26(2), 157–168.

Arcay, D., Tric, E., Doin, M.P., 2007. Slab surface temperature in subduction zones: influence of the interplate decoupling depth and upper plate thinning processes. Earth and Planetary Science Letters 255, 324–338.

Bai, Z., Zhong, H., Naldrett, A.J., Zhu, W., Xu, G. 2012. Whole-Rock and Mineral Composition Constraints on the Genesis of the Giant Hongge Fe-Ti-V Oxide Deposit in the Emeishan Large Igneous Province, Southwest China. Economic Geology 107, 507-524.

Barnes, S.J., Roeder, P.L., 2001. The Range of Spinel Compositions in Terrestrial Mafic and Ultramafic Rocks. J. Petrol. 42, 2279–2302.

Beard, J.S., 1986. Characteristic mineralogy of arc-related cumulate gabbros: implications for the tectonic setting of gabbroic plutons and for andesite genesis. Geology 14, 848–851.

Beard, J.S., and Barker, F., 1989, Petrology and tectonic significance of gabbros, tonalities, shoshonites, and anorthosites in a late Paleozoic arc-root complex in the Wrangellia terrane, southern Alaska: Journal of Geology, v. 97, p. 667–683.

Bernard-Griffiths, J., Peucat, J.-J. and Menot, R.-P., 1991. Isotopic Rb–Sr, U–Pb and Sm–Nd and trace element geochemistry of eclogites from the PanAfrican belt: A case study of REE fractionation during high-grade metamorphism.Lithos, 27,43–57.

Beurlen, H. and Lira, R.B., 1988. Bodoco and Floresta, PE two atypical Fe-Ti occurrences in northeast Brazil. 7 Congr. Latino Americano Geol. Anals, 1:185-200.

Beurlen, H. 1988. Fazenda Esperança (Bodocó) e Riacho da Posse (Floresta): Duas ocorrências atípicas de Fe-Ti no Estado de Pernambuco. Universidade Federal de Pernambuco.

Beurlen, H., & Villarroel, S. 1990. Petrografia de duas ocorrências de provável eclogito em Bodocó e Floresta no estado de Pernambuco, Brasil. Revista Bras. de Geoc, 20, 111–121.

Beurlen, H., Silva, A. F. Da, Guimarães, I. P., & Brito, S. B. 1992. Proterozoic C-type eclogites hosting unusual Ti-Fe-Cr-Cu mineralization in northeastern Brazil. Precambrian Research, 58, 195–214.

Blake, M.C. Jr., Morgan, B.A. 1976. Rutile and sphene in blueschist and related high-pressure facies rocks. U.S. Geological Survey. Professional Paper 959C, p.C1-C6.

Brasilino, R.G., Miranda, A.W.A., Morais, D.M.F de, Lages, G.A. 2014. Programa Geologia do Brasil. Carta Geológica Escala 1:100.000: Folha Mirandiba SC.24-X-A-I. CPRM/Serviço Geológico do Brasil.

Brito, M.F.L. & Cruz, R.F., 2009. O Complexo Metavulcanossedimentar da região de Salgueiro/PE, Zona Transversal, Província Borborema, NE do Brasil. In: SBG, Simpósio de Geologia do Nordeste, 24. Fortaleza. Anais... p. 201.

Brito Neves B.B. 1975. Regionalização geotectônica do Pré-cambriano Nordestino. Tese de Doutorado, IGc - Universidade de São Paulo. São Paulo-SP. 198 p.

Brito Neves B.B. 1983. O Mapa Geológico do Nordeste Oriental do Brasil, Escala 1:1 000000. Tese de Livre Docência, Instituto de Geociências da Univ. de S. Paulo, 171p.

Brito Neves B.B., Van Schmus W.R, Santos E.J, Campos Neto M.C.C. 1995. O Evento CaririsVelhos na Província Borborema: integração de dados, implicações e perspectivas. Rev. Bras. de Geoc., 25:151-182.

Brito Neves B.B., Santos E.J., Van Schmus W.R. 2000. Tectonic history of the Borborema Province. In: Cordani U.G. et al.. (eds). Tectonic evolution of the South America. 31st International Geological Congress, p.151-182.

Brito Neves B.B., Campos Neto M.C.C., Van Schmus W.R., Santos E.J. 2001a. O Sistema Pajeú-Paraíba e o Maciço São José do Campestre no Leste da Borborema. Rev. Bras. de Geoc. 31:173-184.

Brito Neves B.B., Campos Neto M.C.C., Van Schmus W.R., Fernandes M.G.G., Souza S.L. 2001b. O Terreno Alto Moxotó no Leste da Paraíba (Maciço Caldas Brandão). Rev. Bras. de Geoc. 31:185-194.

Brito Neves B.B., Van Schmus W.R., Kozuch M., Santos E:J., Petronilho L. 2005. A Zona Tectônica Teixeira Terra Nova –ZTTTN –Fundamentos da Geologia Regional e Isotópica. Revista do Instituto de Geociências – USP. Série Cientifica. 5:57-80.

Brügmann, G.E., Reischmann, T., Naldrett, A.J., Sutcliffe, R.H., 1997. Roots of an Archean volcanic arc complex: the Lac des Iles area in Ontorio, Canada. Precambrian Research. 81, 223–239.

Bühn, B. M., Pimentel, M, M., Matteini, M., Dantas, E.L., 2009. High spatial resolution analysis of Pb and U isotopes for geochronology by laser ablation multi-collector inductively coupled plasma mass spectrometry (LA-MC-ICP-MS. Anais da Academina Brasileira de Ciências. v. 81, p. 1-16.

Burg, J.P., Bodinier, J.L., Gerya, T., Bedini, R.M., Boudier, E., Dautria, J.M., Prikhodko, V., Efimov, A., Pupier, E., Balanec, J.L., 2009. Translithospheric mantle diapirism: geological evidence and numerical modeling of the Kondyor zoned ultramafic complex (Russian Far-East). Journal of Petrology 50, 289–321.

Caby, R., Sial, A.N., Arthaud, M. & Vauchez, A. 1991. Crustal evolution and the Brasiliano orogeny in Northeast Brazil. In: Dallmeyer, R.D. & Lecorché, P. (Eds.).The West African orogens and Circum-Atlantic correlatives. Springer-Verlag, pp. 373-397.

Cai, K., Sun, M., Yuan, C., Zhao, G., Xiao, W., & Long, X. 2012. Keketuohai mafic–ultramafic complex in the Chinese Altai, NW China: Petrogenesis and geodynamic significance. Chemical Geology, 294-295, 26–41.

Carmichael, I.S.E. 1967. The iron-titanium oxides of salic volcanic rocks and their associated ferromagnesian silicates. Contributions to Mineralogy and Petrology, 14, 36-64.

Chavagnac, V. 2004. A Geochemical and Nd Isotopic Study of Barberton Komatiites (South Africa): Implication for the Archean Mantle. Lithos. 75 (3-4), 253–81.

Chen, B., Suzuki, K., Tian, W., Jahn, B.M., Ireland, T., 2009. Geochemistry and Os–Nd–Sr isotopes of the Gaositai Alaskan-type ultramafic complex from northern North China Craton: implications for mantle–crust interaction. Contributions to Mineralogy and Petrology 158, 683–702.

Coleman, R. G., Lee, D. E., Beatty, L. B., & Brannock, W. W. 1965. Geological Society of America Bulletin Eclogites and Eclogites : Their Differences and Similarities. Geological Society of America Bulletin, 76, 483–508.

Coleman, R.G., 1971. Plate tectonic emplacement of upper mantle peridotites along continental edges. Journal of Geophysical Research. 76, 1212–1222.

Conrad, W.K., and Kay, R.W., 1984, Ultramafic and mafic inclusions from Adak Island: crystallization history, and implications for the nature of primary magmas and crustal evolution in the Aleutian arc: Journal of Petrology, v. 25, p. 88-125.

Corfu, F., Hanchar, .M., Hoskin, P. . W. O., & Kinny, P. 2003. Atlas of Zircon Textures. Reviews in Mineralogy and Geochemistry, 53(1), 469–500.

Corsini, M., Vauchez, A., Archanjo, C.J. 1991. Strain transfer at continental scale from a transcurrent shear zone to a transpressional fold belt: The Patos-Seridó System, Northeastern Brazil. Geology, 19: 586-589.

Crawford, A.J., Beccaluva, L., Serri, G., 1981. Tectono-magmatic evolution of the west Philippine–Mariana region and the origin of boninites. Earth and Planetary Science Letters 54, 346–356.

Dantas, E.L. 1996. Geocronologia U-Pb e Sm-Nd de Terrenos Arqueanos e Paleoproterozóicos do Maciço Caldas Brandão, NE do Brasil. Tese de Doutorado. Unesp, 208p.

DeBari, S.M., and Coleman, R.G., 1989, Examination of the deep levels of an island arc: evidence from the Tonsina ultramafic-mafic assemblage, Tonsina, Alaska: Journal of Geophysical Research, v. 94-B, p. 4373-4391.

Deer, W. A; Howie, R. A; Zussman, J. 1966. An introduction to the rock - forming minerals. London: Longman. 528 p.

Depaolo, D.J., Wasserburg, G.J., 1976. Nd isotopic variations and petrogenetic models. Geophys. Res. Lett. 3, 3–6.

Depaolo, D.J. 1981. A neodymium and strontium isotopic study of the Mesozoic calc alkaline granitic batholits of the Sierra Nevada and Peninsular Ranges. California Journal Geophysical Research, v. 86, p. 10470-10488.

Depaolo, D.J. 1988. Neodymium Isotope Geochemistry. Springer-Verlag, Berlin, 187p.

Deschamps, F., Godard, M., Guillot, S., & Hattori, K. 2013. Geochemistry of subduction zone serpentinites: A review. Lithos, 178, 96–127.

Dilek, Y. 2003. Ophiolite concept and its evolution. In: Dilek, Y., Newcomb, S. (Eds.), Ophiolite Concept and the Evolution of Geological Thought: Geological Society of America Bulletin Special Publication, 373, pp. 1–16.

Dilek, Y., Robinson, P.T. 2003. Ophiolites in Earth History, Special Pu. ed. Geological Society, London.

Eugster, H.P., Wones, D.R. 1962. Stability Relations of the Ferruginous Biotite, Annite. J. Petrol. 3, 82–125.

Eyuboglu, Y., Dilek, Y., Bozkurt, E., Bektas, O., Rojay, B., & Sen, C. 2010. Structure and geochemistry of an Alaskan-type ultramafic–mafic complex in the Eastern Pontides, NE Turkey. Gondwana Research, 18(1), 230–252.

Eyuboglu, Y., Santosh, M., Bektas, O., & Chung, S.-L. 2011. Late Triassic subduction-related ultramafic–mafic magmatism in the Amasya region (eastern Pontides, N. Turkey): Implications for the ophiolite conundrum in Eastern Mediterranean. Journal of Asian Earth Sciences, 42(3), 234–257.

Farahat, E.S., Helmy, H.M., 2006. Abu Hamamid Neoproterozoic Alaskan-type complex, south Eastern Desert, Egypt. J. African Earth Sci. 45, 187–197.

Farahat, E.S., 2008. Chrome-spinels in serpentinites and talc carbonates of the El Ideid-El Sodmein District, central Eastern Desert, Egypt: their metamorphism and petrogenetic implications. Chemie der Erde - Geochemistry 68, 193–205.

Ferreira, V.P., Sial, A.N., Jardim de Sá, E.F. 1998. Geochemical and isotopic signatures of Proterozoic Granitoids in terranes of the Borborema structural province, northeast Brazil. Journal of South American Earth Sciences, v. 11 (5) - 438-455.

Fleet, M.E., Barnett, R.L., 1978. Al^{IV}/Al^{VI} partitioning in calciferous amphiboles from the mine, Sudbury, Ontario. Canadian Mineralogist 16, 527–532.

Force, E.R., 1991. Geology of Titanium-Mineral Deposits. Geol. Soc. Am. Special paper 259. 112 p.

Franz, L., Wirth, R., 2000. Spinel inclusions in olivine of peridotite xenoliths from TUBAF seamount (Bismarck Archipelago/Papua New Guinea): evidence for the thermal and tectonic evolution of the oceanic lithosphere. Contributions to Mineralogy and Petrology. 140, 283–295.

Fuck, R.A., Brito Neves, B.B., Schobbenhaus, C., 2008. Rodinia descendants in South America. Precambrian Res. 160, 108–126.

Gao, J.F., Zhou, M.F., Lightfoot, P.C., Wang, C.Y., Qi, L., 2012. Origin of PGE-poor and Cu-rich magmatic sulfides from the Kalatongke deposit, Xinjiang, Northwest China. Economic Geology. 107, 481–506.

Gass, L.G. 1968. Is the Troodos massif of Cyprus a fragment of Mesozoic ocean floor? Nature. 221, 926–930.

Gass, I.G. 1980. The Troodos massif: Its role in the unravelling of the ophiolite problem and its significance in the understanding of constructive plate margin process. IN Panayistou, A. (ed.) Ophiolites. p. 23-35, Geol.Surv.Cyprus.

Gióia, S.M.C.L., Pimentel, M.M., 2000. The Sm-Nd isotopic method in the geocrhronology laboratory of the University of Brasilia. Anais da Academia Brasileira de Ciências v. 72, p. 219-245.

Gomes, H.A. and Santos, E.J. 2001.Mapa Geológico do estado de Pernambuco.E: 1:500.000. CPRM, Recife.

Gray, F., Page, N.J., Carlson, C.A., Wilson, S.A., Carlson, R.R., 1986. Platinium group element geochemistry of zoned ultramafic intrusive suites, Klamath Mountains. California and Oregon. Economic Geology 181, 1252–1260.

Green, T.H., Pearson, N.J., 1987. An experimental study of Nb and Ta partitioning between Ti-rich minerals and silicate liquids at high pressure and temperature. Geochimica et Cosmochimica Acta 51, 55–62.

Griffin, W.L. 1987. On the eclogites of Norway - 65 years lates. Mineralogical Magazine. v.51, p. 333-343.

Grütter, H.S., Gurney, J.J., Menzies, A.H., Winter, F., 2004. An updated classification scheme for mantle-derived garnet, for use by diamond explorers. Lithos. 77, 841–857.

Guimarães, I.P., Silva Filho, A.F., Almeida, C.N., Van Schmus, W.R., Araújo, J.M.M., Melo, S.C., Melo, E.B. 2004. Brasiliano (Pan-African) granitic magmatism in the Pajeú-Paraíba belt, Northeast Brazil: an isotopic and geochronological approach. Precambrian Research. 135, 23-53.

Hart, S.R., 1988. Heterogeneous mantle domains: signature, genesis and mixing chronologies. Earth and Planetary Science Letters. 90, 273–296.

Hattori, K.H., Guillot, S., Saumur, B.-M., Tubrett, M.N., Vidal, O., Morfin, S., 2010a. Corundum-bearing garnet peridotite from northern Dominican Republic: A metamorphic product of an arc cumulate in the Caribbean subduction zone. Lithos. 114, 437–450.

Hattori, K., Wallis, S., Enami, M., Mizukami, T., 2010b. Subduction of mantle wedge peridotites: Evidence from the Higashi-akaishi ultramafic body in the Sanbagawa metamorphic belt. Isl. Arc. 19, 192–207.

Hawkesworth, C.J., Hergt, J.M., McDermott, F., Ellam, R.M., 1991. Destructive margin magmatism and the contributions from the mantle wedge and subducted crust. Australian Journal of Earth Sciences. 38, 577–594.

Hawkesworth, C., Kelley, S., Turner, S., Le Roux, A., Storey, B., 1999. Mantle processes during Gondwana break-up and dispersal. J. Afr. Earth Sci. 28, 239–261.

Helmy, H.M., El Mahallawi, M.M., 2003. Gabro Akarem mafic–ultramafic complex, Eastern Desert, Egypt: a late Precambrian analogue of Alaskan-type complexes. Mineralogy and Petrology 77 (1–2), 85–108.

Helmy, H. M., El-Rahman, Y. M. A., Yoshikawa, M., Shibata, T., Arai, S., Tamura, A., & Kagami, H. 2014. Petrology and Sm-Nd dating of the Genina Gharbia Alaskan-type complex (Egypt): Insights into deep levels of Neoproterozoic island arcs. Lithos. doi: 10.1016/j.lithos.2014.03.028.

Helz, R.T., 1973. Phase relations of basalts in the melting range at PH_2O=5 kb as a function of oxygen fugacity: Journal of Petrology, v. 14, p. 249-302.

Himmelberg, G. R., & Loney, R. A. 1995. Characteristics and Petrogenesis of Alaskan-Type Ultramafic-Mafic Intrusions, Southeastern Alaska. Professional Paper 1564. U.S Geological Survey, 43 p.

Hofmann, A. W. 1988. Chemical differentiation of the Earth: the relationship between mantle, continental crust, and oceanic crust. Earth and Planetary Science Letters. 90(3), 297–314.

Hollanda, M.H.B.M., Marulanda, C.O., Archanjo, C.J. 2013. Proveniência U-/Pb in situ de H fem zircões detríticos de sucessões metassedimentares da Zona Transversal. In: III Simpósio da Borborema/XXV Simpósio de Geologia do Nordeste, 2013, Gravatá. Boletim de Resumos do XXV Simpósio de Geologia do Nordeste. Gravatá: SBG, 2013. p. 505-506.

Hou, T., Zhang, Z., Encarnacion, J., Santosh, M. 2012. Petrogenesis and Metallogenesis of the Taihe Gabbroic Intrusion Associated with Fe–Ti-Oxide Ores in the Panxi District, Emeishan Large Igneous Province, Southwest China. Ore Geology Reviews. 49, 109–27.

Irvine, T.N., 1967. Chromian spinel as a petrogenetic indicator. Part II, Petrogenetic applications. Canadian Journal of Earth Science 4, 72–103.

Irvine, T.N., 1974. Petrology of the Duke Island Ultramafic Complex Southeastern Alaska. Geol. Soc. Am. 244.

Ishiwatari, A., Ichiyama, Y., 2004. Alaskan-type plutons and ultramafic lavas in Far East Russia, Northeast China and Japan. International Geology Review. 46, 316–331.

Jahn, B., Caby, R. and Monie, P., 2001. The oldest UHP eclogites of the World: age of UHP metamorphism, nature of protoliths and tectonic implications. Chem. Geol., 178, 143–158.

James, O.B., 1971. Origin and emplacement of the ultramafic rocks of the Emigrant Gap Area, California. Journal of Petrology 12, 523–560.

Jan, M.Q., Windley, B.F., 1990. Chromium-spinel silicate chemistry in ultramafic rocks of the Jijal complex. Northwestern Pakistan. Journal Petrology 31, 667–715.

Janoušek, V., Farrow, C. M. & Erban, V. 2006. Interpretation of whole-rock geochemical data in igneous geochemistry: introducing Geochemical Data Toolkit (GCDkit). Journal of Petrology 47(6):1255-1259.

Jardim de Sá E.F., Macedo, M.H.E., Fuck, R.A. e Kawashita, K. 1992. Terrenos proterozóicos na Província Borborema e a margem norte do Cráton São Francisco. Rev. Bras. de Geoc. 22(4): 472-480.

Jardim de Sá E.F. 1994. A Faixa Seridó (Província Borborema, NE do Brasil) e o seu significado geodinâmico na cadeia Brasiliana/Pan-Africana. Tese de Doutorado, IGc - Universidade de Brasília. Brasília-DF. 804 p.

Jarrard, R.D., 1986. Terrane motion by strike-slip faulting of forearc slivers. Geology 14, 780–783.

Johan, Z. 2002. Alaskan-type complexes and their platinum-group element mineralization. In: Cabri, L.J., (Ed.), Geology, Geochemistry, Mineralogy and Mineral Beneficiation of Platinum-Group Elements. Canadian Institute of Mining, Metallurgy and Petroleum, pp. 669–719.

Kamenetsky, V., Crawford, A.J., Meffre, S., 2001. Factors controlling chemistry of magmatic spinel: an empirical study of associated olivine, Cr-spinel and melt inclusions from primitive rocks. J. Petrol. 42, 655–671.

Kelemen, P.B., Hanghoj, K., Greene, A.R., 2003. One view of the Geochemistry of Subduction-related magmatic Arcs, with an emphasis on Primitive Andesite and Lower Crust, in: Treatise on Geochemistry. pp. 594–649.

Kozuch, M. 2003. Isotopic and trace element geochemistry of early neoproterozoic gneissic and metavolcanic rocks in the Cariris Velhos orogen of the Borborema

Province, Brazil, and their bearing on tectonic setting. Tese (Doutorado)-Department of Geology, University of Kansas, Kansas, 199p.

Krause, J., Brügmann, G. E., & Pushkarev, E. V. 2007. Accessory and rock forming minerals monitoring the evolution of zoned mafic–ultramafic complexes in the Central Ural Mountains. Lithos, 95(1-2), 19–42.

Le Bas, M.J., 1962. The role of aluminum in igneous clinopyroxenes with relation to their parentage. Am. J. Sci. 260, 267–288.

Leake, B. E., Woolley, A. R., Arps, C. E. S., Gilbert, M. C., Grice, J. D., Hawthorne, F. C., … Whittaker, E. J. W. 1997. Nomenclature of amphiboles. The Canadian Mineralogist, 35, 219–246.

Leake, B. E., Woolley, A. R., Birch, W.D., Burke, E.A.J., Ferraris, G., Grice, J.D., Hawthorne, F. C., … Whittaker, E. J. W. 2004. Nomenclature of amphiboles: Additions and revisions to the International Association's amphibole nomenclature. American Mineralogist, 89, 883–887.

Lepage, L.D., 2003. ILMAT: an Excel worksheet for ilmenite–magnetite geothermometry and geobarometry. Comput. Geosci. 29, 673–678.

Leterrier, J., Maury, R.C., Thonon, P., Girard, D., Marchal, M., 1982.Clinopyroxene composition as a method of identification of the magmatic affinities of paleo-volcanic series. Earth and Planetary Science Letters 59, 139–154.

Li, Z.H., Gerya, T.V., 2009. Polyphase formation and exhumation of high- to ultrahigh-pressure rocks in continental subduction zone: numerical modeling and application to the Sulu ultrahigh-pressure terrane in eastern China. Journal of Geophysical Research 114, B09406.

Li, Z.X., Bogdanova, S.V., Collins, A.S., Davidson, A., De Waele, B., Ernst, R.E., Fitzsimons, I.C.W., Fuck, R.A., Gladkochub, D.P., Jacobs, J., Karlstrom, K.E., Lu, S., Natapov, L.M., Pease, V., Pisarevsky, S.A., Thrane, K., Vernikovsky, V., 2008. Assembly, configuration, and break-up history of Rodinia: a synthesis. Precambrian Research 160, 179–210.

Loucks, R.R., 1990. Discrimination of ophiolitic from nonophiolitic ultramafic-mafic allochthons in orogenic belts by the Al / Ti ratio in clinopyroxene. Geology 346–349.

Ludwig K.R. 1993. PBDAT. A computer program for processing Pb-U-Th isotope data. USGS Open File Report 88-542, 34 p.

Ludwig, K.R., 2001. User´s Manual for Isoplot/Ex version 2.47. A geochronological toolkit for Microsoft Excel. Berkeley Geochronology Center Special Publication 1a, 55 pp.

Macdonald, R., Hawkesworth, C.J., Heath, E., 2000. The Lesser Antilles volcanic chain: a study in arc magmatism. Earth Sci. Rev. 49, 1–76.

Mateinni, M., Junges, S. L., Dantas, E.L., Pimentel, M.M., Buhn, B. M., 2009. In situ zircon U-Pb and Lu-Hf isotope systematic on magmatic rocks: Insights on the crustal evolution of the Neoproterozoic Goiás Magmatic Arc, Brasília belt, Central Brazil. Gondwana Research. v. 16, p. 200-212.

McDonough, W.F., Sun, S.S., 1995. The composition of the Earth. Chem. Geol. 120, 223–253.

Medeiros, V. C., Jardim de Sá, E. F., Macedo, M. H. F., Souza, Z. S. 1993. Estruturas Tangenciais e Metagranitóides Transamazônicos na Faixa Salgueiro-Cachoeirinha a Oeste de Parnamirm-PE.. In: XV Simpósio de Geologia do Nordeste, Natal: Sociedade Brasileira de Geologia (SBG). p. 284-287.

Medeiros, V.C. 2004. Evolução geodinâmica e condicionamento estrutural dos terrenos Piancó- Alto Brígida e Alto Pajeú, Domínio da Zona Transversal, NE do Brasil. Tese de Doutorado, Programa de Pós-Graduação em Geodinâmica e Geofísica, Universidade Federal do Rio Grande do Norte, 200 pp.

Medeiros, V.C., Sá, E.F.J. de. 2009. O Grupo Cachoeirinha (Zona Transversal, NE do Brasil) redefinição e proposta de formalização. Rev. de Geologia UFC. V.22(2): 124-136.

Mendes, V.A. 1983. Projeto Cachoeirinha. Folha Bodocó: Mapas e Nota explicativa. Recife, CPRM, v.1.

Moores, E.M. 1982. Origin and emplacement of ophiolites. Reviews of Geophysics 20, 735–760.

Moraes, J.F.S. 1992. Petrologia das máficas e ultramáficas da sequencia vulcano-sedimentar de Monte Orebe, PE/PI. UFBA. Dissertação de mestrado. 98p.

Morimoto, N. 1988. Nomenclature of Pyroxenes. Mineralogy and Petrology, 39, 55–76.

Murray, C.G., 1972, Zoned ultramafic complexes of the Alaskan type: feeder pipes of andesitic volcanoes, in Shagam, R., and others, eds., Studies in earth and space sciences: Geological Society of America Memoir 132, p. 313-335.

Nascimento, M.A.L., Antunes, A.F., Galindo, A.C., Jardim de Sá, E.F. e Souza, Z.S. de. 2000. Geochemical Signature of the Brasiliano-Age Plutonism in the Seridó Belt,

Northeastern Borborema Province (NE Brazil). Revista Brasileira de Geociências, São Paulo, v.30, n.1, p. 161-164.

Nascimento, M.A.L. do, Medeiros, V.C de, Galindo, A.C. 2008. Magmatismo Ediacarano no Domínio Rio Grande do Norte, Província Borborema, NE do Brasil. Estudos Geológicos, UFPE, v.18, n.1, p. 4-25.

Neves, S.P., Mariano, G., Guimarães, I.P., Silva Filho, A.F., Melo, S.C. 2000. Intralithospheric differentiation and crustal growth: Evidence from the Borborema province, northeastern Brazil. Geology. 28(6): 519-522.

Neves, S.P. 2003. Proterozoic history of the Borborema Province (NE Brazil): correlations with neighboring cratons and Pan-African belts, and implications for the evolution of western Gondwana. Tectonics 22, 1352.

Neves, S.P., Monie, P., Bruguier, O., da Silva, J.M.R., 2012. Geochronological, thermochronological and thermobarometric constraints on deformation, magmatism and thermal regimes in eastern Borborema Province (NE Brazil).J. S. Am. Earth Sci., 38,129–146.

Oliveira, E.P., Windley, B.F., Araújo, M.N.C. 2010. The Neoproterozoic Sergipano orogenic belt, NE Brazil: A complete plate tectonic cycle in western Gondwana. Precambrian Research 181, 64–84.

Oliveira, R. G. 2008. Arcabouço geofísico, isostasia e causas do magmatismo cenozóico da Província Borborema e de sua margem continental (Nordeste do Brasil). Natal, 411p. Tese (Doutorado) - Programa de Pós-graduação em Geodinâmica e Geofísica, UFRN.

Pearce, J.A., and Cann, J.R., 1973, Tectonic setting of basic volcanic rocks determined using trace element analyses: Earth and Planetary Science Letters, v. 19, p. 290-300.

Pearce, J.A., 1975. Basalt geochemistry used to investigate past tectonic environments on Cyprus. Tectonophysics 25, 41–67.

Pearce, J.A., 1982. Trace element characteristics of lavas from destructive plate boundaries. In: Thorpe, R.S. (Ed.), Andesites. Wiley, Chichester, pp. 525–548

Pearce, J.A., Lippard, S.J., Roberts, S. 1984. Characteristics and tectonic significance of supra-subductionzoneophiolites.In:Kokelaar,B.P.,Howells,M.F.(Eds.), Marginal Basin Geology: Geological Society of London, Special Publication, 16, pp. 77–89.

Pearce, J. a., 2008. Geochemical fingerprinting of oceanic basalts with applications to ophiolite classification and the search for Archean oceanic crust. Lithos 100, 14–48.

Pearce, J.A., Robinson, P.T. 2010. The Troodos ophiolitic complex probably formed in a subduction initiation, slab edge setting. Gondwana Research. 18, 60–81.

Pettigrew, N. T., & Hattori, K. H. 2006. The Quetico Intrusions of Western Superior Province: Neo-Archean examples of Alaskan/Ural-type mafic–ultramafic intrusions. Precambrian Research, 149(1-2), 21–42.

Ringwood, A.E., 1990. Slab-mantle interactions: 3. Petrogenesis of intraplate magmas and structure of the upper mantle. Chemical Geology. 82, 187–207.

Ripley, E.M., 2009. Magmatic sulfide mineralization in Alaskan-type complexes. In: Li, C.S., Ripley, E.M., (Eds.), New Developments in Magmatic Ni–Cu and PGE Deposits, pp. 219–228.

Rollinson, H.R., 1993. Using Geochemical Data: Evaluation, Presentation, Interpretation. Longman Geochemistry Society, London. 352 p.

Rublee, V.J., 1994, Chemical petrology, mineralogy and structure of the Tulameen Complex, Princeton area, British Colombia. M.Sc. thesis: University of Ottawa, Canada, p.179.

Salem, a. K. a., Khalil, a. E., Ramadan, T.M., 2012. Geology, geochemistry and tectonic setting of Pan-African serpentinites of Um Salim-Um Salatit area, Central Eastern Desert, Egypt. Egypt. J. Remote Sens. Sp. Sci. 15, 171–184.

Sales, A.O., dos Santos, E.J., Lima, E.S., Santos, L.C.M.D.L., de Brito Neves, B.B., 2011. Evolução Petrogenética e Tectônica do Evento Cariris Velhos na Região de Afogados da Ingazeira (PE), Terreno Alto Pajeú , Província Borborema. Geol. USP. Série Científica 11, 101–121.

Santos E.J. & Brito Neves B.B. 1984. Província Borborema. In: Almeida F.F.M & Hasui T. O Pré-Cambriano do Brasil. São Paulo, Edgar Blucher, 123-186.

Santos, E. J. dos. 1995. O complexo granítico Lagoa das Pedras: acresção e colisão na Região de Floresta (Pernambuco), Província Borborema. Sao Paulo. 220 p. 2 mapas. Tese (Doutorado em Geociências, Área de Concentração Geoquímica Geotectônica)-Universidade de São Paulo. Instituto de Geociências.

Santos, E.J., 1996. Ensaio preliminar sobre terrenos e tectônica acrescionária na Província Borborema. in: Congresso Brasileiro DE Geologia, 39, Salvador. anais... Salvador: SBG, 7v., il., v.6, p.47-50.

Santos E.J. & Medeiros V.C. 1999. Constraints from granitic plutonism on proterozoic crustal grownth of the Zona Transversal Domain, Borborema Province, NE Brazil. Rev. Bras. de Geoc.29:73-84.

Santos E.J, Van Schmus W.R., Brito Neves B.B., Oliveira R.G., Medeiros V.C. 1999. Terrane and their boundaries in the Proterozoic Borborema Province, Northeast Brazil. In: Anais do VII Simpósio Nacional de Estudos Tectônicos (SNET), resumos expandidos. p.121-124.

Santos E.J., Ferreira C.A., Silva Júnior J.M.F. 2002. Geologia e recursos minerais do Estado da Paraíba: texto explicativo do mapa geológico e de recursos minerais. CPRM – Serviço Geológico do Brasil, 142p. 2 mapas. Escala 1:500.000.

Santos, E.J., Van Schmus, W.R., Kozuch, M., Brito Neves, B.B de. 2010. The Cariris Velhos tectonic event in Northeast Brazil. Journal of South American Eath Sciences, 29: 61-76.

Santos, E.J., Lira Santos, L.C.M., Guimarães, I.P., Armstrong, R. 2014. New age and tectonic constraints of the Riacho do Icó Suite, Alto Pajeú Terrane, Borborema Province based on Sm-Nd and u-Pb SHRIMP systematics. In: 9th South American Symposium on Isotope Geology. Boletim de Resumos. São Paulo: Usp, 2014. p. 159.

Santos, T. J. S., Amaral, W. S., Ancelmi, M. F., Pitarello, M. Z., Fuck, R. A., Dantas, E. L. 2014. U-Pb age of the coesite-bearing eclogite from NW Borborema Province, NE Brazil: Implications for western Gondwana assembly,Gondwana Research, doi:10.1016/j.gr.2014.09.013.

Seo, J., Oh, C. W., Choi, S. G., & Rajesh, V. J. 2013. Two ultramafic rock types in the Hongseong area, South Korea: Tectonic significance for northeast Asia. Lithos, 175-176, 30–39.

Silva Filho, M.A.; Nesi, J.R. & Mendes, V.A. 1985.Projeto Cachoeirinha. DNPM/CPRM, relat.final, v.1. (inédito).

Shaw, J.E., Baker, J.A., Menzies, M.A., Thirlwall, M.F., Ibrahim, K.M., 2003. Petrogenesis of the largest intraplate volcanic field on the Arabian plate (Jordan): a mixing lithosphere–asthenosphere source activated by lithospheric extension. J. Petrol. 44, 1657–1679.

Shervais, J.W. 2001. Birth, Death and Resurrection: The life Cycle of Supra Subduction Zone Ophiolites. G-Cubed: Geochemistry Geophysics Geosystems 2, Paper No. 2000GC000080.

Sisson, T.W., Grove, T.L., 1993. Experimental investigations of the role of H_2O in calc-alkaline differentiation and subduction zone magmatism. Contributions to Mineralogy and Petrology 113, 143–166.

Song, X.Y., Xie, W., Deng, Y.F., Crawford, A.J., Zheng, W.Q., Zhou, G.F., Deng, G., Cheng, S.L., Li, J., 2011. Slab break-off and the formation of Permian mafic–ultramafic intrusions in southern margin of Central Asian Orogenic Belt, Xinjiang, NW China. Lithos 127, 128–143.

Spandler, C., Hermann, J., Arculus, R., Mavrogenes, J., 2003. Redistribution of trace elements during prograde metamorphism from lawsonite blueschist to eclogite facies; implications for deep subduction-zone processes. Contrib. to Mineral. Petrol. 146, 205–222.

Stormer, J. C. Jr. 1983. The effects of recalculation on estimates of temperature and oxygen fugacity from analyses of multicomponent iron-titanium oxides. American Mineralogist. 68, 586-59.

Su, B., Qin, K., Sakyi, P.A., Malaviarachchi, S.P.K., Liu, P., Tang, D., Xiao, Q.-H., Sun, H., Ma, Y.-G., Mao, Q., 2012. Occurrence of an Alaskan-type complex in the Middle Tianshan Massif , Central Asian Orogenic Belt : inferences from petrological and mineralogical studies. Int. Geol. Rev. 54, 37–41.

Su, B.-X., Qin, K.-Z., Santosh, M., Sun, H., Tang, D.-M. 2013. The Early Permian mafic–ultramafic complexes in the Beishan Terrane, NW China: Alaskan-type intrusives or rift cumulates? J. Asian Earth Sci. 66, 175–187.

Su, B.-X., Qin, K.-Z., Zhou, M.-F., Sakyi, P.A., Thakurta, J., Tang, D.-M., Liu, P.-P., Xiao, Q.-H., Sun, H., 2014. Petrological, geochemical and geochronological constraints on the origin of the Xiadong Ural–Alaskan type complex in NW China and tectonic implication for the evolution of southern Central Asian Orogenic Belt. Lithos 200-201, 226–240. doi:10.1016/j.lithos.2014.05.005

Sun, S. S., McDonough, W. F. 1989. Chemical and isotopic systematics of oceanic basalts: implications for mantle composition and processes. Geological Society, London, Special Publications, 42(1), 313–345.

Taylor Jr., H.P., 1967. The zoned ultramafic complexes of the Southeastern Alaska, Part 4. III. In: Wyllie, P.J. (Ed.), Ultramafic and Related Rocks. John Willey, New York, pp. 96–118.

Thakurta, J., Ripley, E.M., Li, C.S. 2008. Geochemical constraints on the origin of sulfide mineralization in the Duke Island complex, southeastern Alaska. Geochemistry Geophysics Geosystems Q07003.

Thanh, N. X., Hai, T. T., Hoang, N., Lan, V. Q., Kwon, S., Itaya, T., & Santosh, M. 2014. Backarc mafic–ultramafic magmatism in Northeastern Vietnam and its regional tectonic significance. Journal of Asian Earth Sciences, 90, 45–60.

Tian, W., Chen, B., Ireland, T.R., Green, D.H., Suzuki, K., Chu, Z., 2011. Petrology and geochemistry of dunites, chromitites and mineral inclusions from the Gaositai Alaskan-type complex, North China Craton: Implications for mantle source characteristics. Lithos 127, 165–175.

Tindle, A.G., Webb, P.C., 1994. Probe-AMPH—A spreadsheet program to classify microprobe-derived amphibole analyses. Comput. Geosci. 20, 1201–1228. doi:10.1016/0098-3004(94)90071-X.

Van Schmus, W. R., Brito Neves, B.B. de, Hackspacher, P., Babinski, M. 1995. U/Pb and Sm/Nd geochronologic studies of the eastern Borborema Province, northeastern Brazil: initial conclusions. J. S. Am. Earth Sci. v.8, p.267–288.

Van Schmus, W.R., Oliveira., Silva Filho, A.F., Toteu, F., Penaye, J., Guimarães, I.P., 2008. Proterozoic links between the Borborema Province, NE Brazil, and the Central African Fold Belt. Geological Society, London, Special Publications. v. 294, p. 66-69.

Van Schmus, W. R., Kozuch, M., & de Brito Neves, B. B. 2011. Precambrian history of the Zona Transversal of the Borborema Province, NE Brazil: Insights from Sm–Nd and U–Pb geochronology. Journal of South American Earth Sciences, 31(2-3), 227–252.

Vauchez, A., Neves, S.P., Caby, R., Corsini, M., Egidio-Silva, M.. Arthaud, M., Amaro, V. 1995. The Borborema shear zone system, NE Brazil. Journal of South American Earth Sciences. v.8, p.247-266.

Wang, Z., Wilde, S. a., Wan, J., 2010. Tectonic setting and significance of 2.3–2.1Ga magmatic events in the Trans-North China Orogen: New constraints from the Yanmenguan mafic–ultramafic intrusion in the Hengshan–Wutai–Fuping area. Precambrian Res. 178, 27–42.

White, W.M., Duncan, R.A., 1996. Geochemistry and geochronology of the Society island: new evidence from deep mantle recycling. In: Basu, A., Hart, S.R. (Eds.), Earth Processes: Reading the Isotopic Code. : Geophysical Monograph, 95. AGU, Washington, DC, pp. 183–206.

Wilson, M. 1989. Igneous Petrogenesis - A global tectonic aproach. Springer, 466p.

Xiao, W.J., Huang, B., Han, C., Sun, S., Li, J., 2010. A review of the western part of the Altaids: a key to understanding the architecture of accretionary orogens. Gondwana Research 18, 253–273.

Xie, Z., Hattori, K., Wang, J., 2013. Origins of ultramafic rocks in the Sulu Ultrahigh-pressure Terrane, Eastern China. Lithos 178, 158–170.

Xie, W., Song, X.-Y., Chen, L.-M., Deng, Y.-F., Zheng, W.-Q., Wang, Y.-S., Ba, D.-H., Yin, M.-H., Luan, Y., 2014. Geochemistry Insights on the Genesis of the Subduction-Related Heishan Magmatic Ni-Cu-(PGE) Deposit, Gansu, Northwestern China, at the Southern Margin of the Central Asian Orogenic Belt. Econ. Geol. 109, 1563–1583.

Xiong, X.L., 2006. Trace element evidence for growth of early continental crust by melting of rutile-bearing hydrous eclogite. Geology 34, 945–948.

Yavuz, F., 2013. WinPyrox : A Windows program for pyroxene calculation classification and thermobarometry. Am. Mineral. 98, 1338–1359.

Yellappa, T., Venkatasivappa, V., Koizumi, T., Chetty, T. R. K., Santosh, M., & Tsunogae, T. 2014. The mafic-ultramafic complex of Aniyapuram, Cauvery Suture Zone, southern India: Petrological and geochemical constraints for Neoarchean suprasubduction zone tectonics. Journal of Asian Earth Sciences.

Zaccarini, F., Pushkarev, E., Garuti, G., 2008. Platinum-group element mineralogy and geochemistry of chromitite of the Kluchevskoy ophiolite complex, central Urals (Russia). Ore Geol. Rev. 33, 20–30.

Zhang, Z.C., Mao, J.W., Chai, F.M., Yan, S.H., Chen, B.L., Pirajno, F., 2009. Geochemistry of the Permian Kalatongke mafic intrusions, Northern Xinjiang, Northwest China: implications for the genesis of magmatic Ni–Cu sulfide deposits. Economic Geology 104, 185–203.

Zhang, M., Li, C., Fu, P., Hu, P., Ripley, E.M., 2011. The Permian Huangshanxi Cu–Ni deposit in western China: intrusive–extrusive association, ore genesis and exploration implications. Mineralium Deposita 46, 153–170.

Zimmer, M., Kroner, A., Jochum, K.P., Reischmann, T., Todt, W., 1995. The Gabal Gerf complex: a Precambrian N-MORB ophiolite in the Nubian Shield, NE Africa. Chemical Geology 123, 29–51.

Zindler, A., Hart, S., 1986. Helium: problematic primordial signals. Earth Planet. Sci. Lett. 79, 1–8.

3.9. APPENDIX

Appendix A - Fe-chromites from Bodocó mafic-ultramafic complex (BMUC)*

Analyse	LB-01	LB-01a	LB-01b	LB-01c	LB-01d	LB-01e	LB-01f	LB-05	LB-05a	LB-05b	LB-12	LB-12a	LB-12b	LB-12c	LB-12d	LB-11	LB-11a	LB-11b	LB-11c	LB-11d	LB-11e	LB-11f	LB-11g	LB-11h	LB-11i
Type	grain 1	grain 2	grain 2	grain 3	grain 4	grain 5	grain 6	grain 1	grain 1	grain1	grain 1	grain 1	grain 2	grain 2	grain 3	grain 1	grain2	grain 3	grain 4	grain 5	grain 6	grain 7	grain 8	grain 9	grain 10
	core	rim	core	core	core	core	core	core	rim	rim	core	rim	core	rim	core	core									
Rock	chromitite	chromitite	chromitite	chromitite	chromitite	chromitite	chromitite	chromitite	chromitite	chromitite	chromitite	chromitite	chromitite	chromitite	chromitite	chromitite	chromitite	chromitite	chromitite	chromitite	chromitite	chromitite	chromitite	chromitite	chromitite
Location	Lagoa das Baraunas	Lagoa das Baraunas	Lagoa das Baraunas	Lagoa das Baraunas	Lagoa das Baraunas	Lagoa das Baraunas	Lagoa das Baraunas	Lagoa das Baraunas	Lagoa das Baraunas	Lagoa das Baraunas	Lagoa das Baraunas	Lagoa das Baraunas	Lagoa das Baraunas	Lagoa das Baraunas	Lagoa das Baraunas	Lagoa das Baraunas	Lagoa das Baraunas	Lagoa das Baraunas	Lagoa das Baraunas	Lagoa das Baraunas	Lagoa das Baraunas	Lagoa das Baraunas	Lagoa das Baraunas	Lagoa das Baraunas	Lagoa das Baraunas
SiO_2																									
TiO_2	12.27	2.74	15.86	1.15	5.47	6.14	3.84	20.71	8.65	0.92	6.15	3.29	3.58	3.33	3.21	5.82	5.71	3.28	12.96	7.82	9.48	3.11	6.78	7.8	4.13
Al_2O_3	3.45	3.12	2.74	11.96	4.06	3.1	3,045	1.24	2.19	3.17	0.76	1.49	1.38	10.78	0.93	0.64	1.53	4.45	2.34	1.42	1.33	2.2	2.06	1.13	4.68
Cr_2O_3	20.88	24.08	20.91	21.08	24.27	24.86	27	15.47	21.87	23.95	26.87	32.05	25.73	15.25	31.41	32.27	32.97	28.24	25.1	32.46	31.57	34.68	31.51	32.51	27.14
FeO	41.49	28.96	45.8	34.13	35.74	36.25	33.53	49.32	38.44	31.27	35.29	32	30.83	28.44	33	35.96	35.6	31.48	41.15	37.48	38.81	32.84	35.08	37.86	32.2
Fe_2O_3	16.53	32.71	11.93	9.62	26.48	25.73	24.15	8.03	24.84	33.73	27.02	22.59	16.02	2.99	27.33	23.06	20.58	14.09	11.45	17.72	14.62	20.25	15.72	18.36	14.21
MnO	0.29		0.16	0.12	0.11	0.15	0.12	0.38	0.47	0.35	0.11	0.31	0.03	0.26	0.1	0.41	0.38	0.16	0.44	0.4	0.28	0.49	0.04	0.28	0.4
MgO	0.64	1.52	0.35	8.23	1.01	0.23	0.39	0.04	0.11	1.29	0.5	1.37	7.54	17.92	0.32	0.23	1.6	7.56	3.78	0.56	0.72	2.07	2.38	0.46	8.38
CaO																									
Na_2O																									
K_2O																									
BaO																									
ZnO	0.5	0.23	0.03	0.1	0.44	0.34	0.05	0.22		0.05	0.05	0.47	0.64	0.15	0.75		0.33	0.42	0.06						0.02
V_2O_3														95.63											
NiO	0.24						0.2		0.05	0.03	0.12	0.12		0.24		0.12	0.08	0.57	0.13			0.05			
Total	97.05	95.13	98.15	96.52	98.4	97.05	93.87	95.86	96.85	96.36	97.68	95.31	95.51		97.43	97.66	100.04	97.66	100.22	98.07	97.55	97.65	95.14	98.63	98.72
Si																									
Ti	0.35	0.08	0.45	0.03	0.15	0.18	0.11	0.6	0.25	0.03	0.18	0.1	0.1	0.08	0.09	0.17	0.16	0.09	0.35	0.22	0.27	0.09	0.19	0.22	0.11
Al	0.15	0.14	0.12	0.47	0.18	0.14	0.14	0.06	0.10	0.14	0.03	0.07	0.18	0.39	0.04	0.03	0.07	0.18	0.10	0.06	0.06	0.10	0.09	0.05	0.19
Cr	0.62	0.73	0.62	0.56	0.71	0.75	0.84	0.47	0.66	0.72	0.81	0.98	0.72	0.37	0.96	0.97	0.96	0.77	0.71	0.97	0.95	1.02	0.95	0.97	0.73
Fe^{3+}	0.47	0.95	0.34	0.24	0.74	0.74	0.72	0.23	0.72	0.07	0.78	0.66	0.43	0.07	0.79	0.66	0.57	0.37	0.31	0.50	0.42	0.57	0.45	0.52	0.36
Fe^{2+}	1.31	0.93	1.44	0.95	1.11	1.16	1.11	1.60	1.24	1.01	1.13	1.03	0.91	0.74	1.06	1.14	1.09	0.91	1.22	1.19	1.23	1.02	1.12	1.19	0.92
Mn																									
Mg	0.04	0.09	0.02	0.41	0.06	0.01	0.02	0.00	0.01	0.07	0.03	0.08	0.40	0.83	0.02	0.01	0.09	0.39	0.20	0.03	0.04	0.11	0.14	0.03	0.43
#Cr	80.52	83.91	83.78	54.37	79.78	84.27	85.71	88.68	86.84	83.72	96.43	93.33	80.00	48.68	96.00	97.00	93.20	81.05	87.65	94.17	94.06	91.07	91.35	95.10	79.35
#Mg	2.96	8.82	1.37	30.15	5.13	0.85	1.77	0.00	0.80	6.48	2.59	7.21	30.53	52.87	1.85	0.87	7.63	30.00	14.08	2.46	3.15	9.73	11.11	2.46	31.85

Appendix B - Recalculated pyroxenites compositions from BMUC mafic-ultramafic complexes recompiled from Beurlen (1988)*

Sample	BO305-1	BO305-2	BO305-3	BO305-4	BO305-5	BO305-6	BO305-7	BO305-8	BO305-9	BO305-10	BO103-1	BO103-2	BO103-3	BO103-4	BO103-5	BO103-6	BO103-7	BO103-8	BO103-9	BO436-1	BO436-2	BO436-3	BO436-4	BO436-5	BO436-6	BO436-7	BO436-8	BO436-9	BO436-10	BO436-11	BO436-12	BO436-13	BO436-14
Rock	Cpx tremolitite										Metapiroxenite																Eclogite						
Location	core	rim	core	rim	core	rim	symplectite	symplectite	symplectite	symplectite	core	core	rim	core	rim	core	rim	symplectite	symplectite	core	rim	core	rim	core	rim	symplectite	symplectite	symplectite	symplectite	symplectite	symplectite	symplectite	symplectite
SiO_2	53.85	52.44	53.60	51.96	51.45	51.08	55.00	54.66	55.08	54.88	53.63	53.91	53.63	54.15	53.17	53.37	54.16	53.86	55.14	56.33	60.63	56.43	56.39	56.55	56.47	52.63	51.87	56.29	57.16	56.31	55.86	56.27	56.61
TiO_2	0.00	0.00	0.26	0.00	0.77	1.32	0.00	0.00	0.00	0.00	0.00	0.00	0.18	0.00	0.28	0.00	0.00	0.03	0.14	0.00	0.00	0.00	0.30	0.00	0.00	0.44	0.00	0.23	0.00	0.00	0.00	0.13	0.15
Al_2O_3	0.37	0.90	0.76	0.81	1.37	1.68	0.00	0.00	0.00	0.00	1.33	1.68	1.94	2.01	1.86	1.42	2.08	0.83	2.09	10.12	12.97	11.14	10.95	10.83	11.08	4.90	22.86	10.19	11.94	21.65	22.82	10.54	11.08
Cr_2O_3	0.25	0.23	0.27	0.42	0.48	0.54	0.00	0.00	0.00	0.00	0.00	0.00	0.00	0.00	0.00	0.00	0.00	0.00	0.12	0.00	0.00	0.00	0.00	0.00	0.00	0.00	0.00	0.00	0.00	0.00	0.00	0.00	0.00
FeO	3.74	5.58	3.99	4.72	5.39	5.31	3.47	3.46	3.98	3.53	2.17	2.20	2.31	2.49	2.57	2.46	2.40	2.87	2.79	5.99	3.19	3.99	4.06	4.08	4.13	13.15	5.43	4.92	9.27	6.01	4.75	6.52	4.50
MnO	0.00	0.24	0.23	0.24	0.27	0.20	0.00	0.00	0.00	0.36	0.14	0.45	0.19	0.26	0.00	0.19	0.16	0.14	0.19	0.00	0.00	0.00	0.00	0.00	0.00	0.00	1.23	0.00	0.00	0.00	0.00	0.00	0.00
MgO	16.36	16.24	16.38	15.91	16.20	16.41	17.22	16.10	16.42	17.27	16.61	16.55	16.31	16.76	15.77	16.19	16.26	16.80	15.57	7.82	6.15	8.09	8.30	8.20	7.97	14.80	1.23	8.02	7.07	2.43	2.35	7.34	6.96
CaO	23.86	23.88	23.64	23.21	22.80	21.83	23.70	25.05	24.25	22.96	25.42	25.63	25.39	24.37	24.49	25.26	24.56	24.15	24.67	13.58	10.23	13.12	13.37	13.53	13.28	12.89	14.40	13.31	6.49	6.69	6.87	13.36	13.46
Na_2O	0.69	0.00	0.49	0.53	0.39	0.44	0.44	0.36	0.40	0.44	0.31	0.38	0.45	0.38	0.44	0.57	0.59	0.55	0.73	6.75	6.68	7.64	7.42	7.26	7.20	1.34	2.98	7.14	5.31	6.47	6.47	6.55	6.78
K_2O	0.00	0.00	0.00	0.41	0.00	0.00	0.00	0.00	0.00	0.00	0.00	0.00	0.00	0.08	0.00	0.00	0.00	0.00	0.21	0.00	0.00	0.00	0.00	0.00	0.00	0.15	0.37	0.00	0.00	0.77	0.49	0.00	0.00
Total	99.12	99.51	99.62	98.21	99.12	98.81	99.83	99.63	100.13	99.44	99.61	100.80	100.40	100.50	98.58	99.46	100.21	99.23	101.65	100.59	99.85	100.41	100.79	100.45	100.13	100.30	100.37	100.10	97.24	100.33	99.61	100.71	99.54
Si	1.98	1.94	1.97	1.93	1.90	1.90	2.00	2.00	2.01	2.01	1.96	1.94	1.94	1.96	1.96	1.95	1.96	1.97	1.98	2.00	1.96	1.98	1.98	1.99	2.00	1.93	1.66	2.00	1.93	1.80	1.77	2.00	2.00
Al^{IV}	0.02	0.04	0.03	0.04	0.06	0.07	0.00	0.00	0.00	0.00	0.05	0.06	0.06	0.04	0.04	0.06	0.04	0.03	0.02	0.00	0.04	0.02	0.02	0.01	0.00	0.07	0.34	0.00	0.07	0.20	0.23	0.00	0.00
Al^{VI}	0.00	0.00	0.00	0.00	0.00	0.00	0.00	0.00	0.00	0.00	0.01	0.01	0.02	0.04	0.04	0.01	0.05	0.01	0.06	0.42	0.45	0.44	0.43	0.44	0.46	0.15	0.52	0.43	0.41	0.62	0.63	0.44	0.46
Fe^{3+}	0.07	0.08	0.05	0.14	0.10	0.08	0.02	0.02	0.01	0.02	0.06	0.07	0.06	0.03	0.01	0.08	0.03	0.06	0.01	0.04	0.00	0.09	0.08	0.06	0.04	0.00	0.00	0.06	0.00	0.00	0.00	0.00	0.00
Fe^{2+}	0.05	0.09	0.07	0.00	0.07	0.09	0.08	0.09	0.11	0.09	0.01	0.00	0.01	0.04	0.07	0.00	0.04	0.03	0.07	0.14	0.49	0.03	0.04	0.06	0.09	0.42	0.70	0.09	0.66	0.61	0.61	0.20	0.20
Ti	0.00	0.00	0.01	0.00	0.02	0.04	0.00	0.00	0.00	0.00	0.00	0.00	0.01	0.00	0.01	0.00	0.00	0.00	0.00	0.00	0.00	0.00	0.00	0.01	0.00	0.01	0.00	0.01	0.00	0.00	0.00	0.00	0.00
Cr	0.01	0.01	0.01	0.01	0.01	0.02	0.00	0.00	0.00	0.00	0.00	0.00	0.00	0.00	0.00	0.00	0.00	0.00	0.00	0.00	0.00	0.00	0.00	0.00	0.00	0.00	0.00	0.00	0.00	0.00	0.00	0.00	0.00
Mn	0.00	0.01	0.01	0.01	0.01	0.01	0.00	0.00	0.00	0.01	0.00	0.01	0.01	0.01	0.00	0.01	0.01	0.00	0.01	0.00	0.00	0.00	0.00	0.00	0.00	0.00	0.03	0.00	0.00	0.00	0.00	0.00	0.00
Mg	0.90	0.89	0.90	0.88	0.89	0.91	0.94	0.88	0.89	0.94	0.90	0.89	0.88	0.90	0.87	0.88	0.88	0.92	0.83	0.41	0.30	0.42	0.43	0.43	0.42	0.81	0.06	0.43	0.36	0.12	0.11	0.39	0.37
Ca	0.94	0.95	0.93	0.93	0.90	0.87	0.93	0.98	0.95	0.90	0.99	0.99	0.98	0.94	0.97	0.99	0.95	0.95	0.95	0.52	0.35	0.49	0.50	0.51	0.50	0.51	0.49	0.51	0.24	0.23	0.23	0.51	0.51
Na	0.05	0.00	0.04	0.04	0.03	0.03	0.03	0.03	0.03	0.03	0.02	0.03	0.03	0.03	0.03	0.04	0.04	0.04	0.05	0.47	0.42	0.52	0.51	0.50	0.49	0.10	0.18	0.49	0.35	0.40	0.40	0.45	0.46
K	0.00	0.00	0.00	0.02	0.00	0.00	0.00	0.00	0.00	0.00	0.00	0.00	0.00	0.00	0.00	0.00	0.00	0.00	0.01	0.00	0.00	0.00	0.00	0.00	0.00	0.01	0.02	0.00	0.00	0.03	0.02	0.00	0.00
Wo	49.94	48.97	48.98	51.06	48.55	46.58	47.65	50.39	48.54	46.53	52.06	52.67	52.45	49.97	50.78	52.86	50.86	50.11	51.11	48.24	31.18	52.40	51.42	51.03	49.83	29.15	39.39	49.54	18.81	24.05	24.40	46.22	47.37
En	47.65	46.33	47.23	48.70	48.00	48.72	48.17	45.06	45.73	48.70	47.33	47.33	46.88	47.81	45.50	47.14	46.85	48.50	44.88	38.65	26.08	44.96	44.42	43.03	41.61	46.56	4.68	41.54	28.51	12.16	11.61	35.33	34.08
Fs	2.41	4.70	3.79	0.24	3.45	4.70	4.19	4.55	5.73	4.77	0.61	0.00	0.67	2.22	3.73	0.00	2.29	1.40	4.01	13.10	42.74	2.64	4.16	5.94	8.56	24.29	55.93	8.92	52.68	63.79	63.99	18.45	18.54
#Mg	95.22	90.76	92.55	99.55	93.22	91.16	91.94	90.82	88.86	91.10	98.69	100.00	98.54	95.55	92.44	100.00	95.33	97.24	91.83	74.73	37.90	94.43	91.37	87.96	82.84	65.75	7.77	82.36	35.11	16.02	15.33	65.71	64.78
Pyx. Grou	Ca-Mg-Fe	Ca-Mg-Fe	Ca-Mg-Fe	Ca-Mg-Fe	Ca-Mg-Fe	Ca-Mg-Fe	Ca-Mg-Fe	Ca-Mg-Fe	Ca-Mg-Fe	Ca-Mg-Fe	Ca-Mg-Fe	Ca-Mg-Fe	Ca-Mg-Fe	Ca-Mg-Fe	Ca-Mg-Fe	Ca-Mg-Fe	Ca-Mg-Fe	Ca-Mg-Fe	Ca-Mg-Fe	Ca-Na	Ca-Na	Ca-Na	Ca-Na	Ca-Na	Ca-Na	Ca-Mg-Fe	Ca-Na	Ca-Na	Ca-Na	Ca-Na	Ca-Na	Ca-Na	Ca-Na
Pyx. Name	Diopside	Diopside	Diopside	Diopside	Diopside	Augite	Diopside	Diopside	Diopside	Diopside	Diopside	Diopside	Diopside	Diopside	Diopside	Diopside	Diopside	Diopside	Diopside	Omphacite	Omphacite	Omphacite	Omphacite	Omphacite	Omphacite	Augite	Omphacite	Omphacite	Omphacite	Omphacite	Omphacite	Omphacite	Omphacite

* Classification scheme based on IMA (Morimoto et al., 1988)

Appendix C - Recalculation and classification scheme for amphiboles from BMUC* and FMUC (Riacho da Posse deposit)

Sample number	BO-436	BO-436	BO-436	BO-436	BO-103	BO-103	BO-103	BO-103	BO-103	BO-409	BO-409	BO-409	BO-409	BO-409	BO-409	BO-409	BO-409	BO-409	BO-409	BO-409	BO-409	BO-409	BO-409	RP-614*	RP-614	RP-614	RP-614	RP-614	RP-614
Rock type	eclogite				metapyroxenite					amphibolite														garnet amphibolite					
analyse	1	2	3	4	1	1	2	3	4	1	1	1	2	2	2	3	3	4	4	5	6	7	1	1	1	2	2	3	3
Location	fine symplectite	fine symplectite	fine symplectite	fine symplectite	core	rim	symplectite	symplectite	symplectite	core	core	core	core	core	rim	core	rim	core	rim	grain	grain	grain	core	rim	grain	core	rim	core	rim
SiO_2	50.26	44.45	48.21	56.85	51.63	57.09	55.59	54.52	55.39	45.76	41.28	43.67	40.86	43.70	42.90	45.69	44.89	44.39	42.24	45.52	45.75	45.33	46.53	41.35	46.20	41.63	40.06	46.06	42.38
TiO_2	0.19			0.25	0.25	0.10	0.11			0.34	0.27	0.26	0.31	0.36	0.31	0.42	0.28	0.42	0.51	0.27	0.32	0.32	0.42	0.35	0.39	0.17	0.28	0.32	0.18
Al_2O_3	10.04	18.82	11.62	8.09	7.89	5.41	1.96	3.68	3.87	10.80	11.99	11.54	16.11	12.69	12.52	10.02	10.40	10.19	12.99	10.62	10.21	13.25	9.49	14.31	10.20	14.95	16.56	10.11	12.73
FeO	12.32	18.33	16.60	17.84	6.47	4.67	5.36	5.11	5.99	17.47	18.83	19.36	19.51	18.38	18.57	18.51	18.09	17.94	18.21	18.02	17.27	18.54	17.75	18.83	17.75	17.97	18.54	17.86	18.45
MnO	0.14	0.22	0.17	0.15		0.23		0.34	0.34				0.23				0.19													
MgO	13.72	6.42	11.55	10.60	18.03	16.95	20.24	19.30	19.78	11.31	13.22	10.80	7.03	9.29	9.21	11.03	10.47	11.73	8.78	11.35	10.71	8.99	11.48	7.89	11.05	8.62	7.32	11.06	9.25
CaO	10.00	10.72	8.04	11.26	12.63	11.41	12.65	12.54	12.34	8.63	6.26	6.72	10.24	10.54	10.82	7.67	9.11	7.74	10.99	8.08	7.48	10.52	7.72	10.43	7.71	10.91	9.92	7.56	9.39
Na_2O	2.63	2.19	2.54	1.57	1.67	2.38	0.66	1.05	1.12	2.17	1.75	1.95	2.20	2.24	2.39	1.93	2.14	1.89	2.41	2.07	2.32	2.61	1.99	2.93	2.42	2.41	2.78	2.25	2.72
K_2O	0.45	0.09	0.44	0.57	0.22	0.08		0.06	0.19	0.87	0.49	0.14	0.48	0.26	0.20	0.49	0.34	0.44	0.28	0.59	0.76	0.44	0.62	0.31	0.76	0.41	0.24	0.47	0.26
NiO	0.18					0.27				0.23						0.34					0.20		0.38		0.34			0.23	0.22
Total	99.49	97.12	98.79	99.13	98.96	98.61	96.77	95.63	99.06	97.62	94.09	95.02	96.98	97.63	96.91	96.09	95.92	94.73	96.42	96.77	95.18	98.09	96.24	96.65	96.86	97.3	95.72	96.72	95.69
Si	7.01	6.30	6.73	7.55	7.19	7.81	7.80	7.68	7.60	6.58	6.08	6.37	6.10	6.44	6.40	6.60	6.61	6.47	6.37	6.56	6.71	6.54	6.70	6.25	6.67	6.20	6.04	6.67	6.34
Al^{IV}	0.99	1.70	1.27	0.45	0.81	0.19	0.20	0.32	0.40	1.42	1.92	1.63	1.90	1.56	1.60	1.40	1.39	1.53	1.63	1.44	1.29	1.46	1.30	1.75	1.33	1.80	1.96	1.33	1.66
Al^{vi}	0.66	1.44	0.64	0.82	0.48	0.69	0.13	0.29	0.23	0.41	0.16	0.35	0.94	0.65	0.60	0.30	0.42	0.22	0.67	0.36	0.48	0.79	0.31	0.80	0.40	0.83	0.98	0.39	0.58
Ti	0.02	0.00	0.00	0.02	0.03	0.01	0.01	0.00	0.00	0.04	0.03	0.03	0.03	0.04	0.03	0.05	0.03	0.05	0.06	0.03	0.04	0.03	0.05	0.04	0.04	0.02	0.03	0.03	0.02
Fe^{3+}	0.52	0.38	1.46	0.00	0.03	0.00	0.07	0.00	0.21	1.51	2.32	2.36	0.89	0.80	0.74	2.00	1.36	2.19	0.54	1.84	1.58	0.53	1.85	0.57	1.65	0.67	0.85	1.81	1.19
Fe^{2+}	0.92	1.79	0.48	1.98	0.73	0.53	0.56	0.60	0.47	0.59	0.00	0.00	1.55	1.46	1.57	0.23	0.87	0.00	1.76	0.33	0.54	1.71	0.29	1.81	0.49	1.56	1.49	0.35	1.12
Mn	0.02	0.03	0.02	0.02	0.00	0.03	0.00	0.04	0.04	0.00	0.00	0.00	0.03	0.00	0.00	0.00	0.02	0.00	0.00	0.00	0.00	0.00	0.00	0.00	0.00	0.00	0.00	0.00	0.00
Mg	2.85	1.36	2.40	2.10	3.74	3.46	4.23	4.05	4.05	2.42	2.90	2.35	1.56	2.04	2.05	2.37	2.30	2.55	1.97	2.44	2.34	1.93	2.46	1.78	2.38	1.91	1.65	2.39	2.06
Ni	0.02	0.00	0.00	0.00	0.00	0.03	0.00	0.00	0.00	0.03	0.00	0.00	0.00	0.00	0.00	0.04	0.00	0.00	0.00	0.00	0.02	0.00	0.04	0.00	0.04	0.00	0.00	0.03	0.03
Ca	1.49	1.63	1.20	1.60	1.88	1.67	1.90	1.89	1.81	1.33	0.99	1.05	1.64	1.67	1.73	1.19	1.44	1.21	1.77	1.25	1.18	1.63	1.19	1.69	1.19	1.74	1.60	1.17	1.50
Na	0.71	0.60	0.69	0.40	0.45	0.63	0.18	0.29	0.30	0.61	0.50	0.55	0.64	0.64	0.69	0.54	0.61	0.53	0.70	0.58	0.66	0.73	0.56	0.86	0.68	0.70	0.81	0.63	0.79
K	0.08	0.02	0.08	0.10	0.04	0.01	0.00	0.01	0.03	0.16	0.09	0.03	0.09	0.05	0.04	0.09	0.06	0.08	0.05	0.11	0.14	0.08	0.11	0.06	0.14	0.08	0.05	0.09	0.05
Total	17.28	17.25	16.97	17.04	17.37	17.06	17.08	17.17	17.15	17.09	16.99	16.72	17.37	17.35	17.46	16.82	17.11	16.82	17.53	16.93	16.98	17.44	16.86	17.61	17.01	17.52	17.46	16.89	17.34
Amphibole gro	Ca	Ca	Na-Ca	Ca	Ca	Ca	Ca	Ca	Ca	Ca	Ca	Ca	Ca	Ca	Ca	Ca	Ca	Ca	Ca	Ca	Ca	Ca	Ca	Ca	Na-Ca	Ca	Ca	Ca	Ca
$Mg/(Mg+Fe^{2})$	0.76	0.43	0.83	0.51	0.84	0.87	0.88	0.87	0.89	0.80	1.00	1.00	0.50	0.58	0.57	0.91	0.73	1.00	0.53	0.88	0.81	0.53	0.90	0.50	0.83	0.55	0.52	0.87	0.65
Amphibole nar	Mg-Hbl	Fe-tschermakitic Hbl	barroisite	actinolite	Mg-Hbl	actinolite	actinolite	actinolite	actinolite	Mg-Hbl	tscherma kite	tscherma kitic Hbl	tscherma kite	tscherma kitic Hbl	tscherma kitic Hbl	Mg-Hbl	Mg-Hbl	tscherma kitic Hbl	ferroan pargasiti c Hbl	Mg-Hbl	Mg-Hbl	Mg-Hbl	Mg-Hbl	ferroan pargasitic Hbl	barroisit e	ferroan pargasite	tscherma kite	Mg-Hbl	tscherma kitic Hbl

No. of oxygens = 23 *raw data of BMUC (BO prefix) and FMUC (RP prefix) analyses were extracted from Beurlen (1988) ** Abbrevs. Hbl - Hornblende;

Appendix D - Whole-rock chemistry data for Rocks of BMUC and FMUC (Riacho da Posse)

Sample	Locality	Rock type	SiO_2	TiO_2	Al_2O_3	Fe_2O_3	FeO	MnO	MgO	CaO	Na_2O	K_2O	P_2O_5	Cr_2O_3	Ni	Co	V	Cu	Rb	Ba	Sr	Zr	Y	La	Ce	Nd	Sm	Eu	Gd	Dy	Ho	Er	Yb	Lu
RP-603B	Riacho da Posse	Dunite	39.00	5.30	16.50	3.10	12.35	0.15	8.00	9.90	0.96	0.60	0.01	0.069	420	95	500	125	29	190	450	21	<10	1.5	2.8	2.4	0.50	0.49	0.50	0.36	0.06	0.20	0.25	0.05
RP-694	Riacho da Posse	Olivine cumulate	26.10	10.40	0.63	14.00	18.70	0.71	22.40	0.28	0.07	0.01	-0.01	0.235	890	300	800	70	<10	570	<10	39	12	0.89	1.9	0.91	0.25	0.11	0.20	0.27	0.07	0.23	0.23	0.07
RP-6103	Riacho da Posse	Olivine cumulate	15.90	19.40	2.00	12.70	26.05	0.30	14.10	0.63	0.23	0.01	0.03	0.246	1200	400	1120	1120	<10	360	<10	74	12	0.82	1.3	1.00	0.20	0.10	0.23	0.21	0.05	0.18	0.33	0.07
RP-6105	Riacho da Posse	Olivine cumulate	23.80	8.90	1.80	18.40	21.50	0.30	19.20	0.38	0.04	0.02	0.01	0.235	420	280	1400	182	<10	240	<10	26	<10	1.2	2.4	1.2	0.42	0.17	0.50	0.38	0.08	0.20	0.23	0.14
RP-625	Riacho da Posse	Olivine cumulate	38.60	10.80	2.20	5.10	23.40	0.21	15.00	0.38	0.05	1.30	-0.01	0.179	880	146	800	520	64	120	<10	39	<10	0.69	1.4	0.97	0.20	0.13	0.29	0.24	0.06	0.29	0.46	0.05
RP-659	Riacho da Posse	Olivine cumulate	20.60	21.80	0.34	12.40	20.25	0.31	18.40	0.11	0.01	0.02	0.01	0.087	690	200	1120	125	<10	110	<10	60	<10	0.67	1.4	0.75	0.16	0.10	0.18	0.10	0.02	0.07	0.20	0.05
RP-691B	Riacho da Posse	Olivine cumulate	13.80	25.30	1.50	13.70	25.80	0.26	13.20	0.20	0.05	0.03	0.02	0.295	750	220	1120	900	<10	140	<10	46	17	0.99	2.4	1.2	0.33	0.09	0.23	0.15	0.03	0.12	0.11	0.02
RP-641	Riacho da Posse	Olivine cumulate	28.10	9.40	0.10	15.50	18.60	0.31	22.00	0.19	0.04	0.01	-0.01	0.007	910	165	550	150	31	54	<10	20	<10	0.89	1.7	0.79	0.21	0.10	0.20	0.18	0.05	0.14	0.19	0.05
RP-626	Riacho da Posse	Olivine cumulate	27.80	20.20	1.90	2.50	29.00	0.33	13.30	1.40	0.03	0.41	0.02	0.144	2000	380	940	1100	22	970	<10	67	11	1.1	2	1.1	0.39	0.11	0.40	0.30	0.06	0.19	0.34	0.07
RP-633	Riacho da Posse	Olivine cumulate	41.20	9.50	1.30	5.10	20.75	0.30	17.30	0.43	0.09	0.71	-0.01	0.161	530	172	800	550	39	110	<10	25	<10	0.84	1.6	1.0	0.22	0.10	0.25	0.26	0.06	0.27	0.25	0.07
RP-6472	Riacho da Posse	Olivine cumulate	33.40	12.20	1.20	3.30	23.75	0.26	16.62	0.35	0.28	0.55	-0.01	0.071	665	192	700	580	31	75	<10	32	<10	0.69	1.7	1.1	0.12	0.11	0.21	0.24	0.06	0.38	0.26	0.06
BO-315	Bodocó	Tremolite-pyroxenite	52.30	0.88	2.60	1.40	6.85	0.17	16.60	16.50	0.42	0.13	0.02	0.411	320	62	2600	120	<10	78	50	42.0	17	5.8	12.1	11.3	3.0	0.91	3.0	2.1	0.40	0.95	0.69	0.09
BO-103	Bodocó	Tremolite-pyroxenite	47.30	0.41	4.50	0.18	3.35	15.00	12.20	23.10	1.80	0.07	0.02	0.009	42	11	1240	10	<10	24	790	16	14	25.8	47.2	22.8	4.5	0.43	2.6	1.4	0.29	0.85	0.50	0.08
BO-108	Bodocó	Tremolite-pyroxenite	45.50	0.57	2.00	2.00	0.90	0.09	18.70	24.50	0.05	0.01	2.20	0.015	210	20	220	38	<10	24	15	22	32	27.8	41.2	20.0	4.2	0.83	3.8	2.7	0.54	1.6	0.8	0.09
RP-697A	Riacho da Posse	Metahornblendite	36.90	8.90	8.40	3.00	21.70	0.18	9.10	7.20	1.10	1.00	-0.01	0.08	445	118	800	100	40	150	32	46	<10	1.5	3.9	4.0	1.7	0.52	1.2	0.72	0.13	0.38	0.36	0.10
RP-658A	Riacho da Posse	Metahornblendite	36.00	6.70	12.60	3.50	19.05	0.20	8.60	8.40	1.60	0.89	-0.01	0.038	780	124	940	35	27	150	120	260	37	11.3	22.5	12.6	3.0	1.1	3.1	3.1	0.61	2.0	2.0	0.33
RP-658X	Riacho da Posse	Metahornblendite	39.00	5.10	21.80	6.80	10.40	0.10	7.60	3.50	1.40	1.30	-0.01	0.089	1250	200	940	40	72	290	1240	102	17	2.9	6.1	5.3	1.1	0.53	0.90	0.83	0.16	0.60	0.67	0.13
RP-637	Riacho da Posse	Metahornblendite	37.20	1.30	12.00	2.60	22.50	0.20	10.80	5.40	0.95	2.50	-0.01	0.037	1400	480	380	1100	120	550	14	300	40	45.7	95.9	39.2	7.4	1.1	6.5	4.9	0.94	2.5	1.9	0.27
RP-607B	Riacho da Posse	Metahornblendite	39.30	5.20	13.80	3.40	14.20	0.17	8.50	10.90	1.80	0.50	0.01	0.095	420	79	620	26	<10	93	159	30	17	1.5	3.3	4.0	1.1	0.42	0.93	0.87	0.2	0.63	0.45	0.07
RP-6106	Riacho da Posse	Metahornblendite	35.80	6.10	2.50	11.10	16.50	0.25	18.20	3.20	0.09	0.58	0.05	0.199	340	200	940	210	24	150	11	29	10	2.0	2.9	2.6	0.96	0.20	0.86	0.77	0.20	0.53	0.36	0.08
RP-0002	Riacho da Posse	Garnet amphibolite	40.90	2.10	16.00	6.20	11.45	0.40	7.80	12.60	0.62	0.47	0.17	0.021	145	61	260	11	10	140	200	126	39	12.0	22.6	13.4	3.8	1.4	3.3	2.3	0.38	0.90	0.48	0.08
BO-126	Bodocó	Eclogite	46.1	1.8	17.9	1.9	7.45	0.14	6.9	12.9	2.1	0.34	0.16	0.019	96	48	320	28	<10	240	860	110	27	14.6	30.8	18.7	4.2	1.3	3.3	2.3	0.54	1.4	0.93	0.16
BO-309	Bodocó	amphibolite	40.9	4.9	12.2	3.3	13	0.3	8.6	11.5	1.7	0.81	0.55	0.085	170	100	500	300	13	380	170	176	38	27.9	88.9	34.4	6.8	3.2	6	3.9	0.62	1.9	1.3	0.21
BO-322	Bodocó	amphibolite	37.90	12.00	11.90	2.90	13.20	0.18	8.50	8.90	1.70	0.46	0.02	0.07	160	116	500	470	110	230	96	72	16	2.4	4.0	3.6	1.0	0.42	2.94	1.00	0.24	0.68	0.56	0.07
RP-602	Riacho da Posse	Metanorthosite	44.20	0.79	26.10	1.82	2.95	0.06	1.40	16.20	2.20	0.10	0.05	0.019	52	16	180	6	<10	45	460	12	<10	4.50	9.0	5.8	1.4	0.69	1.1	1.0	0.21	0.66	0.55	0.09
RP-0001	Riacho da Posse	Metanorthosite	44.60	0.50	30.60	0.79	2.35	0.05	1.50	17.00	1.50	0.07	0.05	0.035	37	11	152	8	<10	51	410	<10	<10	1.1	2.1	1.5	0.39	0.39	0.28	0.24	0.03	0.1	0.09	0.03

*** Prefixes BO and RP are data compiled from Beurlen (1998)**

4. SÍNTESE CONCLUSIVA SOBRE A DISSERTAÇÃO

O conjunto de dados obtidos e reinterpretados para os complexos metamáfico-ultramáficos de Floresta e Bodocó remetem a um protólito ígneo originado por acumulação de um magma hidratado em uma zona de suprasubducção, em provável ambiente de arco/retro-arco ou fazer parte de complexos da região de subarco. A colocação das intrusões pode se dar ao longo de uma das principais zonas de falha geradas como, por exemplo, numa extensão gerada em ambiente de retroarco ou como intrusões injetadas no próprio embasamento.

A idade de cristalização para o Complexo ultramáfico de Floresta (Suíte Serrote das Pedras Pretas) em cerca de 945 Ma configurando-se como intrusões já que, as idades de cerca de 995 Ma obtidas para sequencias vulcânicas (Lagoa das Contendas - Santos et al., 2010) e gnáissicas (Brasilino et al., no prelo) obtidas na parte sul desta área o que pode sugerir a existência de relictos de um arco remanescente separados por uma bacia de retroarco (Complexo São Caetano?) no qual o *front* vulcânico mais recente estaria preservado a norte nas regiões de Manaíra/ Princesa Isabel com idades eruptivas iniciais em torno de ~975 Ma (Kozuch, 2003). As idades mais jovens obtidas para os complexos ultramáficos reforça a possibilidade de serem complexos do tipo-Alaska uma vez que, preferencialmente, são gerados próximo ao fim da subducção. Podem compor, alternativamente, pequenas intrusões pós-orogênicas tipo as que ocorrem no Central Asian Orogenic Belt (China) mineralizadas em Ni-Cu sulfetado ou Fe-Ti (interação de pluma com componente de subducção – Emeishan LIP), estes últimos possuem depósitos de Fe-Ti na parte ultramáfica dos complexos. Na área análoga da Faixa Sergipana, a intrusão pós-tectônica formada pelo Granito Serra Negra (~950 Ma) no arco continental Poço Redondo (980-960 Ma) reforça essa sugestão.

A idade U-Pb obtida, o parametro εNd (t) de +1,8 e idades-modelo entre 1,28 - 1,6 Ga são compatíveis com um evento juvenil de idade Cariris Velhos, onde a natureza deste tipo de intrusão é bastante semelhante a um ambiente de arco continental baseado em concentrações relativas de elementos imóveis, minerais diagnósticos tais como espinélios e clinopiroxênios.

A idade U-Pb em zircão obtida para o sobrecrescimento metamórfico materializado nas bordas destes que possuem baixas razões Th/U (0,008-0,038) em um amostra de meta-horblendito grosso da mina Serrote das Pedras Pretas é relacionada à Orogenese Pan-Africana/Brasiliana de 625 ± 6 Ma, cuja interpretação possui cronocorrelatos tanto em relação ao evento eclogítico (fechamento do oceano Pharusiano-Goiás) quanto a um metamorfismo de alto grau (que neste caso estaria relacionado aos estágios retro-eclogíticos).

O Complexo de Monte Orebe (distante menos de 200 km de Bodocó e 380 km de Floresta) interpretado como relictos de crosta oceânica preservada formada entre o Cráton do São Francisco e o Bloco Pernambuco-Alagoas (Província Borborema) em cerca de ~820 ± 120 Ma (Caxito et al., 2014) é sugestivo da possibilidade de uma bacia oceânica de idade similar ter originado uma zona de subducção do tipo Pacífico envolvendo estas rochas durante o evento brasiliano/Cariris Velhos.

Argumentamos que essas rochas de alta pressão podem representar no contexto da fusão do supercontinente Gondwana occidental, o fechamento do braço de uma bacia oceanica neoproterozoica ao longo dos limites sul e sudoeste dos Domínios Alto Pajeú, Piancó-Alto Brígida, Alto Moxotó e Bloco Pernambuco-Alagoas. Rochas de natureza eclogitica e granulitica de alta pressão, sobretudo na Domínio Ceará Central, vem sendo correlacionados com suas contrapartes na África podendo linkar um grande cinturão collisional que culminou com o fechamento de um grande oceano "Pharusian-Goiás".

Os depósitos de Fe-Ti inclusos como xenolitos dentro da Suíte granítica de Riacho do Icó possuem mineralizações primária viáveis economicamente, que tiveram enriquecimento secundário relacionado a fluidos ígneos hidrotermais tardios que cortam as áreas das minas e percebe-se alteração do tipo cloritização e talco-carbonato nas rochas ultramáficas com remobilização dos óxidos em pequenos veios bem como expurgações e exsoluções que culminaram com formação de grãos de ilmenita livres de lamelas do tipo *trellis* dentre outras. O enriquecimento sob a forma de rutilo de até 12% são comumente atribuidos à condições de alta pressão podendo formarem depósitos subeconôomicos.

5. REFERÊNCIAS DOS CAPÍTULOS 1 a 3

Albarède, F., Télouk, P., Blichert-Toft, J., Boyet, M., Agranier, A., Nelson, B., 2004. Precise and accurate isotopic measurements using multiple-collector ICPMS. Geochim. Cosmochim. Acta 68, p. 2725-2744.

Accioly, A.C. de A. 2000. Geologia, geoquímica e significado tectônico do Complexo Metanortosítico de Passira: província Borborema, nordeste brasileiro. Tese (Doutorado em Geoquímica e Geotectônica)-IG, Usp, São Paulo,168p.

Accioly, A.C.A., Santos, C.A., Rodrigues, J.B, Brito Neves, B.B., Santos, E.J. 2007. Idade Cariris Velhos do Complexo Vertentes na região de Pesqueira-PE, Terreno Rio Capibaribe, Província Borborema. In: XII Simpósio de Geologia do Nordeste. Boletim de resumos, p. 234.

Almeida, C. N. 1995. Estudo das rochas metamáficas de Itatuba (PB) e das ocorrências de Fe-Ti Aassociadas. Recife.131p. Dissertação (Mestrado)-Centro de Tecnologia, Universidade Federal de Pernambuco.

Almeida, C.N., Guimarães, I.P., Beurlen, H., Topitsch,W. 2009. Caracterização Geoquímica de Rochas Metamáficas e Metaultramáficas da Faixa Pajeú-Paraíba, Província Borborema-NE do Brasil. Anuário do Instituto de Geociências (UFRJ. Impresso), v. 32, p. 46-61.

Almeida, F. F. M., Brito Neves, B.B. Fuck, R.A. 1977. Províncias estruturais brasileiras. In: SIMPÓSIO DE GEOLOGIA DO NORDESTE, 8, Campina Grande. Atas do... Campina Grande: SBG. Núcleo Nordeste, p.363-391.

Almeida F.F.M.de, Hasui Y., Brito Neves B.B., Fuck R.A. 1981. Brazilian structural provinces: an introduction. Earth-Sci.Reviews, 17:1-21.

Barbosa O, Baptista M.B., Coelho J.A.L., et al., 1970, Geologia econômica de parte da região do Médio São Francisco. DNPM/DFPM, Bol. 140, 97p.

Beurlen, H. (1988). Fazenda Esperança (Bodocó) e Riacho da Posse (Floresta): Duas ocorrências atípicas de Fe-Ti no Estado de Pernambuco. Universidade Federal de Pernambuco. Tese de livre docência. 72p.

Beurlen, H., & Villarroel, S. (1990). Petrografia de duas ocorrências de provável eclogito em Bodocó e Floresta no estado de Pernambuco, Brasil. Revista Bras. de Geoc, 20, 111–121.

Beurlen, H., Silva, A. F. Da, Guimarães, I. P., & Brito, S. B. (1992). Proterozoic C-type eclogites hosting unusual Ti-Fe-Cr-Cu mineralization in northeastern Brazil. Precambrian Research, 58, 195–214.

Bittar S.M.B., 1998, Faixa Piancó-Alto Brígida: Terreno tectonoestrutural sob regimes metamórficos e deformacionais constrastantes. Tese de Doutourado, IG/USP, 126p.

Bittar, S. M. B. , Guimarães, I. P. , Campos Neto, M. C. , Kozuch, M., Accioly, A.C.A., Lima, E.S. 2001. Geoquímica preliminar dos metabasáticos do complexo Riacho Gravata, domínio Tectonico Rio Pajeu, PE - Brasil. Estudos Geológicos, Recife: Universidade Federal de Pernambuco. Centro de Tecnologia e Geociências, v.11, p. 53-66.

Black, L.P., Kamo, S.L., Allen, C.M., Davis, D.W., Aleinikoff, J. N., Valley, J.W Mundil, R., Campbell, I.H., Korsch, R.J., Williams, I.S., Foudoulis, C., 2004. Improved $^{206}Pb/^{238}U$ microprobe geochronology by the monitoring of a trace-element-related matrix effect, SHRIMP, ID-TIMS, ELA-ICP-MS and oxygen isotope documentation for a series of zircon standards. Chemical Geology, v. 205, p. 115-140.

Brasilino, R.G., Miranda, A.W de A., Lages, G.A., Rodrigues, J.B. 2009. Ortognaisses da Suíte Carnoió-Caturité: Magmatismo do final do estateriana no Domínio da Zona Transversal, Província Borborema. In: XXIII Simp. de Geol. do Nordeste, Fortaleza. Boletim de resumos.

Brasilino, R.G., Miranda, A.W de A., Lages, G.A., Rodrigues, J.B. 2012. Petrography, geochemistry and geochronology (U-Pb) of metamafic rocks from Cabaceiras Complex, Northeast, Brazil: Geodinamic implication. In: VIII SSAGI, Medelin, Colombia. CD de resumos.

Brasilino, R.G., Miranda, A.W.A., Morais, D.M.F de, Lages, G.A. 2014. Programa Geologia do Brasil. Carta Geológica Escala 1:100.000: Folha Mirandiba SC.24-X-A-I. CPRM/Serviço Geológico do Brasil.

Brasilino, R.G. & Miranda, A.W de A. no prelo. Geologia e Recursos Minerais da Folha Santa Cruz do Capibaribe (SB.24-Z-D-VI). CPRM/SBG. Programa Geologia do Brasil. xx p.

Brito Neves B.B. 1975. Regionalização geotectônica do Pré-cambriano Nordestino. Tese de Doutorado, IGc - Universidade de São Paulo. São Paulo-SP. 198 p.

Brito Neves B.B. 1983. O Mapa Geológico do Nordeste Oriental do Brasil, Escala 1:1 000000. Tese de Livre Docência, Instituto de Geociências da Univ. de S. Paulo, 171p.

Brito Neves B.B., Van Schmus W.R, Santos E.J, Campos Neto M.C.C. 1995. O Evento CaririsVelhos na Província Borborema: integração de dados, implicações e perspectivas. Rev. Bras. de Geoc., 25:151-182.

Brito Neves B.B., Santos E.J., Van Schmus W.R. 2000. Tectonic history of the Borborema Province. In: Cordani U.G. et al.. (eds). Tectonic evolution of the South America. 31st International Geological Congress, p.151-182.

Brito Neves B.B., Campos Neto M.C.C., Van Schmus W.R., Santos E.J. 2001a. O Sistema Pajeú-Paraíba e o Maciço São José do Campestre no Leste da Borborema. Rev. Bras. de Geoc. 31:173-184.

Brito Neves B.B., Campos Neto M.C.C., Van Schmus W.R., Fernandes M.G.G., Souza S.L. 2001b. O Terreno Alto Moxotó no Leste da Paraíba (Maciço Caldas Brandão). Rev. Bras. de Geoc. 31:185-194.

Brito Neves B.B., Van Schmus W.R., Kozuch M., Santos E:J., Petronilho L. 2005. A Zona Tectônica Teixeira Terra Nova –ZTTTN –Fundamentos da Geologia Regional e Isotópica. Revista do Instituto de Geociências – USP. Série Cientifica. 5:57-80.

Brito, M.F.L. & Cruz, R.F. 2009. O Complexo Metavulcanossedimentar da região de Salgueiro/PE, Zona Transversal, Província Borborema, NE do Brasil. In: SBG, Simpósio de Geologia do Nordeste, 24., 2009. Fortaleza. Anais... p. 201.

Bühn, B. M., Pimentel, M, M., Matteini, M., Dantas, E.L., 2009. High spatial resolution analysis of Pb and U isotopes for geochronology by laser ablation multi-collector inductively coupled plasma mass spectrometry (LA-MC-ICP-MS. Anais da Academina Brasileira de Ciências. v. 81, p. 1-16.

Campelo, R. C. Análise de terrenos na porção setentrional da Província Borborema, NE do Brasil: Integração de dados geológicos e gravimétricos. Natal, 1999. 130p. Dissertação (Mestrado) - Programa de Pós-graduação em Geodinâmica e Geofísica, UFRN, 1999.

Campos Neto M.C., Brito Neves B.B. & Bittar S.M.B., 1994, Domínio tectônico Rio Pajeú: orogêneses superpostas no ciclo Brasiliano/Panafricano. Relatório Científico, FAPESP, Proc. Geoc. 92/2079, 62p. (inédito).

Carmona, L. C. M. 2006. Estudo geológico e geoquímico da região compreendida entre Fagundes e Itatuba (PB), Terreno Alto Moxotó, Nordeste do Brasil. Recife. 337p. Tese (Doutorado) - Centro de Tecnologia e Geociências, Universidade Federal de Pernambuco.

Coleman, R.G., Lee, D.E., Beatty, L.B., Brannock, W. 1965. Eclogites and eclogites: their differences and similarities. Geol. Soc. Am. Bull. 76: 483-508.

Coney, P.J., Jones, D.L, Monger, J.W.H. 1980. Cordilleran suspect terranes. Nature, v.288, p.329-333.

Coney, P. J. Structural aspects of suspect terranes and accretionary tectonics in western North America. Journ. Strut. Geol., v.11, p.107-125, 1989.

Corsini, M., Vauchez, A., Archanjo, C.J. 1991. Strain transfer at continental scale from a transcurrent shear zone to a transpressional fold belt: The Patos-Seridó System, Northeastern Brazil. Geology, 19: 586-589.

Cruz, R.F. da., Medeiros, V.C., Freire, A.G. 2010. Geologia da Folha Parnamirim - SC.24-V-B-II (Escala 1:100.000). In: 45 CONGRESSO BRASILEIRO DE GEOLOGIA, 2010, Belém, anais, 2010.

Dantas, E.L. 1996. Geocronologia U-Pb e Sm-Nd de Terrenos Arqueanos e Paleoproterozóicos do Maciço Caldas Brandão, NE do Brasil. Tese de Doutorado. UNESP, 208p.

Depaolo, D.J. 1981. A neodymium and strontium isotopic study of the Mesozoic calc alkaline granitic batholits of the Sierra Nevada and Peninsular Ranges. California Journal of Geophysical Research, v. 86, p. 10470-10488.

Depaolo, D.J. 1988. Neodymium Isotope Geochemistry. Springer-Verlag, Berlin, 187p.

Ferreira, V.P., Sial, A.N., Jardim de Sá, E.F. 1998. Geochemical and isotopic signatures of Proterozoic Granitoids in terranes of the Borborema structural province, northeast Brazil. Journal of South American Earth Sciences, v. 11 (5) - 438-455.

Fuck, R.A, Brito Neves, B.B., Schobbenhaus, C. 2008. Rodinia descendants in South America. Precambrian Research. 160: 108-126.

Force, E.R., 1991. Geology of Titanium-Mineral Deposits. Geol. Soc. Am. Special paper 259. p.112.

Gass, I.G. 1980. The Troodos massif: Its role in the unravelling of the ophiolite problem and its significance in the understanding of constructive plate margin process. IN Panayistou, A. (ed.) Ophiolites. PP. 23-35, Geol.Surv.Cyprus.

Gióia, S.M.C.L., Pimentel, M.M., 2000. The Sm-Nd isotopic method in the geocrhronology laboratory of the University of Brasilia. Anais da Academia Brasileira de Ciências v. 72, p. 219-245.

Guimarães, I.P., Silva Filho, A.F., Almeida, C.N., Van Schmus, W.R., Araújo, J.M.M., Melo, S.C., Melo, E.B. 2004. Brasiliano (Pan-African) granitic magmatism in the Pajeú-Paraíba belt, Northeast Brazil: an isotopic and geochronological approach. Precambrian Research 135, 23-53.

Guimarães, I.P. & Brito Neves, B.B., 2004. Geochemistry characterization of part of the Early Neoproterozoic plutonism in the Central Structural Domain of the Borborema Province, NE Brazil. In: Proceedings of the 32nd International Geological Congress, International Union of Geological Sciences, Firenze.

Guimarães, I.P., Silva Filho, A.F., Almeida, C.N., Macambira, M.B., Armstrong, R. 2011. U-Pb Shrimp data constraints on calc-alkaline granitoids with 1.3 – 1.6 Ga Nd Tdm Model Ages from the Central Domain of the Borborema Province, Ne Brazil. Journal of South American Earth Sciences. 31: 383-396.

Guimarães, I.P., Van Schmus, W.R., Brito Neves B.B., Bittar, S.M.B., Silva Filho, A.F., Armstrong, R. 2012. U–Pb zircon ages of orthogneisses and supracrustal rocks of the Cariris

Velhos belt: Onset of Neoproterozoic rifting in the Borborema Province, NE Brazil. Precambrian Research. 192-195: 52-77.

Hollanda, M.H.B.M., Marulanda, C.O., Archanjo, C.J. 2013. Proveniência U-/Pb in situ de H fem zircões detríticos de sucessões metassedimentares da Zona Transversal. In: III Simpósio da Borborema/XXV Simpósio de Geologia do Nordeste, 2013, Gravatá. Boletim de Resumos do XXV Simpósio de Geologia do Nordeste. Gravatá: SBG, 2013. p. 505-506.

Howell, D. G. 1995. Principles of terrane analysis. New application for global tectonics. 2.ed. [S.l]: Chapman & Hall. 245p.

Jackson, S.E., Pearson, N. J., Griffin, W.L., Belousova, E.A., 2004. The application of laser ablation-inductively coupled plasma-mass spectrometry to in situ U-Pb zircon geochronology. Chemical Geology, v. 211, p. 47-69.

Jardim de Sá E.F., Macedo, M.H.E., Fuck, R.A. e Kawashita, K. 1992. Terrenos proterozóicos na Província Borborema e a margem norte do Cráton São Francisco. Rev. Bras. de Geoc. 22(4): 472-480.

Jardim de Sá E.F. 1994. A Faixa Seridó (Província Borborema, NE do Brasil) e o seu significado geodinâmico na cadeia Brasiliana/Pan-Africana. Tese de Doutorado, IGc - Universidade de Brasília. Brasília-DF. 804 p.

Jardim de Sá, E. F., Medeiros, W. E., Castro, D. L. Contribuição da gravimetria aos modelos de estruturação crustal da Província Borborema, Nordeste do Brasil. In: SIMPÓSIO DE GEOLOGIA DO NORDESTE, 17, 1997, Fortaleza. Resumos expandidos. Fortaleza: SBG. Núcleo Nordeste, 1997. 537p. il. (Boletim do Núcleo Nordeste da SBG, 15) p.352-357.

Kozuch, M., Bittar, S. M. B., Van Schmus, S. M., Brito Neves, B. B. de. 1997. Late mesoproterozoic and middle neoproterozoic magmatism in the Zona Transversal of the Borborema Province, Brazil. In: SIMPOSIO DE GEOLOGIA DO NORDESTE, 17, 16-19 nov. 1997, Fortaleza. Resumos expandidos. Fortaleza: SBG. Núcleo Nordeste, 537p. (Boletim Núcleo Nordeste da SBG, 15). p. 47–50.

Kozuch, M. 2003. Isotopic and trace element geochemistry of early neoproterozoic gneissic and metavolcanic rocks in the Cariris Velhos orogen of the Borborema Province, Brazil, and their bearing on tectonic setting. Tese (Doutorado)-Department of Geology, University of Kansas, Kansas, 199p.

Lages, G.A., Marinho, M.S., Rodrigues,J.B., Medeiros, V.C., Rodrigues, S.W.O, Silva, J.F.V. 2010. Sm-Nd Isotopic patterns and new paleoproterozoic nuclei basement on boundary between alto pajeú and Alto Moxotó domains, Borborema Province, NE-Brazil. In: VII South American Symposium on Isotope Geology. Brasília.

Lages, G.A., Dantas, E.L., Rodrigues, J.B., Santos, L.M.L. 2013. O magmatismo estateriano/caliminiano e os ortognaisses Coloete: Indício geoquímico de granito orogênico no leste da Província Borborema. In: III Simpósio da Borborema/XXV Simpósio de Geologia do Nordeste, 2013, Gravatá. Boletim de Resumos do XXV Simpósio de Geologia do Nordeste. Gravatá: SBG. p. 509-510.

Lages, G.A., Dantas, E.L., Santos, L.C.M.L. 2014. Sítio do Icó orthogneiss, east of Transversal Zone, Borborema Province: stenian orthogneiss with juvenile caractheristics. In: 9th

South American Symposium on Isotope Geology, 2014, São Paulo. Boletim de Resumos. São Paulo: Usp. p. 113.

Lages, G.A. no prelo. Geologia e Recursos Minerais da Folha Boqueirão, estado da Paraíba (SB.24-Z-D-III). CPRM/SBG. Programa Geologia do Brasil. 248p. ISBN: 978-85-7499-152-8.

Leake, B. E., Woolley, A. R., Arps, C. E. S., Gilbert, M. C., Grice, J. D., Hawthorne, F. C., … Whittaker, E. J. W. 1997. Nomenclature of amphiboles. The Canadian Mineralogist, 35, 219–246.

Lira Santos, L.C.M de. 2012. O paleoproterozóico (2.3 a 1.6 Ga) do Terreno Alto Moxotó, Província Borborema: significado e implicações para o Gondwana ocidental. Dissertação de Mestrado, IGd - Universidade de Brasília. Brasília-DF. xxx p.

Lira Santos, L.C.M., Dantas, E.L., Santos, E.J. dos, Santos, R.V., Lima, H.M., 2014. Early to Late Paleoproterozoic magmatism in NE Brazil: The Alto Moxotó Terrane and its tectonic implications for the Pre-West Gondwana assembly. J. South Am. Earth Sci. doi:10.1016/j.jsames.2014.07.006

Ludwig, K.R., 2001. User´s Manual for Isoplot/Ex version 2.47. A geochronological toolkit for Microsoft Excel. Berkeley Geochronology Center Special Publication 1a, 55 pp.

Mateinni, M., Junges, S. L., Dantas, E.L., Pimentel, M.M., Buhn, B. M., 2009. In situ zircon U-Pb and Lu-Hf isotope systematic on magmatic rocks: Insights on the crustal evolution of the Neoproterozoic Goiás Magmatic Arc, Brasília belt, Central Brazil. Gondwana Research. v. 16, p. 200-212.

Medeiros, V.C. 2004. Evolução geodinâmica e condicionamento estrutural dos terrenos Piancó- Alto Brígida e Alto Pajeú, Domínio da Zona Transversal, NE do Brasil. Tese de Doutorado, Programa de Pós-Graduação em Geodinâmica e Geofísica, Universidade Federal do Rio Grande do Norte, 200 pp.

Medeiros, V.C. & Sá, E.F.J. 2009. O Grupo Cachoeirinha (Zona Transversal, NE do Brasil) redefinição e proposta de formalização. Rev. de Geologia UFC. V.22(2): 124-136.

Melo, O.O de. 1998. Petrologia e Geoquímica das Rochas Gabro-Anortosíticas e Mineralizações de Fe-Ti associadas, de Barro Vermelho, Custódia-PE, Nordeste do Brasil. UFPE, CTG, Tese de Doutoramento, 216p.

Melo, O.O de, Guimarães, I.P., Fetter, A., Beurlen, H. 2002. Idades U/Pb em zircão e idades modelo (Sm/Nd) de ortognaisses e enclaves metamáficos da área de Barro Vermelho-PE, Terreno Alto Moxotó, Província Borborema, Nordeste do Brasil. RBG. v.32(2), pp. 197-204.

Nascimento, M.A.L., Antunes, A.F., Galindo, A.C., Jardim de Sá, E.F. e Souza, Z.S. de. 2000. Geochemical Signature of the Brasiliano-Age Plutonism in the Seridó Belt, Northeastern Borborema Province (NE Brazil). Revista Brasileira de Geociências, São Paulo, v.30, n.1, p. 161-164.

Nascimento, M.A.L. do, Medeiros, V.C de, Galindo, A.C. 2008. Magmatismo Ediacarano no Domínio Rio Grande do Norte, Província Borborema, NE do Brasil. Estudos Geológicos, UFPE, v.18, n.1, p. 4-25.

Neves, S.P., Mariano, G., Guimarães, I.P., Silva Filho, A.F., Melo, S.C. 2000. Intralithospheric differentiation and crustal growth: Evidence from the Borborema province, northeastern Brazil. Geology. 28(6): 519-522.

Neves, S.P. & Mariano, G. 2001. Província Borborema: Orógeno acrescionário ou intracontinental?. Estudos Geológicos, UFPE, v.11, p. 26-36.

Neves, S.P. 2003. Proterozoic history of the Borborema Province (NE Brazil): correlations with neighboring cratons and Pan-African belts, and implications for the evolution of western Gondwana. Tectonics 22, 1031

Neves, S.P., Bruguier, O., Vauchez, A., Bosch, D., Silva, J.M.R., Mariano, G., 2006. Timing of crust formation, deposition of supracrustal sequences, and Transamazonian and Brasiliano metamorphism in the East Pernambuco belt (Borborema Province, NE Brazil): implications for western Gondwana assembly. Precambrian Research 149, 197–216.

Neves, S.P., Bruguier, Olivier, Silva, J.M.R., Bosch, D., Alcantara, V.C., Lima, C.M. 2009. The age distributions of detrital zircons in metasedimentary sequences in eastern Borborema Province (NE Brazil): Evidence for intracontinental sedimentation and orogenesis?. Precambrian Research, p. 187-205.

Neves, S.P., Bruguier, O., Vauchez, A., Mariano, G., Silva, J.M.R. 2011. O magmatismo pós-Cariris Velhos, pré-Brasiliano na porção oriental da Província Borborem: Implicações tectônicas. XIII SNET, Campinas.

Neves, S.P., Lages, G.A., Brasilino, R.G., Miranda, A.W.A., 2014. Paleoproterozoic accretionary and collisional processes and the built-up of the Borborema Province (NE Brazil): geochronological and geochemical evidence from the Central Domain. J. South Am. Earth Sci. doi:10.1016/j.jsames.2014.06.009

Oliveira, E.P., Windley, B.F., Araújo, M.N.C. 2010. The Neoproterozoic Sergipano orogenic belt, NE Brazil: A complete plate tectonic cycle in western. Precambrian Research. 181: 64-84.

Oliveira, R. G. 2008. Arcabouço geofísico, isostasia e causas do magmatismo cenozóico da Província Borborema e de sua margem continental (Nordeste do Brasil). Natal, 411p. Tese (Doutorado) - Programa de Pós-graduação em Geodinâmica e Geofísica, UFRN.

Rodrigues, S.W de O., Medeiros, V.C de, Brasilino, R.G. 2010. U/Pb Geochonology of Salvador Orthogneiss (Paleoproterozoic unit of Transversal Zone, Borborema Province) In Campina Grande sheet (SB.25-Y-C-I). In: VII South American Symposium on Isotope Geology. Brasília.

Sá, J.M., Bertrand, J.M., Leterrier, J. 1997. Geocronologia U-Pb e geoquímica de ortognaisses paleo- e mesoproterozóicos da região de Taqueritinga – PE. In: Simp. Geol. Nordeste, 17. Fortaleza. Resumos expandidos, 108-112.

Santos E.J. & Brito Neves B.B. 1984. Província Borborema. In: Almeida F.F.M & Hasui T. O Pré-Cambriano do Brasil. São Paulo, Edgar Blucher, 123-186.

Santos, E.J., Coutinho, M.G.N., Costa, M.P.A, Ramalho, R. 1984. A região de dobramentos Nordeste e a bacia do Parnaíba, incluindo o Cráton de São Luís e as bacias marginais. In: Schobbenhaus, C., Campos, D.A., Derze, G.R., Asmus, H.E. (Eds.). Geologia do Brasil. DNPM,5, Brasília, p. 131-189.

Santos, E. J. dos. 1995. O complexo granítico Lagoa das Pedras: acresção e colisão na Região de Floresta (Pernambuco), Província Borborema. Sao Paulo. 220 p. 2 mapas. Tese (Doutorado em Geociências, Área de Concentração Geoquímica Geotectônica)-Universidade de São Paulo. Instituto de Geociências.

Santos, E. J., Oliveira, R.G., Paiva, I. P. 1997.Terrenos no domínio Transversal da Província Borborema: controles sobre acresção e retrabalhamento crustais ao sul do lineamento Patos. In: XVII Simpósio de Geologia do Nordeste, Fortaleza. Atas do XVII Simpósio de Geologia do Nordeste (Boletim do Núcleo Nordeste, SBG). Fortaleza : Sociedade Brasileira de Geologia, Núcleo Nordeste, v. 15. p. 141-144.

Santos, E. J. 1999. Belém do São Francisco, Folha SC.24-X-A, estados de PE, AL e BA (Nota Explicativa). Serviço Geológico do Brasil, PGBL, Brasília.

Santos E.J. & Medeiros V.C. 1999. Constraints from granitic plutonism on proterozoic crustal grownth of the Zona Transversal Domain, Borborema Province, NE Brazil. Rev. Bras. de Geoc.29:73-84.

Santos E.J, Van Schmus W.R., Brito Neves B.B., Oliveira R.G., Medeiros V.C. 1999. Terrane and their boundaries in the Proterozoic Borborema Province, Northeast Brazil. In: Anais do VII Simpósio Nacional de Estudos Tectônicos (SNET), resumos expandidos. p.121-124.

Santos E.J., Brito Neves B.B., Van Schmus W.R., Oliveira R.G. & Medeiros V.C. 2000. An overall view on the displaced terrane arrangement of the Borborema Province, NE Brazil. In: International Geological Congress, 31th, Rio de Janeiro, Brazil, General Symposia, Tectonic Evolution of South American Platform, p. 5-9, 1 cd-rom

Santos E.J., Ferreira C.A., Silva Júnior J.M.F. 2002. Geologia e recursos minerais do Estado da Paraíba: texto explicativo do mapa geológico e de recursos minerais. CPRM – Serviço Geológico do Brasil, 142p. 2 mapas. Escala 1:500.000.

Santos, E.J., Nutman, A.P., Brito Neves, B.B. 2004. Idades SHRIMP do Complexo Sertânia: Implicações sobre a evolução tectônica da Zona Transversal, Província Borborema. São Paulo. Geol.USP Ser.Cient. v4,n.1,pp.1-12.

Santos, E.J., Souza Neto, J.A., Carmona, C de M., Sial, A.N., Chemale Jr., F., Brito, R.S.C. 2008. Paleoproterozoic juvenile accretion in the Alto Moxotó Terrane, Borborema Province, Northeast Brazil. In: VI South American Symposium on Isotope Geology. San Carlos de Bariloche, Argentina.

Santos, E.J., Van Schmus, W.R., Kozuch, M., Brito Neves, B.B de. 2010a. The Cariris Velhos tectonic event in Northeast Brazil. Journal of South American Eath Sciences, 29: 61-76.

Santos, E.J., Souza Neto, J.A., Carmona, C de M., Armstrong, R., Basei, M.A, Mendes, D.S, Santos, L.C.M de Lira. 2010b. Collisional intrusive metacarbonates and associated metaplutonics at Itatuba (Paraíba), Alto Moxotó Terrane, Borborema Province. In: VII South American Symposium on Isotope Geology. Brasília.

Silva Filho M.A. 1984. A faixa de dobramento Piancó: Síntese do conhecimento e novas considerações. In XXXIII Congresso Brasileiro de Geologia, 5:3337-3347.

Stacey, J.S., Kramers, J.D., 1975. Aproximation of terrestrial lead isotope evolution by a two-stage model. Earth and Planetary Science letters. v. 26, p. 207-221.

Steiger, R. H., Jager, E., 1977. Subcomission on geochronology: conventions on the use of decay constants in geochronology and cosmochronology. Contributions to the geologic time scale. A.A.P.G. Studies in Geology. v. 6, p. 67-71

Schobbenhaus C., Campos, D.A., Derze, G.R., Asmus, H.E. 1984. Geologia do Brasil. Texto explicativo do mapa geológico do Brasil incluindo depósitos minerais escala 1: 2.500.000. Brasília: DNPM, Brasília, 501p.

Tohver, E., D'Agrella-Filho, M.S., Trindade, R.I.F. 2006. Paleomagnetic record of Africa and South America for the 1200–500 Ma interval, and evaluation of Rodinia and Gondwana assemblies. Precambrian Research. 193-222.

Trompette, R., 1994. Geology of Western Gondwana, Pan African-Brasiliano aggregation of South America and Africa. Rotterdam: A. A. Balkema. 350 p.

Van Schmus, W. R., Brito Neves, B.B. de, Hackspacher, P., Babinski, M. 1995. U/Pb and Sm/Nd geochronologic studies of the eastern Borborema Province, northeastern Brazil: initial conclusions. J. S. Am. Earth Sci. v.8, p.267–288.

Van Schmus, W.R., Brito Neves, B.B., Willians, I.S., Hackspacher, P.C., Fetter, A.H., Dantas, E.L., Babinski, M. 2003. The Seridó Group of NE Brazil, a late Neoproterozoic pre-to syn-collisional basin in West Gondwana: insights from SHRIMP U-Pb detrital zircon ages and Sm-Nd crustal residence (TDM) ages. Precambrian Research, v. 127, n.4, p.287-327.

Van Schmus, W.R., Oliveira., Silva Filho, A.F., Toteu, F., Penaye, J., Guimarães, I.P., 2008. Proterozoic links between the Borborema Province, NE Brazil, and the Central African Fold Belt. Geological Society, London, Special Publications. v. 294, p. 66-69.

Van Schmus, W.R., Kozuch, M., Brito Neves, B.B. Precambrian history of the Zona Transversal of the Borborema Province, NE Brazil: Insights from Sm-Nd and U-Pb geochronology. 2011. J. of South A.E.Sciences. V.31.pp. 227-252.

Vauchez, A., Neves, S.P., Caby, R., Corsini, M., Egidio-Silva, M.. Arthaud, M., Amaro, V. 1995. The Borborema shear zone system, NE Brazil. Journal of South American Earth Sciences. v.8, p.247-266.

Veronese, W.F., Ortiz, L.R.C., Gonzales, S.R., Menor, E.A., Montes, A.S.L., Marques, N.M.G. & Coitinho, J.B.L. Projeto ferro titanado de Floresta (PE). Minérios de Pernambuco/Radambrasil, vol. 2-Metalogenia, 155p. 1985.